2010

Localization and Function Of RNA Interference in the Cerebral Cortex

John T. G. Pena

LOCALIZATION AND FUNCTION OF RNA INTERFERENCE IN THE CEREBRAL CORTEX

A Thesis Presented to the Faculty of

The Rockefeller University

in Partial Fulfillment of the Requirements for

the degree of Doctor of Philosophy

by

John T.G. Pena

June 2010

LOCALIZATION AND FUNCTION OF RNA INTERFERENCE IN THE CEREBRAL CORTEX

John T. G. Pena, Ph.D.
The Rockefeller University 2010

During the course of adult cortical plasticity, a number of signal transduction mechanisms are brought into play. To study regulatory genes implicated in this process, we inhibited gene expression by harnessing the machinery of RNA interference (RNAi) pathway via small hairpin RNAs (shRNA) delivered by viral vectors. Using this technology we sought to influence plasticity of the mouse vibrissal barrel cortex. In this model system, chronic whisker plucking reliably leads to the expansion of the cortical representation of the adjacent non-deprived whiskers. The mechanism underlying this process involves changes in synaptic efficacy and sprouting of axon collaterals. Initial studies describing the molecular events leading to synaptogenesis and remapping have implicated a number of signal transduction pathways, including neurotrophins such as brain derived neurotrophic factor (BDNF). Though previous experiments have shown up-regulation of neurotrophins and their receptors in reorganized cortex, it is necessary to remove these factors to definitively prove their involvement in adult cortical plasticity. We therefore repressed neurotrophic gene expression in the mouse somatosensory cortex to determine if these trophic factors are essential for cortical remodeling after sensory deprivation. We blocked gene expression *in vivo* using a non-replicative adeno-associated virus bearing genes encoding shRNA constructs. The shRNA nucleotide sequences were designed to target and destroy selected neurotrophin messenger RNAs by triggering the RNAi pathway, resulting in a reduction of BDNF protein levels by up to 80% *in vivo*. This knockdown of BDNF expression effectively repressed functional cortical reorganization induced by chronic whisker plucking. Unexpectedly, when transducing the somatosensory cortex with a viral vector carrying a control

shRNA that does not target a gene in mouse, we saw no cortical reorganization after sensory deprivation. These results suggest that a non-specific blockade of cortical plasticity occurs when using shRNAs in the brain. Our results suggest that manipulating gene expression via virally delivered shRNAs may have limited value for blocking expression of specific genes involved in cortical plasticity. However, the results suggest a potential role for RNA interference itself in regulating cortical plasticity.

In the second part of this thesis, we study methods to visualize microRNAs in tissue sections. MicroRNAs (miRNAs) are small regulatory RNAs with many biological functions and disease associations. Association studies are rapidly linking miRNAs with cancers and neurological disorders. miRNAs have specific expression and function in specialized cell types, emphasizing the need to define cell–type–specific miRNA expression patterns. For pathologists, the most common method for visualizing gene expression in specific cell types is *in situ* hybridization (ISH). In our laboratory, conventional ISH worked for highly abundant miRNAs, however examining less abundantly expressed miRNAs often yielded inconsistent or negative results. A review of the literature indicates that zebrafish whole–mount ISH were robust, whereas ISH in *D. melanogaster* embryos were mostly unsuccessful. In tissue sections, several studies set the foundation for establishing miRNA ISH, and were used to support association to disease, or defined expression patterns in multiple cell types present in the brain and eye. The technical difficulties in miRNA ISH also led to development of transgenic or cell sorting methods that monitor cell–type–specific miRNA expression.

To better understand the technical challenges associated with miRNA ISH, we investigated the importance of miRNA fixation and probe hybridization. For fixation of proteins and nucleic acids in tissues, a solution containing 3.7% formaldehyde (10% formalin) is commonly used. Formaldehyde

crosslinks are reverted by incubation at elevated temperature and this process is facilitated by proteinase K treatment. Reversal of the formaldehyde–based nucleic acid base modifications is also necessary for probe hybridization, but it creates the problem of miRNA release and diffusion out of the tissue sections. Therefore, we examined the extent of miRNA escape from tissue during ISH. We conducted a mock ISH for conventionally fixed brain sections, isolated RNA from the tissue sections and the ISH buffer, and probed both fractions for the highly expressed neuronal miRNAs. We showed that *in situ* hybridization (ISH) using conventional formaldehyde fixation results in significant miRNA loss from mouse tissue sections, which can be prevented by fixation with 1–ethyl–3–(3–dimethylaminopropyl) carbodiimide (EDC) that irreversibly immobilizes the miRNA at its 5' phosphate.

Eliminating the possibility of miRNA diffusion by introducing an irreversible crosslink between the 5’ phosphate of the miRNA and protein side chains significantly improves miRNA retention in tissues. The advantage of EDC–based phosphoramidate–linked miRNA is that the sample can be exposed to higher temperatures for a longer time, resulting in a more complete reversion of the formaldehyde induced nucleobase modification of the miRNAs and less interference with probe hybridization. At present, we showed that different tissues and detection systems are compatible with our approach. This method paves the way for reliable disease association studies and the potential use of miRNA *in situ* hybridization expression analysis as a diagnostic tool for biopsy material.

This thesis is dedicated to my family; John W. Pena, Hollie E. Pena, Tracy Pena, Robin Pena, Kris Pena, Jennifer Pena, David Hurley, Chase Hurley, Lauren Hurley, Max Helchowski, Ella Helchowski, and Forrest Ward, and Brandon Helchowski, Genevieve Walton, Harry Pena, Velma Pena, Dr. Overby, Dr. M. Overby, Carey Jenkins, Dr. Forrest, Dr. Reddan, and Dr. Kaplitt.

TABLE OF CONTENTS

LIST OF FIGURES

LIST OF TABLES.....

Chapter I

Regulation of gene expression by RNA interference

Introduction

Cortical plasticity in adult central nervous system

Damage to the central nervous system (CNS) often results in devastating sensory and motor deficits that last a lifetime. Several neural systems demonstrate *limited* ability to partially reorganize damaged circuits after injury. With the loss of afferent input, the adult brain remodels to improve function by shifting neuronal receptive fields away from the damaged region and thereby enhancing the representation of the available sensory input. This observation was described in the adult somatosensory cortex after digit amputation[1]. After removing the forefinger, sensation for the amputated digit was lost, but within several months, the cortical neurons representing the lost digit shifted their receptive fields towards the adjacent fingers. In cases of partial deafness, damaging receptor cells in a restricted area of the cochlea resulted in loss of auditory information from a selected frequency range. Months later, the cortical area previously representing frequencies of the ablated neurons expanded its representation to stimuli collected from cochlear cells adjacent to the lesioned region[2].

In the visual system, several investigators describe cortical remodeling in the primary visual cortex (V1) following focal binocular and monocular retinal lesions in the adult cat and monkey[3-10]. Binocular lesions in the adult monkey silence a corresponding region of the visual cortex, known as the cortical lesion projection zone (LPZ), where neurons are no longer responsive to visual stimuli. After several months, however, neurons in the cortical LPZ recover stimulus-driven activity by shifting their receptive fields to the region of visual space just outside the lesion[3]. These receptive field shifts were determined to be cortically mediated[4,5], by sprouting

of horizontal connections in the adult, which is strongly correlated with, and likely underlies, these changes in receptive field representation[5,11].

In mice, cortical remodeling occurs after partial vibrissectomy as sparing selected rows of vibrissae in adult animals results in the enlargement of areas representing the intact whiskers[12]. To induce plasticity, one can remove a selected group of whiskers for weeks, then after sensory deprivation, the cortical area representing the intact row expands into areas that previously represented chronically removed whiskers (**Figure 1**). Collectively, these studies from sensory systems suggest the adult brain has a remarkable ability to adapt to injury by cortical reorganization. Yet the extracellular signaling molecules and signal transduction pathways that mediate injury induced cortical plasticity are not fully characterized.

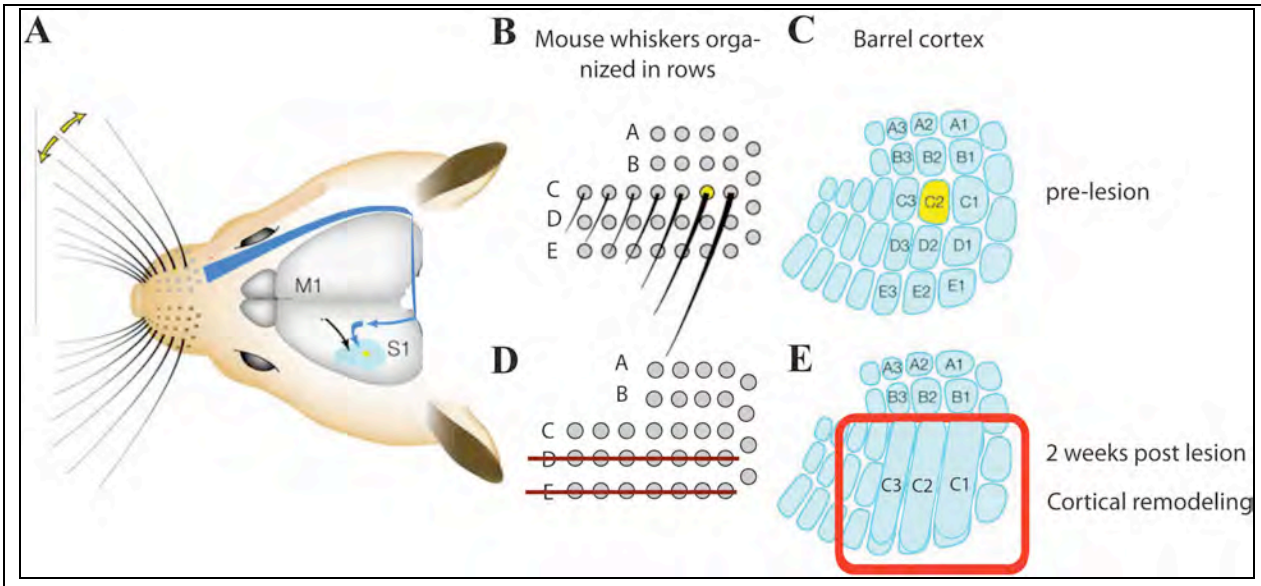

Figure 1: Cortical plasticity in mouse somatosensory cortex induced by sensory deprivation. (a) An illustration showing the mouse vibrissa that are mechanically manipulated and stimuli is then represented in the somatosensory cortex. **(b)** The mouse vibrissa is organized into rows A-E. **(c)** Barrels in the somatosensory cortex represent specific whiskers (light blue circle; letter marks the whisker row and the number identifies the whisker within the row). **(d)** To induce cortical plasticity, whiskers from rows D and E are continuously removed for two weeks (illustrated by line strike). (**e**) The representation from the intact whiskers in row C expand into sensory deprived areas (expanded represenation is denoted by larger retangles).

Neurotrophic factors are potential mediators of cortical remodeling after injury.

Functional recovery of cortical areas after injury requires changes in cortical architecture, a process that must be regulated by signaling molecules. Neurotrophins have emerged as attractive candidates to potentially mediate cortical plasticity. The neurotrophin family of peptides is known to regulate neuronal differentiation[13], axon sprouting[14,15] and synapse formation[16,17].

Nerve growth factor (NGF) was the first neurotrophin family isolated[18], later others were cloned including brain-derived neurotrophic factor (BDNF), and neurotrophin 3 and 4/5 (NT3 and NT4/5)[19]. The mature peptides exert their action by binding to a specific tyrosine kinase receptor (Trk), NGF to TrkA, BDNF and NT4/5 to TrkB and NT3 exerts opposing effects on TrkA, TrkB and TrkC receptors[20]. Ligand-receptor coupling induces the dimerization of receptors, and then activates downstream signal transduction pathways like CREB[16], which modulates axonal growth[16]. Neurotrophins signal changes in axon morphology by retrograde signaling, NGF for example, stimulates axonal sprouting when applied to the distal ends of cultured sympathetic neurons[21]. Other neurotrophins BDNF and NT-3 promote spontaneous synaptic plasticity[22,23]. Interestingly, BDNF and other neurotrophin expression levels elevate with increased neural activity[24-27]. For example, visual stimuli enhances BDNF messenger RNA (mRNA)[27], conversely, rearing animals in the dark blunts BDNF mRNA expression levels. This interdependency between neurotrophin expression and neural activity is a likely mechanism for preferentially strengthening active neural circuits[24,28]. Limited amounts of neurotrophins present in the postsynaptic target neurons, act an activity-dependent retrograde signal, which strengthens more active pre-synaptic inputs. Evidence supporting this hypothesis comes from monocular deprivation (MD) studies in developing animals[24]. Normally, suturing an eyelid shut silences representation of cortical neurons mapped to the deprived eye, however, when NGF is applied in excess during sensory deprived, the neurotrophin rescues the animal from cortical blindness[24,29]. Other neurotrophins like BDNF also influence the formation of ocular dominance columns[16] and the TrkB ligand NT-4 can rescue the visual cortex from MD induced cortical blindness[30]. BDNF

also regulates GABAergic interneurons by stimulating outgrowth, altering gene expression of GABA[31] and regulates maturation of inhibitory neurons in the visual cortex during the critical period[32]. Neurotrophins appear to signal activity-dependent synaptic competition, a mechanism that is important in neuronal development[33,34].

Neurotrophin upregulation can be observed in the adult reorganized cortex. In the adult monkey V1, after a restricted region of the retina is damaged, BDNF, NT-3 and NGF protein expression is enriched at the cortical LPZ (**Figure 2**)[35]. Up-regulation of the TrkA, TrkB, TrkC, and p75 receptors were also observed at early time points (3 days) and for the long-term (up to 87 weeks). Enhanced expression occurred within the large cortical LPZ at early time points, and protein expression patterns shrank in size as the cortical LPZ was filled in over time. The location of enriched neurotrophin expression correlated with the site of the cortical scotoma (also defined as the LPZ) following retinal lesions, suggesting a role for neurotrophins in V1 repair. Yet, no study has directly demonstrated that neurotrophins are necessary for cortical reorganization. To study cortical plasticity in the intact adult brain one can integrate approaches in molecular biology and systems neuroscience to block gene expression *in vivo*.

Figure 2. BDNF expression within the cortical LPZ. Retinal injury enriches BDNF, protein expression within the cortical LPZ in adult primate V1 shown by assaying with immunohistochemistry [35]. Up-regulation of BDNF was observed at early time points (3 days) and for up to 87 weeks.	

Gene delivery using adeno-associated viral vectors

Cortical reorganization occurs over weeks; therefore a gene delivery system to alter this process should persistently attenuate gene expression for the long-term. Adeno-associated virus (AAV) vectors are non-pathogenic human single stranded DNA parvoviruses [36,37], suitable to deliver transgenes into the brain. Since the vast majority of AAV exists as extrachromasomal circular DNA, AAV vectors effectively and stably transduce non-dividing neurons[37]. AAV vectors have proven to be efficient and safe means of transducing non-dividing cells *in vivo*. Up to 80% of the human population is likely to be infected with AAV and no malignancy has been associated with this virus[38]. Nor has AAV infection evoked a stress response[39]. Long-term expression has been demonstrated in the monkey CNS for five years without initiating the host immune system[38]. A small percentage of AAV forms have been reported to recombine into host cell genomes[40], however the side-effects are rare and the potential for complication in brain transduction studies are minimal.

The technical advantages of using these vectors include rapid production of viral stocks, ability to obtain a high titer, and ease of cross-packing AAV plasmids into several different serotypes. The AAV shuttle vector or *cis plasmid* contains two 145 nucleotide (nt) inverted terminal repeats (ITRs), between which are up to 4.8 kb of foreign DNA can be inserted (**Figure 3**). AAV *Rep* and *cap* genes are required for replication of the viral genome and the structural envelope of the capsid, respectively. To complete the life cycle AAV requires a helper virus, usually Adenovirus. While shuttle vectors AAV2 ITRs and *rep* gene usually remain constant, capsid genes coding for various serotypes are interchangeable, these AAV hybrids are called

pseudotypes. Recent studies demonstrate AAV serotype 1 capsid and AAV2 rep gene (termed: AAV2.1) enhance transgene expression and spreads more widely in areas of the midbrain, when compared to wild type AAV2 virus[41]. Transgene expression can be controlled by a *hybrid* CMV-chicken-beta-actin (CBA) promoter, which has enhanced expression when compared to the CMV promoter[42]. To further enrich GFP labeling, one can recombine the Woodchuck hepatitis virus element posttranscriptional regulator (WPRE) to the 3' end of the transgene to increase the steady-state level of mRNA and improve translation efficiency[43].

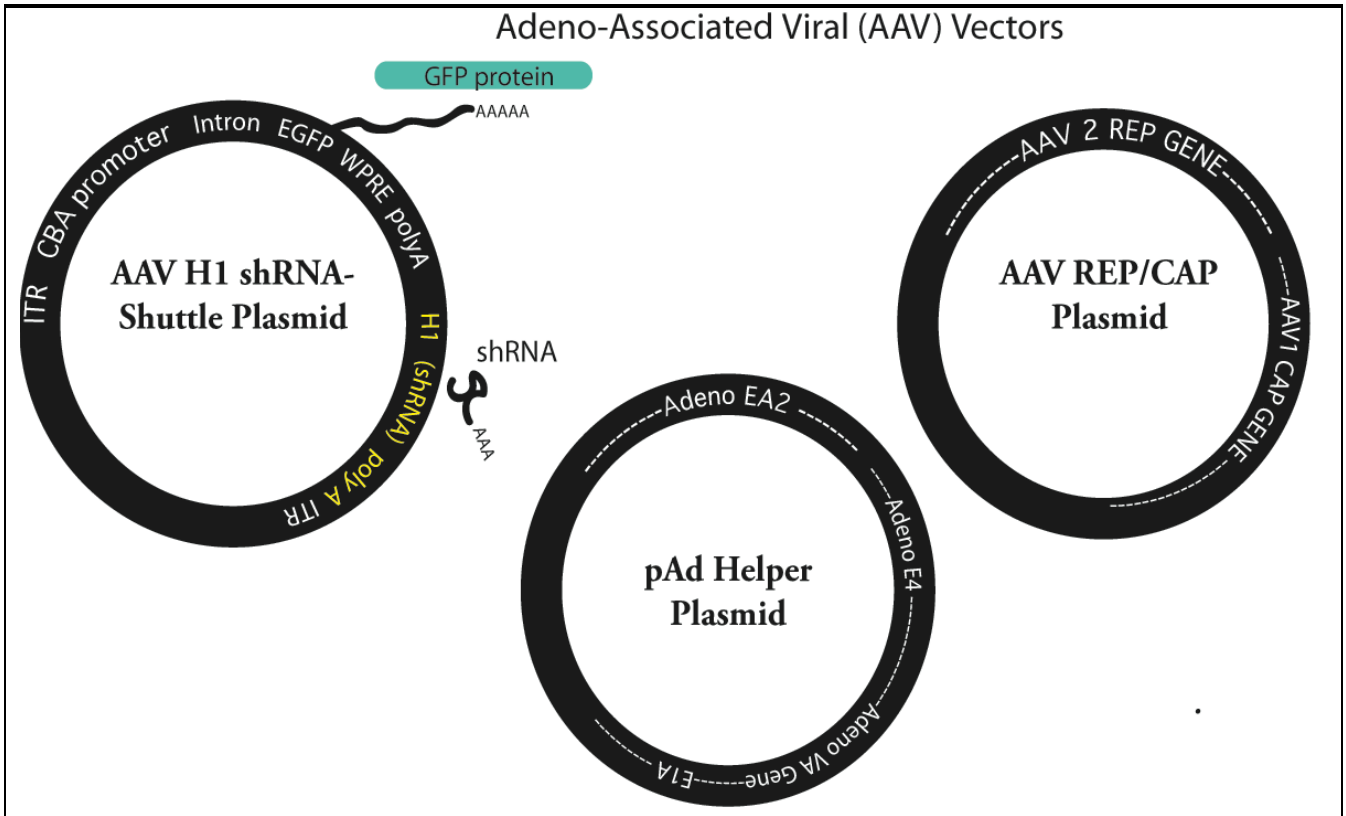

Figure 3: Schema of Adeno-Associated Viral (AAV) vectors encoding small interfering RNAs and a fluorescent protein: (**Top, left**) Diagram of transgenes cloned into an AAV shuttle vector flanked by inverted terminal repeats (ITRs). The shuttle vector contains two separate expression cassettes for a fluorescent protein (eGFP or RFP) and a small interfering RNA (shRNA) duplex. To enrich fluorescent protein levels, the chicken beta actin promoter drives expression, along with a woodchuck hepatitis virus element posttranscriptional regulator (WPRE) recombined toward the 3' end. An RNA polymerase III promoter, H1 controls small hairpin RNA (shRNA) expression. **(Top, right)** To package the DNA between the ITRs of the shuttle vector, AAV requires structural proteins (cap) and non-structural genes (rep) encoded on a separate vector (**top, right**). **(Center)** Completion of the viral life cycle AAV requires proteins and RNA genes from a helper virus Adeno virus vector (**center**).

By combining the AAV gene delivery system with RNA interfering molecules (reviewed

below) one can attenuate gene expression in the living brain. The emergence of the RNAi has revolutionized biological research by harnessing the cell's natural ability to inhibit any gene with specific small RNA triggers.

Post-transcriptional genetic control by small RNAs

The recent discovery of gene regulation by different classes of small non-coding RNAs illustrates the complexity of regulation of gene expression in higher vertebrates[44]. Classes of mammalian small RNAs include ubiquitously expressed microRNAs (miRNAs) and germline-specific piwi-interacting RNAs (piRNAs), as well as synthetic mimics that use the natural RNAi pathway, such as small interfering RNAs (siRNAs) and small hairpin RNAs (shRNAs). miRNAs represent the most abundant family of small regulatory RNAs in animals, but are also present in plants and some viruses[45]. miRNAs are matured from double-stranded RNA (dsRNA) precursors[46-48] and rely on the RNA silencing or RNA interference (RNAi) machinery to destabilize and/or translational repress partially sequence-complementary target mRNAs; fully complementary target mRNAs, though they are extremely rare for animal miRNAs, are effectively cleaved and the mechanism is exploited for siRNA-mediated gene knockdown[49-55].

RNAi processing pathway

miRNAs are encoded within intronic or exonic regions of protein-coding or non-coding transcripts, and miRNAs are often organized in polycistrons[56-58]. The primary transcripts of miRNAs (pri-miRNAs), with exception of some viral miRNAs, are transcribed from polymerase (pol) II promoter[46-48] and matured in a multi-step process (**Figure 4**)[46-48]. Within the pri-miRNA, exists a hairpin RNA known as the pre-miRNA, which is recognized by dsRNA-binding

proteins. These two RNase III enzymes process the pre-miRNA to yield a double-stranded processing intermediate, where one strand represents the miRNA, and the opposing strand is annotated as miRNA*. The mature miRNA is predominatly incorporated into an Argonaute (Ago) protein containing complex, also known as RNA-induced silencing complex (RISC), which facilitates target recognition and mediates the miRNA regulatory function[59-66]. The miRNA* is usually lost during this process and less frequently incorporated in the silencing complex[15]. Humans contain 4 Ago proteins, Ago1 through 4, which bind miRNAs and target RNAs with similar specificity[67];Ago2 is the only protein that has an active endonuclease domain and is responsible for potent cleavage of target RNAs by siRNAs in gene knockdown experiments[68,69]. More recently it was also shown that the three members of the TNRC6 protein family, also known as P-body marker GW182 family, associate with miRNA-containing Ago complexes and their targets[67]. The miRNA-containing ribonucleoprotein complexes (miRNPs) binding reduce the target mRNA and protein levels by interfering with either translation initiation or elongation (**Figure 4**)[70-77].

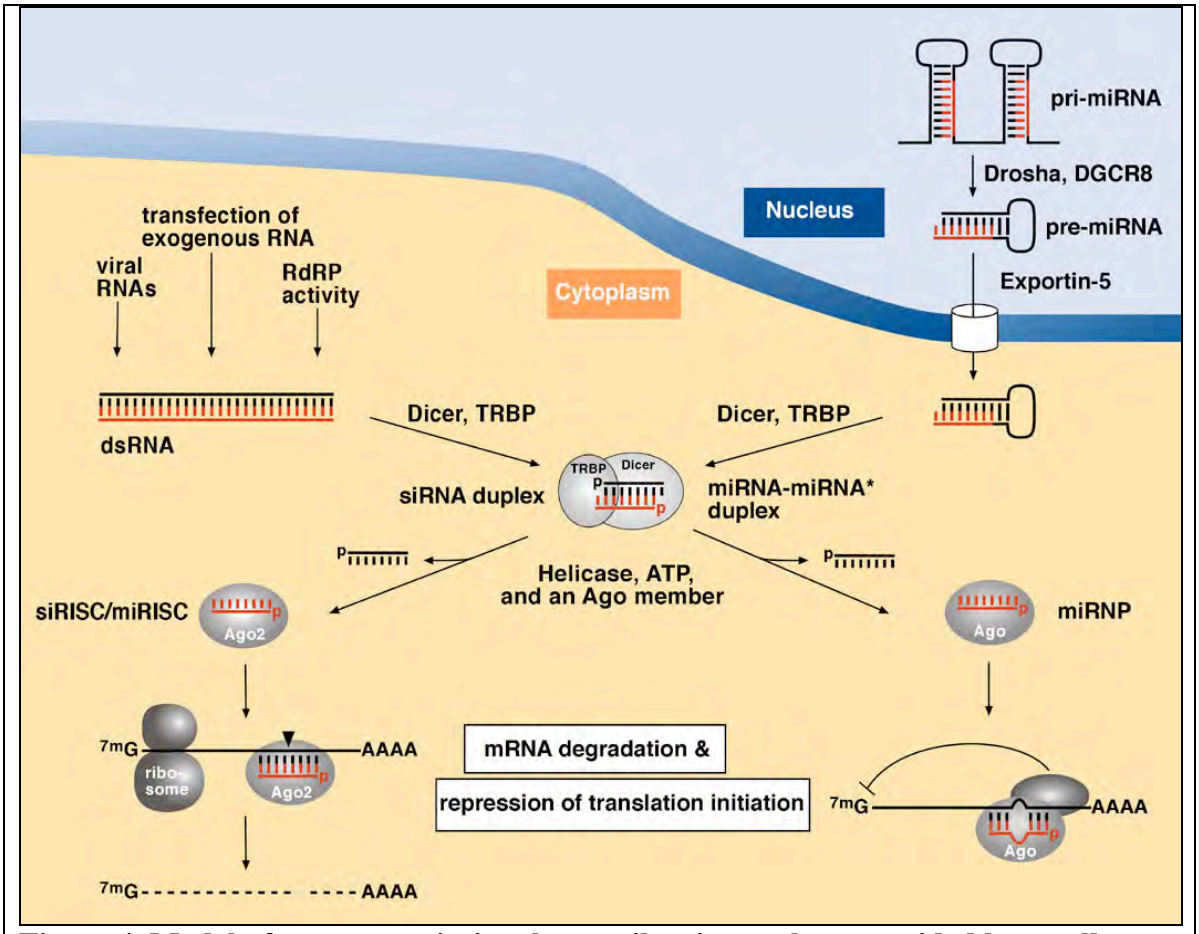

Figure 4. Model of posttranscriptional gene silencing pathways guided by small RNAs. Drosha RNase III and its interacting partner, DGCR8, process pri-miRNA to pre-miRNA. The pre-miRNA is subsequently exported to the cytoplasm using the export receptor exportin-5 and processed by Dicer RNase III to a "siRNA-like" miRNA-miRNA* duplex intermediate. The single-stranded miRNA is loaded onto a member of the Ago protein family and the miRNA* is degraded. miRNPs associate with partially complementary sequences in the 3' UTR to inhibit translation. Both siRNAs and miRNAs can be assembled into Ago2-containing RISC complexes (siRISC, miRISC). Ago2 in mammals mediates the cleavage of complementary targets. Abbreviated.: 7mG, 7-methyl guanosine; AAAA, poly-adenosine tail; p, 5' phosphate.

Blocking gene expression using RNA interference (RNAi)

The recent discovery of RNA interference has emerged as a powerful tool for specific gene knockdown. By activating endogenous RNAi machinery, one can specifically inhibit any transcript in the genome[78,79]. Collectively, the processes of post-transcriptional gene silencing by small double-stranded RNA are termed RNA interference (RNAi), a highly conserved mechanism in eukaryotes (**Figure 4**). Initial studies in *C. elegans* showed exogenous and endogenous double stranded RNA (dsRNA) are more potent silencers of gene expression when compared to antisense RNA alone[80]. Tuschl and colleagues elicited transient degradation of targeted messenger RNA by introducing short 21-28 nucleotide RNA (siRNAs) duplexes *in vitro*[81]. For stable RNAi induction, plasmid based small hairpin RNAs (shRNAs) can be expressed using a polymerase III promoter[82] and shRNA can be inserted into viral vectors for long-term expression. Both shRNA and siRNAs are essentially homologues of processed miRNAs and enter the RNAi pathway at the same stage of the pre-miRNA. The processing of shRNAs is reviewed (**Figure 4**).

Tissue-specific expression patterns of miRNAs

The biological function for many small RNAs is largely unknown, yet the RNA interference pathway plays an essential role in nature, as the sequence of many miRNAs are conserved from invertebrates to humans[85,86]. Moreover, several studies using gene knockouts of several RNAi components proved to be embryonic lethal in mice[87,88]. Cell- and tissue-type-specific mature miRNA expression is best determined by small RNA cDNA library sequencing or more recently by using miRNA microarrays[89,90]. An example of a cell-type enriched and conserved miRNA

family is miR-1 and its close relative miR-206, which are predominantly expressed during development in muscle of vertebrate and invertebrate specimens[91-93], and highly abundant in the heart of adult mammals[86,94]. Other examples of tissue specific miRNAs include miR-122 in the liver[86], miR-124 in neurons[86,95], or miR-375 specific to endocrine cell-types such as pancreatic alpha and beta cells or the pituitary gland[96]. Analysis of expression patterns of close to 100 miRNAs in the developing zebrafish revealed that about 68% of the miRNAs have a distinct expression in tissues during or after the blastula period[91]. Virtually every cell type or tissue examined expresses some unique combination of miRNAs, and miRNA expression profiles were shown to be useful for certain diagnostic applications[97].

miRNAs influence cellular function

The biological relevance and exact gene targets of most miRNAs remain unclear, however the like miRNAs are conserved, so are many of their target sites[98]. Several miRNAs have been implicated in a variety of developmental and physiological processes, affecting cell lineage decisions, cell proliferation, apoptosis, morphogenesis, fat metabolism, hormone secretion, and the stress response[55,99-102]. In *C. elegans*, lin-4 -miRNA is involved in controlling larval developmental steps by targeting sites in the 3' untranslated region (3' UTR) of lin-14 mRNA. Other studies deleted a processing enzyme in the RNAi pathway, the RNase III Dicer, which is essential for miRNA maturation. This perturbation of the miRNA pathway severely affects mouse embryonic development[88,103,104]. To overcome lethality associated with early deletion of dicer in mice, the allele can be removed using a cre-inducible conditional allele, generating a conditional knockout (cKO). Dicer cKO in the mouse impaired T cell differentiation, survival,

and proliferation[105,106]. In another mouse study, dicer cKO expressing cre in the limb mesoderm resulted in perturbed morphogenesis, but no effect was observed for patterning of the developing limb[107]. Attenuating dicer expression in mouse embryonic stem resulted in development defects *in vitro* and *in vivo*, the effect was linked to a lack of miRNAs[108]. Dicer also functions to process other small RNA species in addition to miRNAs[109]. Despite these potential complications, the knockout studies provided the first clues about the physiological function of miRNA regulatory networks in developing vertebrates.

Another approach to gain insight regarding miRNA function in development is to attenuate DGCR8 protein expression *in vivo*. DGCR8 is thought to exclusively be involved in the maturation process of miRNAs[110-112], with no other known cellular function. Inhibiting DGCR8 in mouse embryonic stem cells yielded phenotypes similar to Dicer cKO animals. However, DGCR8 negative embryonic cells showed accelerated growth rate, when compared to Dicer cKO cells[108]. In the mouse skin, DGCR8 cKO mice had abnormal hair follicle development and altered epidermal cell differentiation, phenotypes also observed in Dicer null mice. In the latter study, the observed phenotypes suggest Dicer and DGCR8 removal were responsible for reduced follicle development, solely due to reduction of miRNA levels.

Molecular targets of miRNAs

The precise number of miRNAs targets, especially those not evolutionary conserved, remains unclear. Computational studies provide guidance in addressing this key question[113-128]. Over 500 human miRNAs have been identified and thousands of gene targets predicted. Conservative estimates suggest that over one third of the mammalian genome is potentially regulated by

miRNAs[125]. Yet experimental validation of specific gene targets for the majority of miRNAs remains incomplete. Experimental approaches to pair miRNA and mRNA targets using cDNA array analysis of cells over-expressing miRNAs in cell culture set the foundation for identifying mRNA targets[129]. Immunoprecipitation of Ago proteins and analysis of associated mRNAs by array and deep sequencing shows promise in identifying these interactions[67]. Due to the complexity and the large numbers of genes implicated in these studies, further functional validation is necessary. Almost certainly, given the large number of interactions (mis-expression of miRNAs and/or deletion, insertion or mutation of miRNA targeting sites), this process will likely be linked to some diseases. Most recently it was shown that progressive hearing loss in some families was linked to mutations in miR-96[130,131]. Association of miRNA mis-regulation and various types of cancer have also been described[47,91] and miRNA expression profiles have been suggested to be useful for classifying diseased specimens[132].

The identification and spatial localization of miRNAs in the nervous system

Given the neuron-specific expression of certain conserved miRNAs, it is likely that the RNAi pathway also plays an important regulatory role in the nervous system. The nervous system is comprised of complex cell types with unique functions, and miRNA expression patterns may contribute to this diversity. Several early studies focused on identifying miRNA expression in different brain regions and identified the highly abundant and conserved miR-9, miR-124, and miR-128a, which are specifically expressed in the brain[89,133]. miRNA expression patterns are thought to be characteristic of distinct neuronal lineages[134], as the timed expression of miRNA families correlates with cortical development[135-137].

To elucidate specific expression patterns of miRNAs in complex tissues, several techniques were developed, such as generating transgenic models that express miRNA constructs with reporters[138], using single cell detection by quantitative PCR[139], and profiling FACS sorted hematological cells[89,140]. To localize miRNAs at the sub-cellular level, others combined laser capture microscopy and multiplex PCR to show miRNAs are also present in neuronal dendrites[141]. Several studies set the foundation to image the cell-type specificity of miRNAs in the neuronal and other tissue sections using conventional or a modified *in situ* hybridization techinque[95,142-147]. For example, the highly abundant miR-124 is exclusively expressed in neurons. Other miRNAs such as miR-23, miR-26, and miR-29 were present in neurons and astrocytes[148].

The role of the miRNA pathway in the nervous system

An early example of a miRNA associated with function in the nervous system occurred in *C. elegans*, as the miRNA lsy-6 controlled left/right neuronal asymmetry[149-151]. In cultured cells, exogenous expression of neuron-specific miR-124 in HeLa cells induced a down-regulation of hundreds of target mRNAs, effectively switching the gene expression profile of these human carcinoma cells to mirror gene expression patterns of a mature neuron[129,152]. In neuroblastoma cells, the over-expression of the highly abundant miR-124, induced neuronal differentiation, while blocking miR-124 expression with a 2'-O-methyl RNA oligonucleotide, inhibited neurite outgrowth and synaptogenesis in primary cultured neurons. In the adult brain, miR-124 regulated the process of cell maturation in the subventricular zone (SVZ)[134]. miR-124 expression increased as cells matured and differentiated. Knockdown of miR-124 resulted in increased populations of

cells similar to those present early in the neurogenesis pathway, while over-expression of miR-124 promoted neuronal differentiation. These studies demonstrate that a single strongly expressed miRNA influences function in the brain.

Blocking proteins in the miRNA pathway in neurons

To further investigate the function of miRNAs in the brain, a number of studies manipulate components of the RNAi machinery to block miRNA biogenesis. In zebrafish, depleting mature miRNAs by knocking-out Dicer resulted in abnormal brain morphogenesis[153]. In the adult mouse, Dicer conditional knockout (cKO) in the forebrain resulted in gross abnormalities including microcephaly and reduced dendrite branch elaboration[154]. In the cerebellum of adult mice, removing Dicer resulted in a cerebellar degeneration and ultimately functional ataxia[103]. Engineered mouse strains with 22p11.2 micro-deletions, with one copy of the gene for DCGR8 removed, showed impaired and abnormal biogenesis of miRNAs. The phenotype of the reduced miRNA levels led to smaller dendritic spines and less complex dendritic trees, similar to the Dicer cKO. The functional consequences of reducing miRNA expression from DGCR8 cKO animals caused impaired spatial working memory-dependent tasks and experienced reduced sensorimotor gating[155]. Blocking the miRNA-processing pathway demonstrates that RNAi is an important regulator of the nervous system.

Fragile X mental retardation protein, an RNA binding proteins involved in neurological disease

The importance of the miRNA pathway in the nervous system may be, at least in part, through its reported association with the fragile X mental retardation protein (FMRP)[156,157]. In humans,

Fragile X syndrome is one of the most common inherited cognitive deficiency disorders. The etiology of this disease is related to a trinucleotide repeat expansion of CGG in the 5' untranslated region (UTR), which inactivates the X-linked FMR1 gene that encodes FMRP, ultimately leading to the reduction in FMRP. FMRP is an RNA binding protein, which regulates mRNAs at the post-transcriptional level. While the mechanism of FMRP-dependent regulation remains unknown, FMRP appears to control protein synthesis in response to synaptic activity[158]. FMRP is also thought to be critical for messenger RNA transport within dendrites, possibly affecting axon guidance, synaptic development and formation of neuronal circuits. In *Drosophila*, FMRP was shown to associate with RISC protein components[157,159,160]. A compelling model is that FMRP elicits its function through an association with the RISC complex. There appears genetic evidence that FMRP and RISC functions do overlap. Studies in flies using olfactory conditioning showed that long-term memory formation requires FMRP and Ago proteins[159]. Future studies are still needed to prove miRNAs and FMRP function directly together to regulate protein translation in neural systems.

miRNAs in synaptogenesis

In the neuron, the size, shape, and number of postsynaptic structures are dynamically regulated throughout its life. miRNAs have emerged as potentially important molecular mediators of synaptic plasticity. At the neuromuscular junction (NMJ), the conserved miRNA let-7 is highly expressed, and when artificially mutated in the fly, the NMJ develops abnormally. The loss of let-7 results in a phenotype of abnormal flight, impaired motility, and infertility[161]. In the rodent, the neuron specific miR-134 is located near dendritic spines and regulates dendrite spine size, via

down-regulation of the Lim domain containing protein kinase (Limk1). When stimulated with brain derived neurotrophic factor, the inhibition of miR-134 is released and limK mRNA is upregulated, showing miRNA participation in activity dependant plasticity[162]. Interestingly, BDNF is also involved in a regulatory loop with miR-132 and methyl CpG-binding protein 2 (MeCP2)[163]. MeCP2 mutations are responsible for the pathology in Rett's syndrome, a neuro-developmental disorder with X-linked inheritance. Blockade of miR-132 in cultured rat neurons resulted in up-regulation of MeCP2 and BDNF, possibly forming a miRNA-regulated control mechanism. While further validation is necessary to assess the role of most miRNAs in the brain, these studies suggest the miRNA pathway is an important regulator of gene expression in the nervous system.

Summary of Thesis

The present thesis will describe methods to manipulate and study the RNAi pathway in neuronal tissues. In the second chapter, we used RNAi to block brain derived neurotrophic factor (BDNF) to determine if BDNF is a molecular mediator that facilitates cortical plasticity after sensory deprivation. In the latter part of the thesis, we describe a modified *in situ* hybridization (ISH) method that we developed to image high, medium, and low abundant miRNAs in neuronal tissues. Together, these findings studied the RNAi pathway as a candidate regulation mechanism in neurons, by which gene-expression is likely modified to support dynamic events including cortical plasticity.

Chapter II

Using virally delivered RNA interference molecules to influence cortical plasticity

Summary of Chapter II

During the course of adult cortical plasticity, a number of signal transduction mechanisms are brought into play. To study regulatory genes implicated in this process, we inhibited gene expression by harnessing the machinery of RNA interference (RNAi) pathway via small hairpin RNAs (shRNA) delivered by viral vectors. Using this technology we sought to influence plasticity of the mouse vibrissal barrel cortex. In this model system, chronic whisker plucking reliably leads to the expansion of the cortical representation of the adjacent non-deprived whiskers. The mechanism underlying this process involves changes in synaptic efficacy and sprouting of axon collaterals. Initial studies describing the molecular events leading to synaptogenesis and remapping have implicated a number of signal transduction pathways, including neurotrophins such as brain derived neurotrophic factor (BDNF). Though previous experiments have shown up-regulation of neurotrophins and their receptors in reorganized cortex, it is necessary to remove these factors to definitively prove their involvement in adult cortical plasticity. We therefore repressed neurotrophic gene expression in the mouse somatosensory cortex to determine if these trophic factors are essential for cortical remodeling after sensory deprivation. We blocked gene expression *in vivo* using a non-replicative adeno-associated virus bearing genes encoding shRNA constructs. The shRNA nucleotide sequences were designed to target and destroy selected neurotrophin messenger RNAs by triggering the RNAi pathway, resulting in a reduction of BDNF protein levels by up to 80% *in vivo*. This knockdown of BDNF expression effectively repressed functional cortical reorganization induced by chronic whisker plucking. Unexpectedly, when transducing the somatosensory cortex with a

viral vector carrying a control shRNA that does not target a gene in mouse, we saw no cortical reorganization after sensory deprivation. These results show a non-specific blockade of cortical plasticity occurs when using shRNAs in the brain. Our results suggest that manipulating gene expression via virally delivered shRNAs may have limited value for blocking expression of specific genes involved in cortical plasticity. However, the results suggest a potential role for RNA interference itself in regulating cortical plasticity.

Introduction

Injuries to the central nervous system (CNS) often result in debilitating sensory and motor function. Several neural systems demonstrate limited ability to partially reorganize damaged circuits after injury. Whereas cortical plasticity during a critical period in early postnatal life is a well established phenomenon, a growing body of evidence indicates that, for certain cortical connections, plasticity is maintained well into adulthood. Adult cortical reorganization was seen in the somatosensory cortex after digit amputation[1]. Similar cortical recovery also occurs in instances of partial deafness[2], incomplete spinal cord injury[164,165], and focal binocular retinal lesions[3-10]. Vibrissectomy sparing selected vibrissae in adult mice results in the enlargement of areas representing the intact whiskers[12]. Studies from these sensory systems suggest that the adult brain adapts to lesions by adjusting the cortical representation of sensory neurons. These receptive field shifts after injury were determined to be cortically mediated[4,5], by anatomical sprouting of horizontal connections in the adult, which is strongly correlated with, and likely underlies, these changes in receptive field representation[5,11].

During the course of adult cortical plasticity, a cascade of signal transduction molecules likely supports the shift in receptive field maps. Initial studies describing molecular events leading to synaptogenesis and remapping have implicated a number of signal transduction pathways, in including neurotrophins. The neurotrophin protein family regulates neuronal differentiation[13], axon sprouting[14,15] and synapse formation[16,17]. Brain derived neurotrophin (BDNF) promotes spontaneous synaptic plasticity[22,23] and expression levels were upregulated with increased neural activity[24-27]. A molecular association between neurotrophin expression and neural activity is a potential mechanism for preferentially strengthening active neural circuits[24,28]. Though previous experiments have shown up-regulation of neurotrophins and their receptors in reorganized cortex[35,166], attenuating neurotrophin expression is required to establish a direct link to adult cortical plasticity. We hypothesize that neurotrophins are the signaling molecules that mediate remapping of the barrel cortex after sensory deprivation. Therefore, we integrated molecular, physiologic and anatomical modalities to block the neurotrophin BDNF's gene expression to study injury induced cortical plasticity

To study cortical reorganization, we used the adeno-associated viral (AAV) vector gene delivery system to stably transduce transgenes in non-dividing neurons of the brain[36,37]. We combined this technology with RNA interference (RNAi), which utilizes the cell's native ability to regulate gene expression with specific small RNA triggers. By activating endogenous RNAi machinery, one can specifically block any transcript in the genome[78,79]. For stable RNAi induction, plasmid based small hairpin RNAs (shRNAs) are expressed using a polymerase III promoter[82] and shRNA can be inserted into viral vectors for long-term studies. Using this

approach, we explored using RNAi to study cortical reorganization.

Results

Silencing BDNF gene expression

To block BDNF using RNAi, we designed small hairpin RNAs (shRNA) to target and reduce all BDNF isoforms (BDNF variants 1-4) (**Figure 1**). We designed candidate shRNAs according to siRNA rules[167], then chemically synthesized and recombined these constructs into an expression vector upstream of a H1, RNA polymerase III promoter (**Figure 2**). To validate these oligonucleotide duplexes *in vitro*, we screened several BDNF shRNA plasmids and tested the knockdown potency using an artificial dual-luciferase reporter assay (**Figure 2**). We created a BDNF messenger RNA reporter vector by recombining the Renilla-Luciferase (RL) gene with BDNF-mRNA, generating a BDNF-reporter fusion product (BDFN-RL). Candidate shRNAs were co-transfected with the BDNF–RL reporter vector *in vitro* and reduced reporter activity by 50% (**Figure 2**). Effective BDNF shRNA constructs (shRNA BDNF #1 and #2) and a control luciferase shRNA (shRNA luc) were later packaged into adeno-associated viral (AAV) vectors for *in vivo* validation.

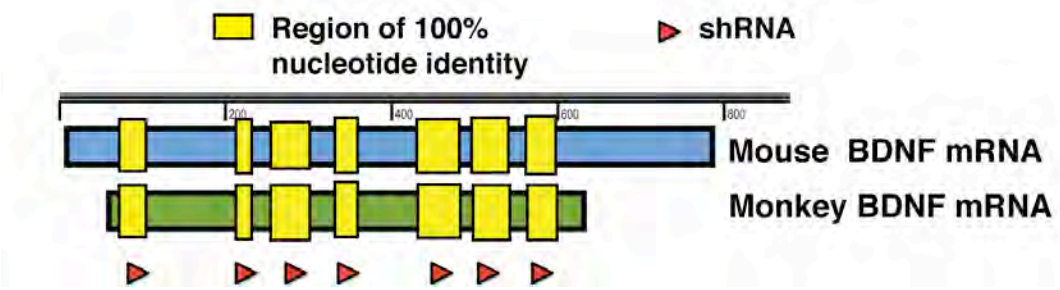

Figure 1: **Design of small hairpin RNAs targeting BDNF:** BDNF nucleotide sequences were aligned to identify regions of 100% identity in mouse, human, rat and monkey. A computer algorithm was employed to select shRNA candidates. Several shRNAs were designed to target the messenger RNA within these homologous regions (red arrows).

Packaging small hairpin RNAs shuttle vector into AAV

Cortical reorganization in the barrel cortex occurs over a period of weeks[12], therefore we chose a gene delivery system to persistently block BDNF protein levels for the long-term. We delivered shRNAs and other transgenes in the mouse brain using adeno-associated viral (AAV) vectors, which are ideal vehicles for delivering foreign genes to the brain[36,37]. The AAV constructs served dual purposes, labeling neurons with a fluorescent protein and/or delivering a RNA interfering molecule. To infect neurons in the barrel cortex more effectively, we pseudotyped AAV serotype-1 capsid and AAV2 replication (rep) gene (abbreviated; AAV2.1), which has enhanced gene expression in the brain[41]. AAV shuttle plasmids encoded eGFP or RFP (AAV2.1 eGFP or AAV2.1 RFP) for neuron labeling. Other shuttle plasmids contained an shRNA cassette (shRNA BDNF #1, shRNA BDNF #2, or shRNA luc) downstream of a separate RFP expression cassette. AAV shuttle plasmids were packaged into AAV2.1 pseudotype, with a final viral titer

yield of at least $1x10^{13}$ viral particles/mL (**Figure 2 and 3**).

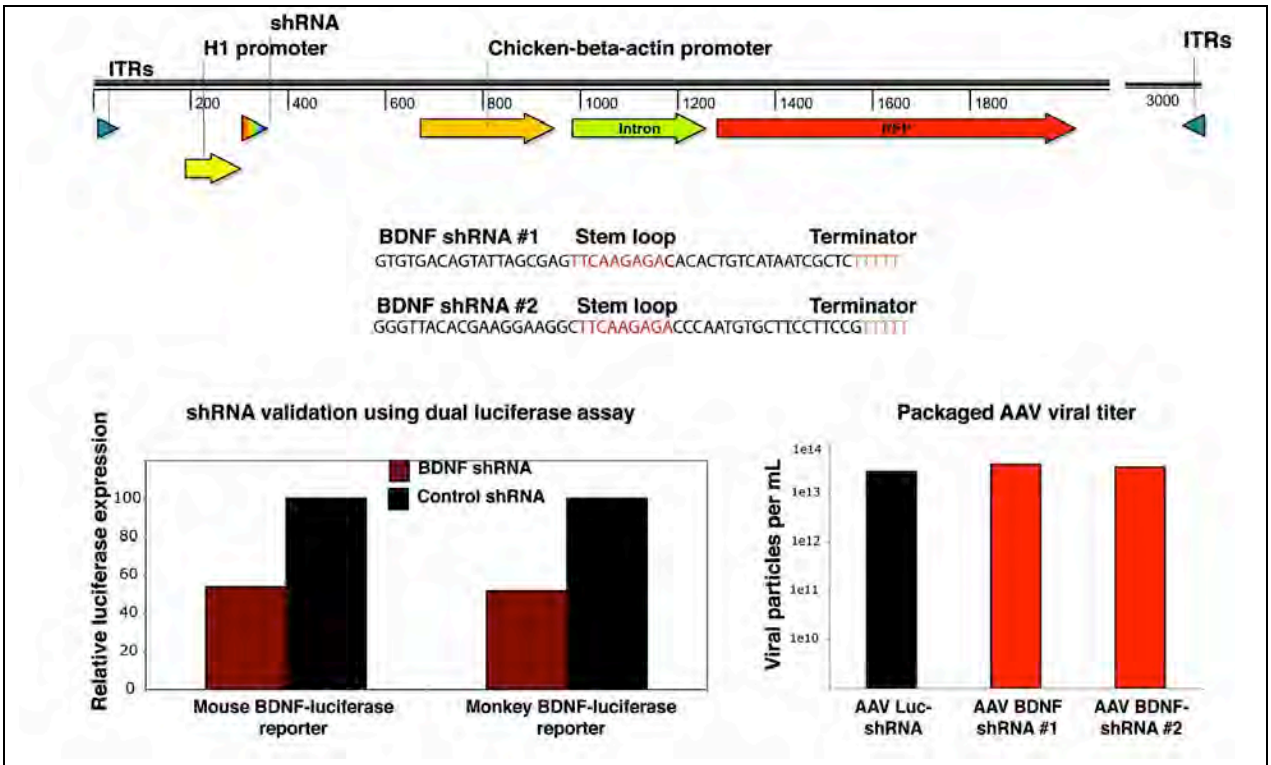

Figure 2: small hairpin RNAs reduce mouse BDNF *in vitro*: (top panel) Schematic diagram of a custom designed AAV vector expressing a small hairpin RNA. AAV shuttle vector silences gene expression using an shRNA cassette driven by an RNA polymerase III H1 promoter and expresses a fluorescent protein controlled by a hybrid CMV-chicken-beta-actin (CBA) promoter. (**Middle**) Representation of two BDNF shRNAs cassette sequences including the stem loop structure and terminator sequence. (**Bottom)** Results from *in vitro* screening of BDNF shRNAs by a dual luciferase reporter assay showed the shuttle vector encoding a BDNF specific-shRNA reduced luciferase activity in the mouse BDNF-RL reporter by approximately 45-50%.

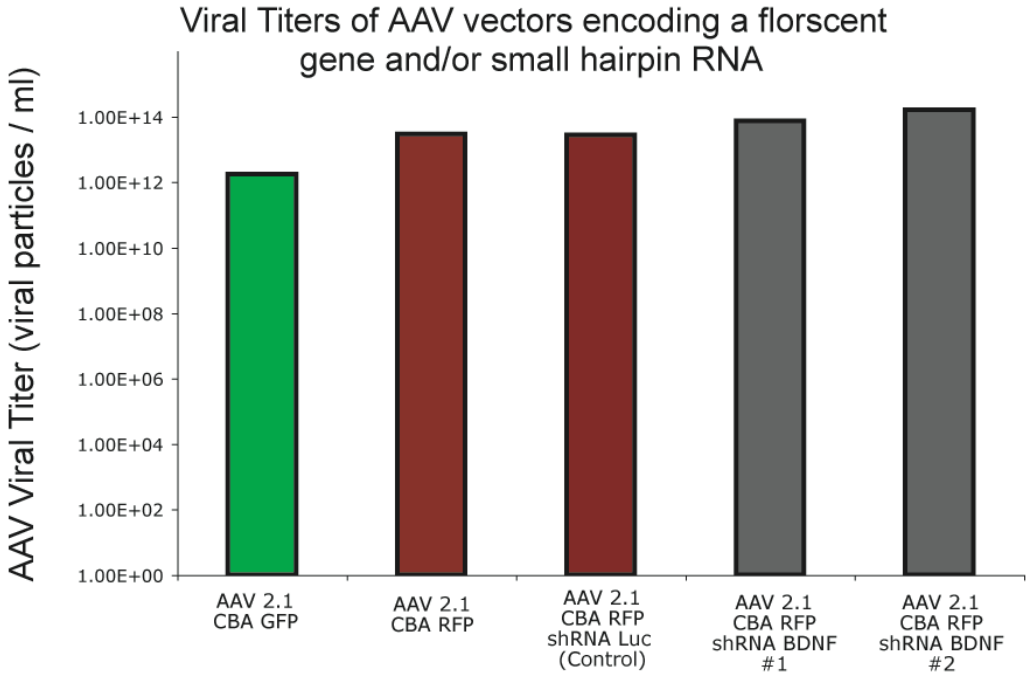

Figure 3: AAV viral vectors packaged at high titers: Graph illustrating the viral titer of AAV vectors expressing eGFP, RFP, and shRNAs vectors targeting luciferase as a control (AAV 2.1 shRNA luc), and two different shRNAs targeting mouse BDNF (AAV 2.1 shRNA BDNF #1 and #2) with a titer measured in viral particles/mL.

BDNF-specific shRNAs delivered via AAV reduced protein expression by 80% *in vivo*.

To directly test the potency of these BDNF RNAi constructs *in vivo*, we stereotaxically injected the AAV 2.1 shRNA virus into the mouse hippocampus, which is rich in BDNF expression. On one side of the hippocampus, we delivered a bolus of AAV2.1 shRNA BDNF (shRNA BDNF #1 or #2). In the contralateral hemisphere and at the same depth, we injected a control (AAV2.1 shRNA Luc or saline). Six week post-surgery, animals were sacrificed and the hippocampus was

immediately dissected and tissues were isolated. The samples were homogenized and the total protein lysates were measured and then analyzed by western blotting. After transfer, we probed the membrane with an anti-BDNF (Sigma) or anti-beta-actin (Chemicon) antibody, and immunoreactive bands were quantified by densitometry (**Figure 4**). shRNAs targeting BDNF demonstrated a potent blockade of BDNF protein in the adult mouse hippocampus, reducing BDNF protein levels in this region by 80% (AAV 2.1 BDNF shRNA #1) and 65% (AAV 2.1 BDNF-shRNA #2), respectively. These data support that the RNAi viral vectors effectively inhibit BDNF protein levels *in vivo*.

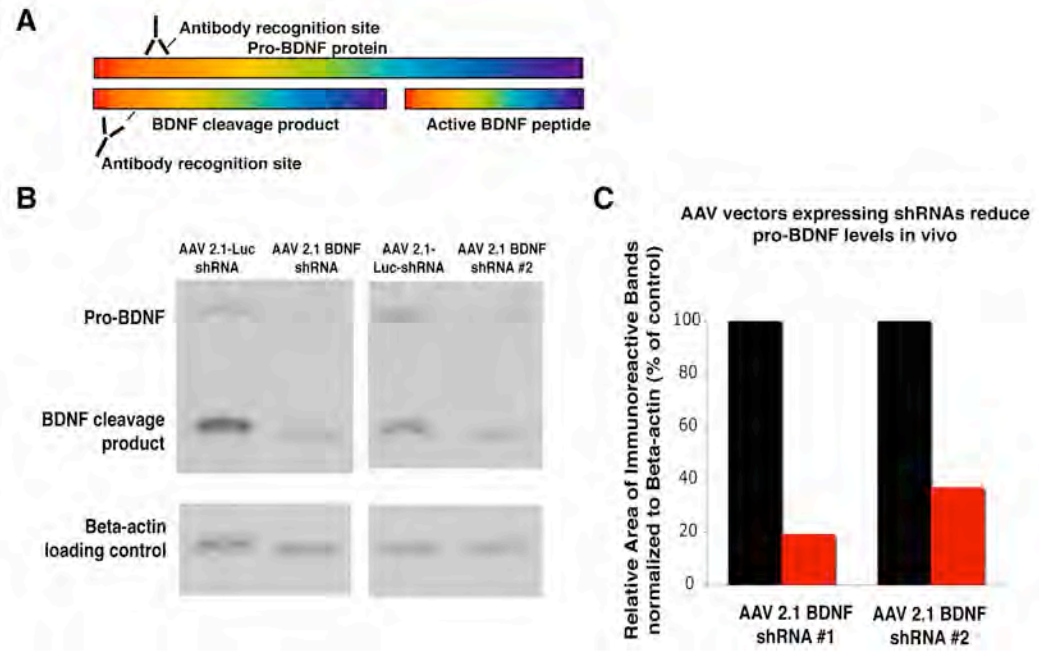

Figure 4: BDNF shRNA delivered substantially inhibit endogenous BDNF protein levels *in vivo*: (**a**) Image detailing Pro-BDNF processing. The shRNAs targeting BDNF block the mRNA transcript, reducing the pro-BDNF protein and the mature form and the BDNF cleavage product. BDNF knockdown was validated using an anti-BDNF antibody (Sigma) that detected the pro-BDNF peptide and the BDNF cleavage product. **(b)** Western blotting image demonstrates pro-BDNF and the BDNF cleavage product protein levels were reduced in the mouse hippocampus after transduction with AAV vectors encoding two different small hairpin RNAs targeting BDNF. Beta-actin protein levels were also analyzed (**b, bottom image**). (**c**) Immunoreactive bands were quantified (ImageJ) and reduction in BDNF protein levels graphically represented. Viral vectors encoding BDNF shRNA #1 reduced endogenous BDNF protein level in the mouse hippocampus by 80% compared to the control, and AAV delivering BDNF shRNA #2 reduced BDNF protein levels 65%. BDNF bands were normalized to beta-actin controls.

shRNAs delivered by viral vectors block cortical plasticity *in vivo*.

We sought to alter plasticity in the mouse vibrissa barrel cortex by blocking neurotrophin gene expression with AAV vectors carrying RNAi constructs. First, we mapped the cortical representation of each vibrissa by mechanically stimulating the whisker and then recorded the location of the corresponding receptive field using electrophysiology (**Figure 5a)**. Following cortical mapping, we transduced viral vectors (AAV2.1 RFP; AAV2.1 shRNA BDNF #1; AAV shRNA BDNF #2; AAV shRNA luc; or saline), in and immediately surrounding the superficial layer of the cortex representing the vibrissa positioned in row C (**Figure 5b**). One month after surgery, we remapped the barrel cortex of AAV injected animals and observed no changes in the barrel map.

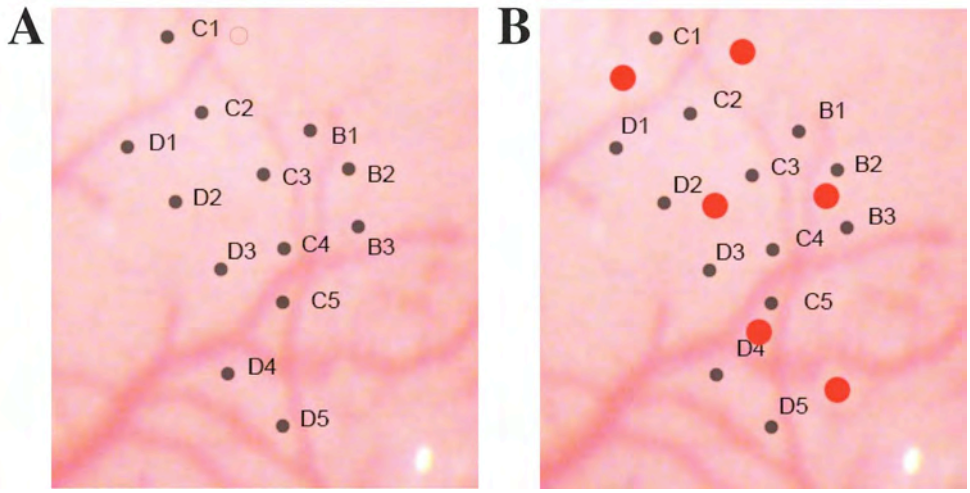

Figure 5: Electrophysiology guided injection of viral vectors into mouse somatosensory cortex: (a) Photograph of mouse somatosensory cortex and vasculature structures. The vibrissa receptive fields (RF) were mapped in the mouse barrel cortex using electrophysiology following mechanical stimulation of the mouse vibrissa. Whiskers in rows B, C, and D were mechanically manipulated and the receptive field location recorded, then plotted on the photograph (location of the RF marked with black dot; the letter and number describe the vibrissa stimulated). (**b**) Photograph of the somatosensory cortex demonstrating the location of AAV vector injections at selected sites (red dot) in and surrounding RF representing vibrissa stimulated in row C.

To induce cortical remodeling in the barrel cortex, we removed vibrissa from row D and E continuously for 2 weeks. Following sensory deprivation, we remapped the location of the receptive fields (RF) in the barrel cortex. In saline (n=3) and AAV2.1 RFP (n=3) injected animals, the cortical representation of the intact vibrissa in row C expanded into regions that

were sensory deprived (**Figure 6a-b**). Next, we examined the influence of shRNAs that target and destroy BDNF. For AAV2.1 shRNA BDNF #1 injected animals (n=3), the cortical map did not reorganize after injury, as the somatosensory cortex maintained the original RF map prior to sensory deprivation. We tested a second shRNA targeting a different region of the mouse BDNF gene (AAV shRNA BDNF #2; n=3) and the RF map in the somatosensory cortex did not reorganize (**Figure 6 c-d**). We also examined the effect of a control shRNA that does not target a gene expressed in the brain (AAV2.1 shRNA luc), which unexpectedly showed no shift in the cortical map after chronic vibrissa removal (**Figure 6e**). Interestingly, animals transduced in the barrel cortex with any of the described shRNAs failed to show cortical reorganization after whisker removal. Since animals injected with saline or AAV 2.1 RFP consistently reorganized after injury, neither the injection procedure nor the viral vector itself were responsible for blocking cortical plasticity *in vivo*. In these experiments, the presence of a small hairpin RNA was sufficient to inhibit adult cortical plasticity after injury.

Figure 6: AAV delivered shRNAs block cortical plasticity *in vivo*: (a-e) Photographs showing the RF map of the somatosensory cortex following sensory loss. **(a)** RF map after injection of **(a)** saline or **(b)** AAV2.1 RFP showed after persistent whisker trimming. RF representing intact vibrissa in row C expanded into the cortical areas previously represented by vibrissa plucked rows in rows D and E. (**c-e**) RF map in the mouse barrel cortex following transduction of (**c**) AAV2.1 shRNA BDNF #1, (**d**) AAV2.1 shRNA BDNF #2, or (**e**) AAV2.1 shRNA luc showed no cortical reorganization following continuous sensory deprivation.

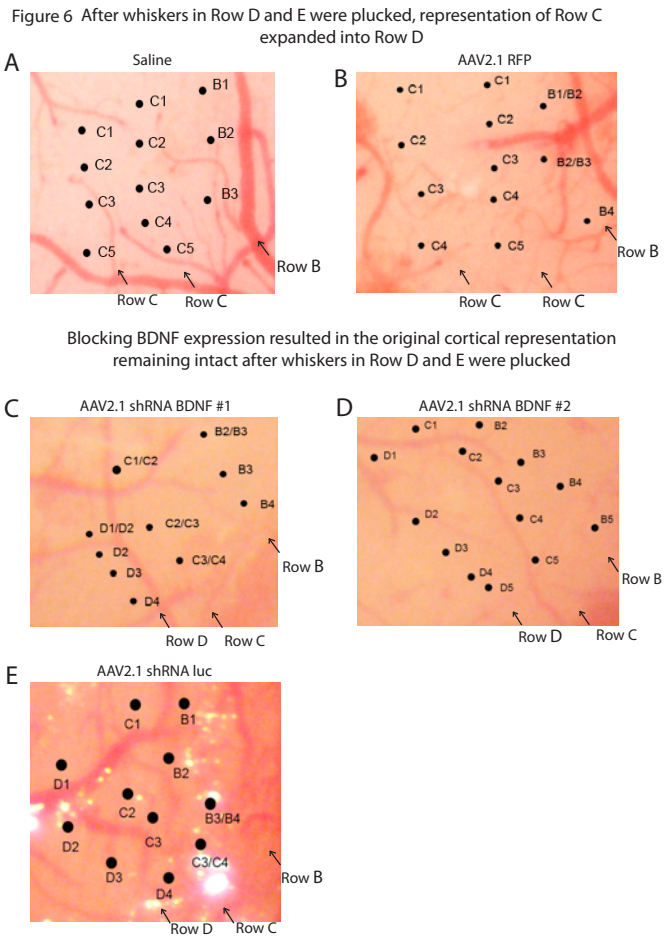

Evaluating potential toxicity associated with AAV delivered shRNAs

A recent study reported sustained high-level shRNA expression caused a lethal phenotype in adult mice[168]. The cause of the mortality was associated with saturation of the nuclear karyopherin exportin-5, a shuttling protein in microRNA pathway, which processes shRNAs and

miRNAs. In our experiments, cell morphology and RF maps remained normal after 5 months post injection for animals transduced with AAV shRNA viruses (**Figure 7**). In addition, to determine if an AAV delivered shRNA reduced microRNA levels in the brain, we transduced the mouse hippocampus with AAV2.1 shRNA luc and on the contralateral side we introduced a non-shRNA containing virus (AAV2.1 RFP). Next, we determined the level of the highly abundant and neuron-specific miR-124 present in AAV2.1 luc and compared this with a non-shRNA carrying virus (AAV2.1 RFP). By using quantitative northern blotting, we determined that miR-124 amounts in AAV shRNA luc injected animals were equivalent to RFP injected controls (**Figure 7**). We also examined levels of miR-124 expressing via *in situ* hybridization and observed that miR-124 expression in AAV2.1 shRNA luc injected animals expressed miR-124 at similar intensity to samples injected with the AAV2.1 RFP alone (**Figure 7**). Using these methods, brain tissue injected with viral vectors carrying shRNAs showed no gross reduction of the most highly abundant miRNA expressed in the brain, when compared to the control.

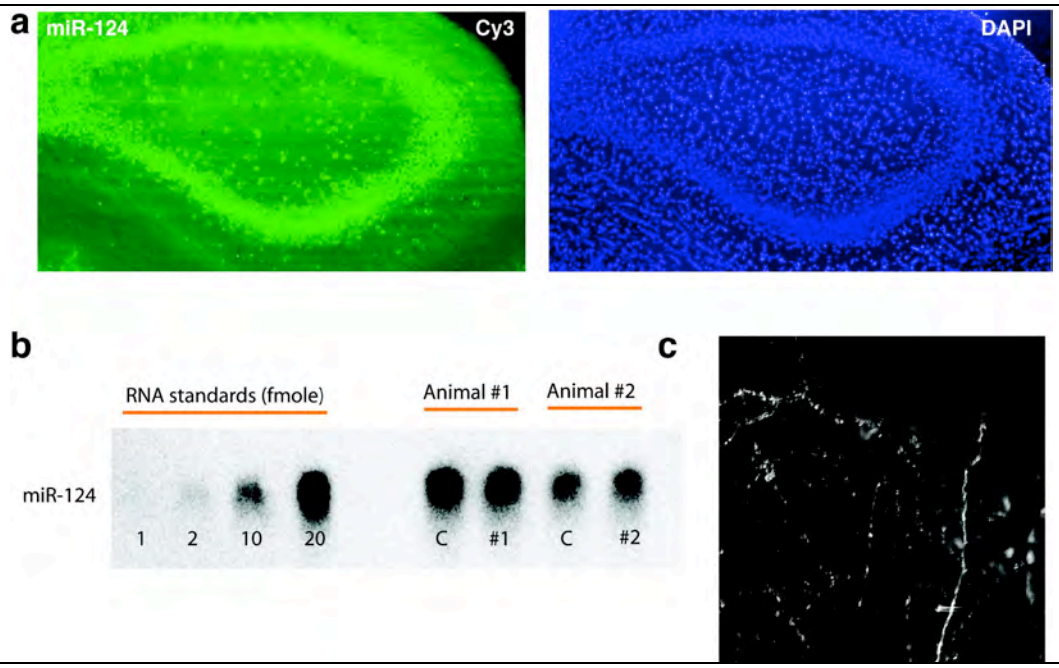

Figure 7: AAV viral vectors encoding shRNAs are not toxic to neurons in vivo. (a) Photomicrographs of mouse brain hippocampus show miR–124 expression detected by in situ hybridization in regions injected with AAV shRNA targeting luciferase. **(b)** Quantitative northern blotting image shows miR–124 levels from brain regions injected with adeno–associated virus expressing RFP (marked; "C") or an AAV virus expressing an shRNA cassette targeting luciferase (marked #1) or an shRNA targeting BDNF (marked #2). **(c)** Two–photon microscopy images of the mouse cerebral cortex area showing expression of an AAV virus expressing a shRNA targeting luciferase with a RFP also encoded in the virus. Image captured 5 months after injection.

Discussion:

Adeno-associated viral vectors employed to deliver small RNAs hold the potential to rapidly block gene expression for long-term *in vivo* studies. Yet, the present data supports that this set of virally delivered shRNAs causes non-specific blockade of cortical recovery after injury. The

phenotype observed in the control shRNA may be due to off-target binding and silencing of an unknown mRNA (other than BDNF), which participates in cortical plasticity. However, this is unlikely since the shRNA does not bind other gene targets with high affinity, according to computational programs that compared the shRNA to the mouse genome.

Alternatively, the effects of sustained shRNA expression in adult mice consistently resulted in the lack of cortical plasticity after shRNA transduction, possibly due to introducing sustained high-levels of shRNA into the neurons. These effects may be due to shRNAs competing with miRNAs for the RNAi machaniery and preventing miRNAs from regulating their gene targets. Moreover, the overexpression of an shRNA may saturate the RNA induced silencing complex (RISC) and exclude endogenous miRNAs from performing their natural function of controlling gene expression. While the specific small RNA that is ultimately involved in dynamically altering the local circuitry is unknown. The results suggest the endogenous RNAi machinery itself may regulate cortical plasticity.

Follow up studies

Determining the relative levels of small RNAs

The regulatory potency of small RNAs depends on relative abundance and the spatio-temporal expression patterning of miRNAs in a given tissue. To determine the relative levels of shRNAs produced, we will profile the small RNA content (both miRNA and shRNA) in AAV shRNA infected tissues and non-shRNA transduced samples. We will characterize the siRNA produced and determine the relative amount of the siRNA verses the endogenous molecular substrate for the RNA interference (RNAi) pathway, the microRNAs (miRNA) fraction[169]. We will infect

brain tissue with an shRNA that does not target any gene expressed in the brain (AAV2.1 luc) and the control samples will be transduced with a non-shRNA containing virus (AAV2.1 RFP). We will then isolate the transduced tissues; prepare RNA from infected areas. miRNA and siRNA cloning will be performed as previously described[170], the cDNA library will be sequenced using 454 sequencing, and miRNA sequences annotated as described[89]. We will compare the clone frequencies of the virally delivered siRNAs to endogenous miRNAs clone frequency. Our expected outcome is that the level of siRNA is equal or greater than the relative amount of the highly abundant miRNAs. For the control tissues injected with AAV RFP, we anticipate that the miRNA profile will show no shifts in miRNA relative abundance when compared to small RNA profiles from naive mice.

Methods:

AAV expression vectors

For recombinant AAV shuttle vectors, the fluorescent protein (GFP or RFP) was controlled by a hybrid CMV-chicken-beta-actin (CBA) promoter. Downstream of this cassette, we recombined a RNA polymerase III, H1 promoter to express an shRNA duplex. The vector was designed for rapid directional insertion of chemically synthesized shRNAs with EcoR1 and Xho1 restriction sites. We generated separate shuttle vectors encoding shRNA BDNF #1, shRNA BDNF #2, and shRNA that targeted a luciferase sequence as a control (shRNA luc; which does not target a gene expressed in the mouse brain). To target BDNF variants (BDNF mRNA variants 1-4), we identified regions of 100% nucleotide identity (Megalign, Lasergene), and selected candidate small hairpin RNAs to target homologous regions. Candidate shRNAs were selected according

to predefined "siRNA rules" using a computer algorithm[167], then chemically synthesized and recombined into our expression vector with a RNA polymerase III termination sequence encoding a six thymidine nucleotides terminator sequence.

shRNA Validation

The shRNAs constructs were prevalidated using an *in vitro* dual-luciferase assay. To assess the degree of knockdown, we recombined a mouse-BDNF-messenger-RNA with a Renilla-Luciferase (RL) gene, creating an mRNA fusion product (BDFN-RL) that is separated by a translational stop codon. To test for shRNA potency, the shRNA plasmid was co-transfected with the reporter vector *in vitro*. Briefly, a BDNF-RL was cloned into psiCHECK-2 and plasmids were cotransfected into HEK293 cells according to manufacturer's protocol. Effective shRNAs targeted the BDNF-reporter mRNA and reduced luciferase activity as measured by a luminometer. Two shRNA duplexes, "BDNF #1" and "BDNF #2" resulted in an *in vitro* knockdown of more than 50% and were chosen for viral packaging and *in vivo* infusion experiments. As control shRNA duplex, a shRNA targeting GL2 firefly luciferase (luc) was used.

AAV vector packaging

Validated AAV shRNA plasmids were packaged into AAV2.1 pseudotype capsids. AAV *shuttle vector*, *rep*/*cap* and helper plasmids were cloned and isolated using a polyethylene glycol (PEG) plasmid purification procedure (Molecular Cloning). The concentration of the purified DNA was determined, and then the integrity of *cis* vector ITR was analyzed by *Sma*I restriction digest. Recombinant AAV vectors were produced by a standard calcium phosphate transfection method

(Molecular Cloning) in HEK 293T cells (ATCC), with the AAV shuttle plasmids, transpackaging (serotype 2.1), and Ad helper (delta F6). The plasmid ratio for the *shuttle vector*, *rep*/*cap* and helper plasmids was 1:2:2, respectively. Viral particles were harvested from cells after a series of freezing and thawing, followed by brief sonication. AAV vectors were purified using a High-trap ion exchange column (Amersham). Packaged virus was concentrated and dialyzed using size filtration columns (Millipore). Vector titers were determined by real-time PCR and the yield was between 1 and 3 x 10^{13} DNase-resistant particles per ml. Vector infectivity was assessed by transduction in a U87 glioblastoma cell line.

Receptive field mapping

The Institutional Animal Care and Use Committee at the Rockefeller University approved all animal protocols. The receptive fields (RF) of the mouse vibrissa were mapped in the barrel cortex via electrophysiology. Briefly, a small craniotomy was performed in anesthesitized, animals directly above and surrounding the mouse barrel cortex (the center of the craniotomy was approximately –2.00 mm posterior and +/– 4.00 mm lateral, relative to the cranial landmark bregma). A picture of the cortical vasculature taken and insulated tungsten microelectrode was placed based on vasculature landmarks. Penetrations were made perpendicular to the cortical surface and restricted to the superficial layers. Multiple recordings were made in each barrel. RFs were mapped according to “minimum response” characteristics after mechanical stimulation of individual vibrissa. Following RF mapping, the bone was replaced, skin sutured, and animal resuscitated. Mice were housed in a controlled temperature environment on a 12-h light/dark cycle.

AAV injection in the barrel cortex

The location of vibrissa receptive fields in the barrel cortex were identified as described above. Viral vectors were pressure injected through glass micropipettes in the superficial layer of the cortex immediately in, and surrounding the cortical areas representing the vibrissa row C. To deliver enough viruses to infect the desired region, we injected AAV2.1 shRNA, AAV2.1 GFP, or AAV2.1 RFP viruses via a series of injections separated from each other by approximately 1 mm. To avoid damaging cortical tissue, small volumes of the AAV vector were delivered at each site (100 nl injected per site; rate 10 nl/min; viral titer of 1 x 10^{13} particles/ml).

AAV injection in the hippocampus

AAV vectors were directly injected into the adult mouse hippocampus area 3A. A craniotomy was burrowed directly above the hippocampus, using stereotaxic surgical coordinates (posterior 2.30 mm and 2.25 mm lateral from a cranial landmark, bregma, described in Paxinos Brain Atlas). A spear–tipped glass pipette penetrated below the surface of the cortex (1.9 mm). We delivered 100 nl of AAV (rate of 10 nl/min, viral titer, 1 x 10^{13} viral particles/ml) expressing an shRNA targeting BDNF (AAV2.1-BDNF-shRNA #1 or AAV 2.1-BDNF-shRNA-#2; n=3) to the hippocampus area 3A. On the opposite side and at the same depth, a control virus expressing an AAV 2.1-RFP (n=3) or saline alone (n=3) was injected under identical conditions. Animals were sutured, resuscitated and placed in Rockefeller University animal housing facility following survival surgery.

Brain tissue collection

Animals were sedated and sacrificed in accordance with NIH Animal Welfare guidelines using ketamine and xylazine cocktail before organ perfusion with 50 ml of Tris-HCl buffered Saline (TBS) containing 50 mM Tris-HCl, 150 mM NaC1 and the pH adjusted to 7.4. The hippocampus was dissected and bisected at the midline, and then isolated and frozen in liquid nitrogen for Northern blotting or Western blotting analysis.

Western blotting analysis

Tissue samples were lysed in lysis buffer (20 mM Tris, pH 8.0/1% Triton X-100/150 mM NaCl/protein and phosphatase inhibitors; Sigma). Total protein lysate was cleared of debris by centrifugation; equal amounts of protein were measured (30 μg of total protein) and were denatured in a sample buffer. Samples were loaded onto a NuPAGE 10% (Bistris [bis(2-hydroxyethyl)amino]tris(hydroxymethyl)methane) gel (Invitrogen) and protein separated by electrophoresis. After transfer, we probed the membrane with an anti-BDNF (Sigma) or anti-beta-actin (Chemicon) antibody, followed by secondary antibodies and enhanced chemiluminescent detection (Amersham Pharmacia Biosciences). Immunoreactive bands were quantified and analyzed by densitometry (Image J). BDNF immunoreactive bands were normalized to the loading control beta-actin.

Northern blotting

Northern blotting was performed as described[89] using Hybond-N+ membrane (Amersham GE healthcare), and the hybridization and wash steps were performed at 50°C. The oligodeoxynucleotide probes were 5'-labelled with [γ-^{32}P] ATP. The probe for miR-124 was 5'

TTGGCATTCACCGCGTGCCTTA. To control for loading of the gel, 5S rRNA was detected by ethidium bromide staining of the polyacrylamide gel prior to transfer. Probe samples were recorded by phosphoimaging and quantified. Northern blotting images were quantitated using ImageJ software[171].

microRNA in situ hybridization

For *in situ* hybridization experiments, mice were sedated and immediately perfused with TBS, and then 4% paraformaldehyde (PFA). Tissues were collected, immersed in 4% PFA for 24 h, then placed in 0.5 M sucrose for 48 h. Tissues were mounted in Tissue-Tek OCT Compound, frozen in a dry-ice/ethanol bath in a Cryomold (Tissue-Tek), immediately serial sectioned at 10 μm with a cryostat (Leica) and mounted on SuperFrost Plus glass slides (Thermo Fisher Scientific). Mouse brain tissue was fixed with formaldehyde–EDC as previously described[147]. After fixation the samples were exposed to 4 pmol of a locked nucleic acid probe complementary to miR-124. The probe was diluted in a formamide-containing solution and hybridized overnight at a temperature 20ºC below the experimentally determined melting temperature[147]. Then tissue sections were subsequently exposed to stringency washes and antibody staining. Finally, miRNA expression was detected using a tyramide Cy3 non-isotopic detection system, then washed in TBS and prepared for microscopy analysis. Images were captured on an Olympus BX50 microscope equipped with a DP70 camera and Olympus DP controller software.

Small RNA cloning protocol

Small RNAs were isolated by gel electrophoresis from total RNA or by immunoprecipitation using anti-Argonaute monoclonal antibodies. First, a chemically preadenylated 3' adapter

oligonucleotide is ligated to the small RNAs. The ligation products are gel-purified and the 5' adapter is ligated with regular RNA ligase in the presence of ATP. The 3' adapter was blocked with an aminolinker at its 3' end. The ligation product is again gel-purified, then reverse transcribed, PCR amplified, concatamerized and sequenced.

Chapter III

In situ hybridization method to detect microRNAs in mammalian tissues

Summary, Chapter III

MicroRNAs (miRNAs) are small regulatory RNAs with many biological functions and disease associations. We showed that *in situ* hybridization (ISH) using conventional formaldehyde fixation results in significant miRNA loss from mouse tissue sections, which can be prevented by fixation with 1–ethyl–3–(3–dimethylaminopropyl) carbodiimide (EDC) that irreversibly immobilizes the miRNA at its 5' phosphate. We determined optimal hybridization parameters for 130 LNA probes by recording nucleic acid melting temperature under ISH conditions.

Introduction:

Association studies are rapidly linking miRNAs[44] with cancer and neurological disorders[172]. miRNAs have specific expression and function in specialized cell types[89], emphasizing the need to define cell–type–specific miRNA expression patterns. For pathologists, the most common method for visualizing gene expression in specific cell types is *in situ* hybridization (ISH). In our laboratory, conventional ISH worked for highly abundant miRNAs, however examining less abundantly expressed miRNAs often yielded inconsistent or negative results. A review of the literature indicates that zebrafish whole–mount ISH were robust[142], whereas ISH in *D. melanogaster* embryos were mostly unsuccessful[92]. In tissue sections, several studies set the foundation for establishing miRNA ISH[95,144,173-175], and were used to support association to disease[176,177], or defined expression patterns in multiple cell types present in the brain[103] and eye[146]. The technical difficulties in miRNA ISH also led to development of transgenic[138] or cell sorting methods[89] that monitor cell–type–specific miRNA expression.

To better understand the technical challenges associated with miRNA ISH, we investigated the importance of miRNA fixation and probe hybridization. For fixation of proteins and nucleic acids in tissues, a solution containing 3.7% formaldehyde (10% formalin) is commonly used[178]. Formaldehyde crosslinks are reverted by incubation at elevated temperature and this process is facilitated by proteinase K treatment[179]. Reversal of the formaldehyde–based nucleic acid base modifications is also necessary for probe hybridization, but it creates the problem of miRNA release and diffusion out of the tissue sections. Therefore, we examined the extent of miRNA escape from tissue during ISH. We conducted a mock ISH for conventionally fixed brain sections, isolated RNA from the tissue sections and the ISH buffer, and probed both fractions for the highly expressed neuronal miR–124 by Northern blotting. At hybridization temperatures above 40ºC, at least 50% of miR–124 initially present in the tissue section accumulated in the buffer as early as 1 h (**Figure 1a–c**). At 4ºC, the hybridization buffer showed no signal for miR–124 (**Figure 1d**), which would suggest that RNA–protein crosslinks were still intact at lower temperatures.

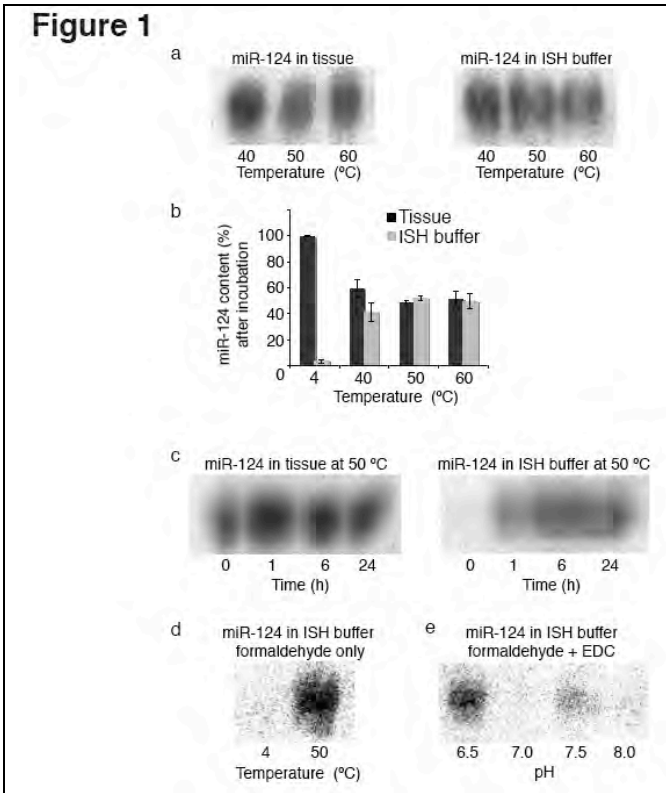

Figure 1: miRNAs retained in formaldehyde + EDC fixed tissues. (**a**) Northern blotting analysis shows escape of miR–124 from formaldehyde–fixed tissues into ISH buffer after 24h incubation at temperatures of 40 ºC and higher. (**b**) Quantification of Northern blots show approx. 50% of miR–124 were present in the hybridization buffer after overnight incubation, $P < 0.05$, $n = 3$. (**c**) Time course of hybridization at 50 ºC shows miR–124 accumulates in ISH buffer after 1 h. (**d**) At 4 ºC, miR–124 was not detectable in the hybridization buffer, which would suggest that RNA–protein crosslinks were intact at lower temperatures. (**e**) Samples fixed with formaldehyde + EDC show negligible amounts of miR–124 in ISH buffer at pH 7.0 and 8.0.

Results

To prevent the loss of miRNAs, we added an additional miRNA fixation step taking advantage of the miRNA 5' phosphate end[44], which does not react with fomaldehyde[178]. The water–soluble 1–ethyl–3–(3–dimethylaminopropyl) carbodiimide, EDC, reacts with phosphate and condenses it with amino groups in the protein matrix to form stable linkages[180,181]. When

formaldehyde–fixed specimens were additionally treated with EDC, miR–124 no longer escaped from the tissue sections, and only trace amounts of miR–124 were detected in the ISH buffer (Figure 1e). EDC treatment alone, without prior formaldehyde fixation insufficiently retained miRNAs in tissues (data not shown).

The second critical factor affecting ISH is probe hybridization. Probes that bind to miRNAs with high thermodynamic stability such as DNA probes containing locked nucleic acid (LNA) residues are well suited for miRNA ISH[142,182]. The melting of LNA/miRNA duplexes can be observed experimentally by UV spectrophotometry[182]. Thermodynamic analysis of LNA–modified deoxynucleotide duplexes led to models that predict their melting temperatures (T_M) for any LNA/RNA pair. Unfortunately the T_Ms cannot be predicted accurately for ISH, as the programs do not consider the presence of formamide denaturant. To derive optimal hybridization conditions, nucleic acid melting studies were conducted and the melting profiles of 130 miRNA/LNA probe pairs were measured (**Supplementary Table 1, appendix**). With these data, we provide a correction factor for these programs, by manipulating the salt parameter of LNA/RNA T_M prediction programs, and obtained useful starting points for estimating hybridization temperature in formamide–containing ISH buffer (**Supplementary Table 1, appendix**). Based on miRNAs expressed with a clone frequency of at least 0.04% based on small RNA library sequencing from 5 regions of the mouse brain (**Supplementary Table 2, appendix**), we generated an LNA probe set.

To determine the range of the ISH sensitivity, we conducted ISH for miRNAs identified at varying frequencies from small RNA cloning libraries in mouse brain; miR–9, 9.3%; miR–124,

8.8%; miR–26a, 3.3%; miR–26b, 0.25%; miR–370, 0.14%; miR–130a, 0.12%; and miR–410, 0.07% (**Supplementary Table 3, appendix**). Tissue sections were fixed with formaldehyde/EDC and then ISH performed (**Methods**). We determined the effect of formaldehyde/EDC versus formaldehyde fixation alone by ISH of the most abundant miR–124 and the 73–fold less abundant miR–130a. ISH images show that signal for miR–124 were improved moderately, but miR–130a signals were only detectable in formaldehyde/EDC–fixed samples (**Figure 2**). Since the abundant miR–124 presumably retained enough miRNA to nearly saturate the signal the improvement remained modest, but for lowly expressed miRNAs, loss by diffusion hindered its detection in formaldehyde alone samples. miR–124 is mostly detected in neuronal cells present in different regions of the brain (**Figure 3a–d** and **Figure 4**) and predominately localized in the cytoplasm, while the cell nuclei were excluded. Another highly expressed miRNA in brain, miR–9, also preferentially localizes in neurons, and is particularly enriched in the Purkinje cell layer (**Figure 3e**). We also observed robust ISH signal for the less abundant miRNAs tested (**Figure 3f–i**), with unique miRNA distributions. Interestingly, miR–26a and miR–26b, which differ by 2 nucleotides (C11U, C21U) and originate from different clusters, showed differential expression patterns in the mouse cerebellum (**Figure 3h,i**). The absolute signal intensities for the miRNAs tested were not directly correlated with the abundance of miRNAs and were likely attributed to differences in kinetics of probe hybridization. Nevertheless, for a given probe, the signal intensities accurately reflected miRNA differential expression.

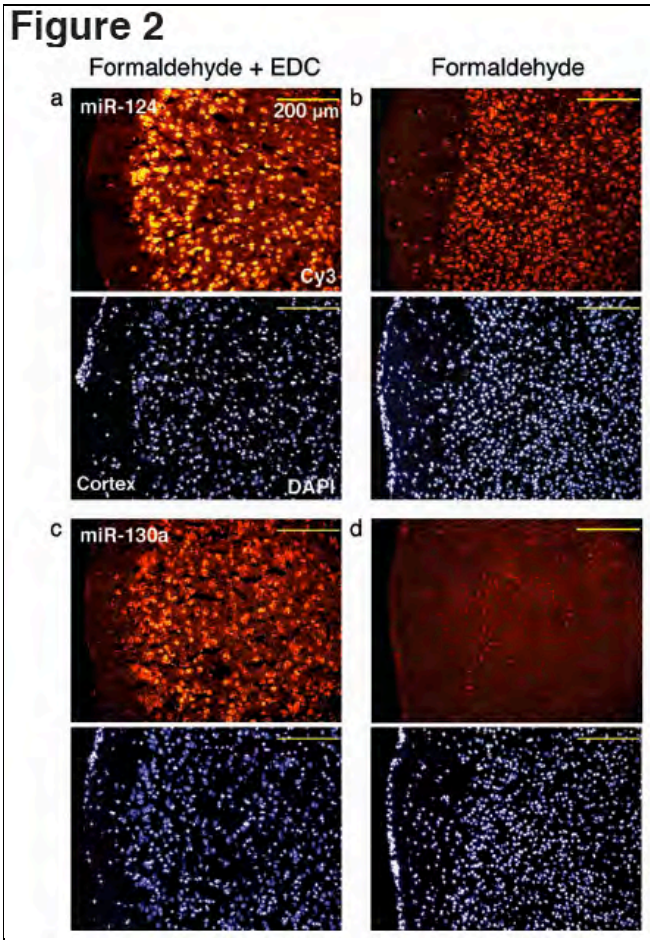

Figure 2: Comparison of formaldehyde + EDC and conventional formaldehyde fixation for detection of a high and low abundance miRNA in mouse brain by ISH. (**a–d**) Fluorescence microscopy images of ISH using mouse brain tissue sections fixed with formaldehyde + EDC (**left**) or conventional formaldehyde alone (**right**), captured with identical camera settings and exposure times. Highly abundant nervous system specific miR–124 (clone count frequency 8.8%) showedformaldehyde + EDC fixation moderately improved signal intensity (**a**), compared to formaldehyde fixation alone (**b**). (**c–d**) Detection of lower expressed miR–130a (clone count frequency 0.12%) using formaldehyde + EDC (**c**). Conventional formalin fixed samples showed no signal (**d**). The digoxigenin–labeled LNA– modified DNA probe was hybridized to a specific miRNA and the signal was amplified using the tyramide–Cy3 (orange) detection system. Cell nuclei were counterstained with DAPI (blue; **bottom panel**). Scale bars were 200 µm

Figure 3

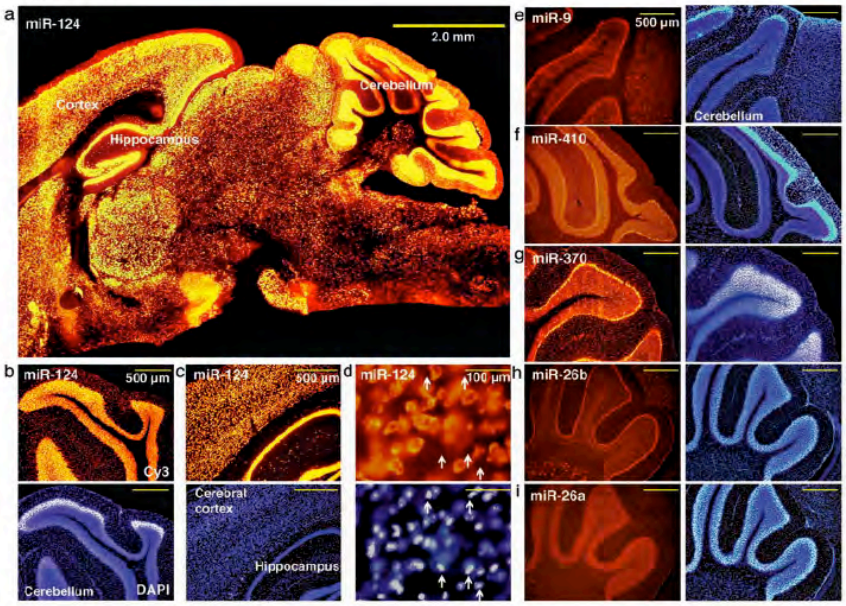

Figure 3: Visualization of miRNAs expressed at different levels in the mouse brain. (a) Low magnification images of nervous system specific miR–124 (orange) shows broad expression in neurons. (**b–c**) High magnification images of miR–124 demonstrate ubiquitous expression in the neurons of the cerebellum (top, orange), (**b**) cerebral cortex and hippocampus (**c**). (**d**) Higher magnification images show that miR–124 signals are not present in all cells, marked with arrows. (**e**) Fluorescence images of mouse brain sections probed for highly expressed miR–9 (Cy3, red) localized in Purkinje cells of the cerebellum. (**f,g**) Image depicting miR–410 (f) and miR–370 (**g**), which have an intermediate expression. (**h,i**) Images demonstrate robust signals for miRNAs differing by 3 nucleotides, miR–26b (**h**) and miR–26a (**i**) and these miRNAs were differentially expressed. Cell nuclei were counterstained with 4', 6–diamino–2–phenylindole dihydrochloride (DAPI, blue; bottom panel of **b–d**; right panel of **e–i**). Scale bars, 500 µm **(f–i).**

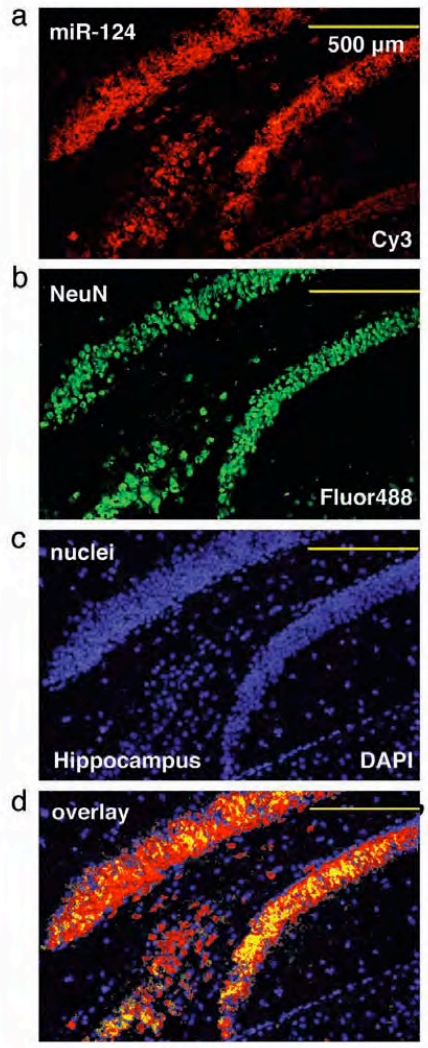

Figure 4: Images of miR–124 ISH show the majority of staining occurs in neurons. (**a**) Photomicrograph from ISH of miR–124 (red; Cy3) in mouse hippocampus (see **Supplemental Methods** for details). (**b**) Prior to miRNA ISH, samples were stained to visualize the localization of neurons with a primary antibody for NeuN (green; Fluor488), a known neuron-specific nuclear protein. (**c**) Nuclear staining (DAPI; blue). (**d**) Overlay of miR–124 (red; Cy3), NeuN (green; Fluor488), and nuclear staining (DAPI; blue). Scale bars, 200 µm (**a–d**). Note: double labeling for the miRNA ISH and immunohistochemistry resulted in a weaker signal for both the immunohistochemistry and miRNA ISH.

To examine probe hybridization specificity, we selected miR–124 and introduced mismatches in the probe seed or central regions. The melting temperatures of the mismatched probe/miR–124 duplexes dropped within the range of 0.7ºC to 14.6ºC (**Supplementary Table 3, appendix**). The ISH was performed at constant temperature 20ºC below the T_M of the fully complementary miR–124 probe. The probes with the greatest difference in T_M showed the least signal and central mismatches abolished detection (**Figure 5**). Interestingly, signal strength

observed for mismatched probes with minor reduction in T_M dropped disproportionately, again indicative of altered kinetics of probe hybridization.

Instead of a mismatch approach to control for probe specificity, conducting ISH using two probes directed against the mature miRNA and miRNA* sequence and/or clustered members may be useful to help rule out signals derived from cross–hybridization. We probed for cistronically expressed miRNAs that are distinct in sequence for co–localization, including members in the mir–99a/mir–125b–1/let–7c–1 cluster. The ISH for let–7c and miR–99a reveal mostly identical patterns that showed superimposable band–like patterns (**Figure 5g**). Other let–7 family members also show similar expression, however, the signal observed in the band–like region of the cortex likely originated from let–7c due to co–localization of miR–99a. We also tested the miRNA* sequences as a specificity control for miRNA ISH signals. We examined miR–140 and its complementary miR–140* sequence, expressed at relative clone frequency of 5 to 1, respectively. The ISH with both probes revealed superimposible expression in the cortex (**Figure 5h**).

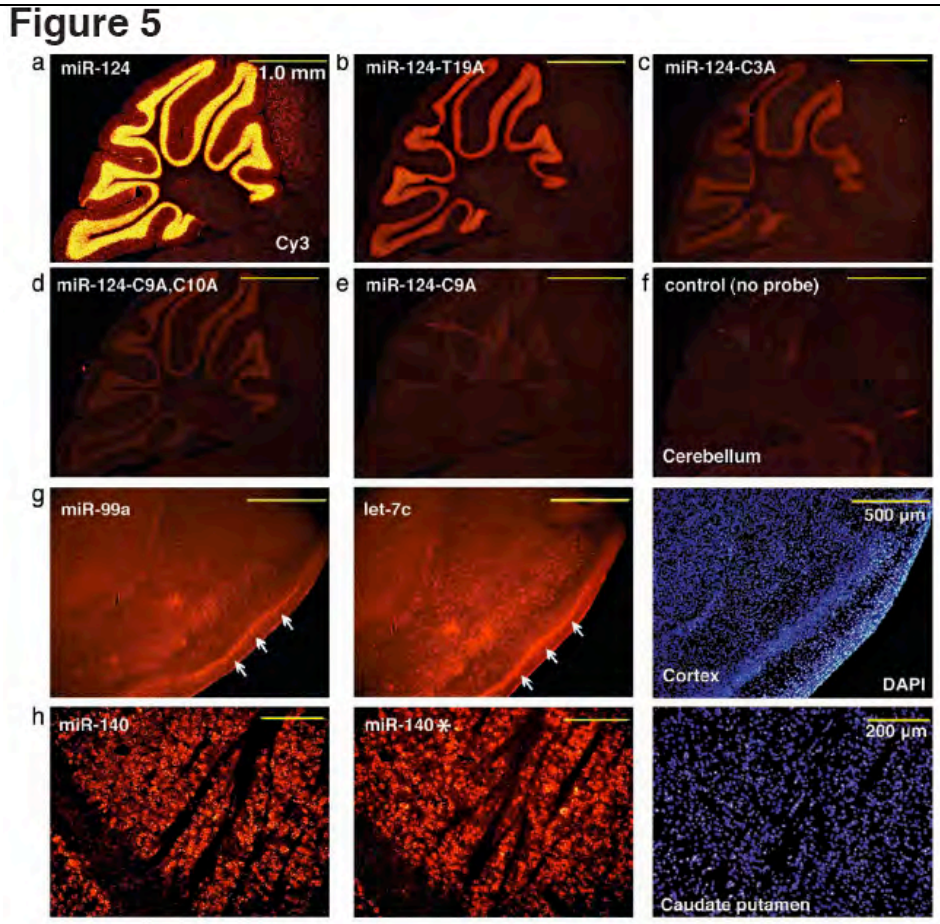

Figure 5: Controls for miRNA probe specificity. The melting temperatures of the mismatched probe–miR–124 duplexes dropped between 0.7ºC to 14.6ºC (Supplementary Table 3). (**a**) Images of neuron–specific miR–124 ISH (Cy3, orange) of fully complementary probes show robust staining in the mouse cerebellum. miR–124 mismatch probes miR–124–T19A (**b**) and miR–124–C3A (**c**) signal is reduced but visible. miR–124 mismatched near the middle or seed region, miR–124–C9A, C10A and miR–124–C9A respectively, show the least signal (**d,e**), similar to background (**f**). (**g**) Cistronically expressed miRNAs miR–99a (**left**, Cy3; red) and let–7c (**center**) exhibit similar band-like distributions in the cortex (Cy3; red), marked by arrows. Nuclei were counter–stained (**right**, DAPI; blue). (**h**) miR–140 (**left**, Cy3; red) and miR–140* (**center**, Cy3; red) co–localize in cortex and DAPI stain (**right**, blue). Scale bars, 1.0 mm (**a–f**), 500 µm (**g**), 200 µm (**h**). For images (**a–e**), ISH was performed at 47.5ºC, which was 20ºC below the TM of the perfect LNA probe–miR–124 duplex determined at 1.5 µM strand concentrations. For image (**g**), a second gene copy of let–7c (clone count frequency 4.1%) is present in the cluster of mir–let–7c–2/mir–let–7b, which was approx. 2.5 fold more abundant than miR–let–7b (clone count frequency 1.7%).

miRNAs are known to localize to subcellular compartments for local regulation of mRNA, possibly to the dendrites of neurons[141,172]. We tested several miRNAs for expression in dendrites including miR–370 (**Figure 6a–d**), miR–9 (**Figure 6e**), and miR–124 (**Figure 6g,h**), which extended up to 50 μm from the cell body. Interestingly, compared to miR-9, the 20–fold less expressed miR–9* did not reveal localization in dendrites (**Figure 6f**). Furthermore, we noted that the ISH signal for a miRNA expressed at higher levels than miR–370, miR–99a (0.9% clone count frequency), also expressed in non–neuronal cells, showed no signal in dendrites (data not shown). Together, these data demonstrate this method detects miRNAs in subcellular compartments.

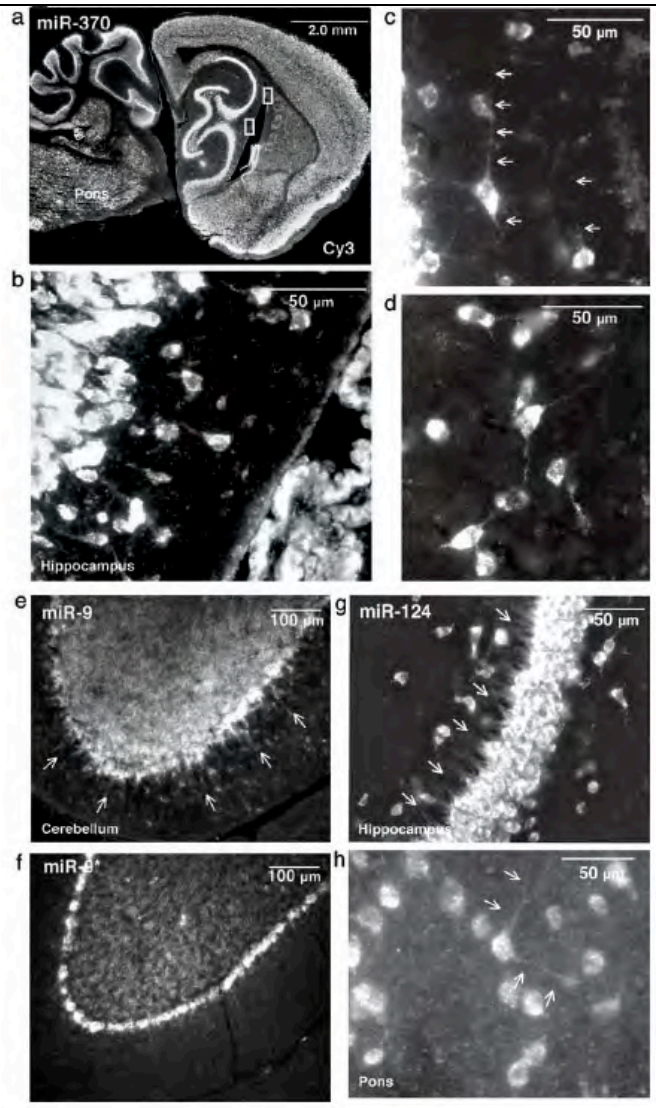

Figure 6: Formaldehyde–EDC–fixed sections show miRNA localized in the dendrites of neurons. (a) Low magnification fluorescent images demonstrate a robust and broad distribution of miR–370 expression (white) with intense staining in the hippocampus (inset). (**b,c**) High magnification images show a single neuron in the CA1 region of the hippocampus for which miR–370 is localized both in the cell body and the dendrites (arrows) (**c,d**), represented by inset (**a**). miR–370 localization extends 50 μm from the cell body (**b**), and 30 μM in other neurons (**c,d**). (**e**) The mature miRNA miR–9 expressed in dendrites of Purkinje cells in the cerebellum, yet the miR–9* (**f**) was absent in dendrites. (**g**) Pyramidal cells in the hippocampus (arrows) show staining of miR–124 in hippocampus dendrites and in neurons located in the pons.

Finally, to broaden this technique for sections not amenable to fluorescent imaging, we compared the NBT/BCIP pigment detection system for miR–370 in the brain to fluorescent detection and observed similar staining (**Figure 7**). We also tested the pigment detection for

miR–122 and miR–126–3p in the mouse liver, miR–1 in the mouse heart, and observed cell–type–specific staining (**Figure 8**). Furthermore, we combined the detection of proteins by immunohistochemistry with miRNA ISH (**Figure 4**), although immunostaining that preceded EDC fixation reduced the signal strength for the miRNA ISH.

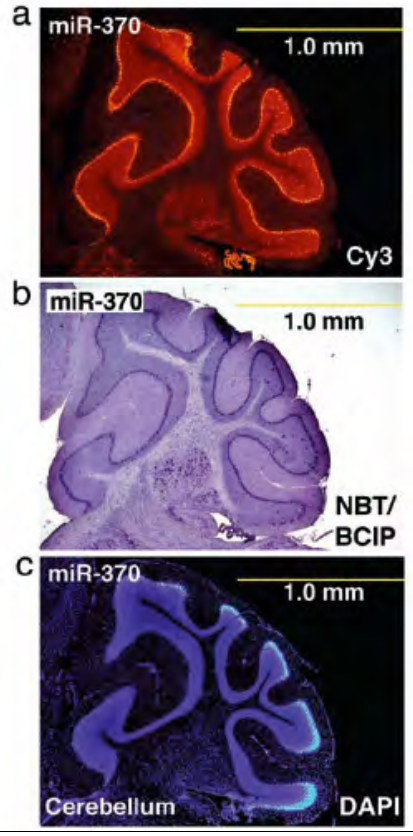

Figure 7: Fluorescence and formazan deposition NBT/BCIP detection systems. (**a**) Fluorescent image of mouse brain cerebellum using Tyramide–Cy3 detection system. (**b**) Light microscopy image of serial sections of mouse brain cerebellum using NBT/BCIP detection system show similar cellular distribution as in fluorescent detection. (**c**) Images of DAPI nuclear stain. Scale bars, 1.0 mm (a–c).

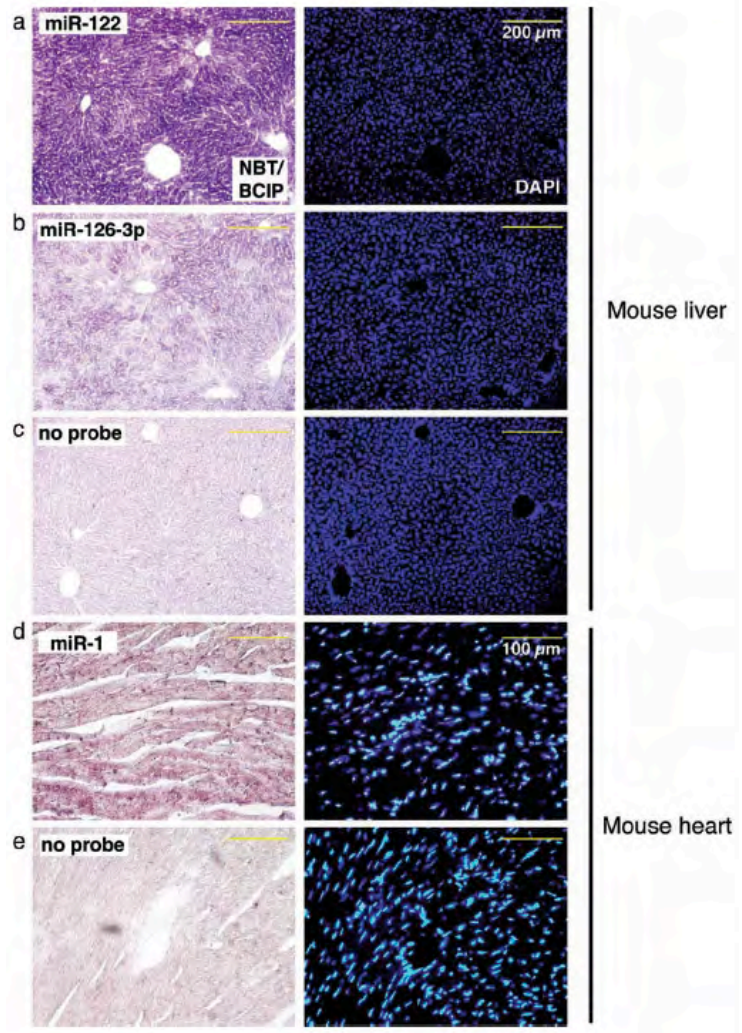

Figure 8: Detection of miRNAs in mouse heart and liver sections using formazan deposition NBT/BCIP detection system. (**a**) Images of a highly abundant miR–122 ISH in the mouse liver sections, (**b**) the lower expressed miR–126, and a no probe control (**c**). (**d**) Images of the mouse heart sections show expression of highly abundant miR–1 (**d**), with a no probe, negative control (**e**). Cell nuclei were counterstained with DAPI (blue; right panel (a–e); Scale bars, 200 μm (a–e).

Discussion and Conclusion

In summary, eliminating the possibility of miRNA diffusion by introducing an irreversible crosslink between the 5' phosphate of the miRNA and protein side chains significantly improves miRNA retention in tissues. The advantage of EDC–based phosphoramidate–linked miRNA is

that the sample can be exposed to higher temperatures for a longer time, resulting in a more complete reversion of the formaldehyde induced nucleobase modification of the miRNAs and less interference with probe hybridization. Furthermore, the melting temperature determined for many probe/miRNA duplexes under ISH conditions more accurately defined ISH hybridization temperatures. At present, we showed that different tissues and detection systems are compatible with our approach. This method paves the way for reliable disease association studies and the potential use of miRNA ISH expression analysis as a diagnostic tool for biopsy material.

Methods

Design and synthesis of LNA-modified oligodeoxynucleotide probes

LNA-spiked oligodeoxynucleotide probes (LNAs) were identical in length and fully complementary to the predominantly cloned mature miRNA or miRNA* sequence[89]. On average, we placed 5 to 8 LNA residues in a 22-nt oligodeoxynucleotide probe. To optimize probe hybridization, we avoided inserting LNA bases in positions that may stabilize internal secondary structures, so LNA residues were placed outside of predicted secondary self-structures (http://www.idtdna.com/analyzer/Applications/OligoAnalyzer/)[183]. The LNA probe sequences are listed in Supplementary Table 1. Probes were synthesized at 0.2 or 0.4 μmol scale on an ABI 3400 DNA synthesizer using 3'-amino-modifier C7 CPG (500 Å) solid glass support (Glen Research) and LNA and DNA phosphoramidites (Sigma-Proligo and Glen Research). The aminolinker Fmoc and phosphate cyanoethyl protecting groups were removed by gently passing back and forth 3 ml of freshly prepared 20% piperidine (Sigma) in N,N-dimethylformamide (DMF, Sigma) for 5 min over each column. Columns were washed three times with 3 ml of

acetonitrile and dried with pressurized air. For further deprotection, the CPG was transferred to a 1.5 ml screw cap tube and incubated with 1.2 ml of 28% aqueous ammonium hydroxide solution for 16 h at 55ºC. The tube was placed on ice for 5 min, and the supernatant transferred to a 13 ml centrifugation tube. 10 ml of 1-butanol was added, vigorously mixed and the LNA pellet was collected by centrifugation at 13,000 rpm in an SS-34 rotor at 4ºC for 20 min in Sorvall RC5C Plus centrifuge. The supernatant was removed completely, the pellet dried in an Eppendorf concentrator and redissolved in 282 µl water. In order to exchange ammonium ions with sodium, the LNA solution was adjusted to 0.3 M NaCl by addition of 18 µl of 5 M NaCl and precipitated by addition of 900 µl of 100% ethanol. The pellet was collected by centrifugation and redissolved in 300 µl water. The LNA concentration was determined by measuring its UV absorbance at 260 nm using an average absorbance coefficient of 11,000 $M^{-1}cm^{-1}$ per nucleotide.

To 3'-digoxigenin-label the LNA probe, an aliquot corresponding to 30 nmol of the LNA, was dried in an Eppendorf concentrator and redissolved in 50 µl of 100 mM sodium carbonate buffer at pH 8.5. 240 nmol of digoxigenin-3-O-methylcarbonyl-ε-aminocaproic acid-N-hydroxysuccinimide ester (Roche) freshly dissolved in 50 µl anhydrous DMF was added, mixed and incubated for 16 h at 25ºC. The yield of a typical labeling reaction was 80%. The DIG-labeled probes, which showed reduced mobility compared to the starting material, were separated on a 43 x 23 x 0.2 cm denaturing 18% PAGE gel (200 ml gel volume) for 6 h at 50 W. Product bands were visualized by UV shadowing, excised, and eluted from the gel slice overnight into 3 volumes (w/v) of 0.3 M NaCl, ethanol precipitated and resuspended in 100 µl water.

DIG-labeling was examined by spotting 1 pmol, 100 fmol and 10 fmol on a Nylon membrane (Amersham Hybond- N+) followed by incubation of the membrane with anti-DIG antibody fragment conjugated to peroxidase antibody (Roche) with NBT/BCIP (Roche). Formazan Blue deposition is observed between 10 min to 1 h for all amounts spotted.

UV Melting profiles of miRNA/LNA-probe duplexes

The UV absorbance change associated with melting of the LNA probe and miRNA duplex was recorded at 280 nm on an Uvikon UV/VIS spectrophotometer (LifePower software) equipped with temperature-controlled cuvette holders. The rate of cuvette heating and cooling was 0.3ºC/min and the absorbance was recorded every min. The melting temperature (T_M) of duplex formation was obtained by curve-fitting the absorbance change as a function of temperature to a two-state model using Meltwin 3.5 software. To prepare samples for T_M analysis, miRNA/probe pairs in a volume of 300 µl of 1.5 µM of unlabeled LNA probe and 1.5 µM of synthetic miRNA in 750 mM NaCl, 75 mM sodium citrate, 50 mM sodium phosphate (pH 7.0) and 50% formamide were incubated for 5 min at 95ºC, for 5 min at 80ºC, gradually cooled for 3 h to 50ºC, and then held at room temperature for 1 h or longer. The solution was then transferred to a quartz cuvette, overlayed with 500 µl mineral oil (Sigma) and degassed for 10 min by applying vacuum to a small dessicator holding the cuvettes.

Adjusted parameters for prediction programs to estimate T_M for miRNA/LNA probe duplex in formamide containing ISH buffer.

To best emulate our experimental T_M analysis, we tested several salt concentrations in the prediction program and determined that 50 mM salt, instead of the actual 750 mM for ISH

buffer, yielded an average predicted T_M of 0.26ºC higher than the average of our experimental values with a standard deviation of 4.4ºC.

We constructed non-parametric prediction intervals to determine the error. From a sample of 127 miRNA/LNA probe pairs, we found that the distribution of the predicted T_M error had a mean of 0.26ºC (the predicted T_M tended to be slightly higher than the real T_M) and a standard deviation of 4.4ºC. To derive estimates for the likelihood that the predicted T_M error will fall within a specified range, we constructed nonparametric prediction intervals[184]. We found that with 95.3% probability, the error in the predicted T_M for any miRNA/LNA probe pair will fall between -9.2ºC and 8.6ºC. With 68.8% probability, the predicted T_M error will fall between -4.1ºC and 4.7ºC. Within a broad range of ±2 standard deviations of the mean, the sampled distribution of predicted T_M errors is closely approximated by a normal distribution with μ = 0.26 ºC and σ = 4.4 ºC. We therefore repeated the same analysis under the assumption of normality and found closely similar results. We found that with a 95.3% probability, the error in the predicted T_M for any miRNA/LNA pair falls within -9.2ºC and 8.6ºC of the experimental T_M in formamide-containing ISH buffer or a 68% probability that the true T_M will fall between -3ºC and 5.1ºC.

Tissue preparation and processing

Male, 2-month-old C57BL/6J mice (Jackson Labs) were maintained on a 12 h light/dark cycle. Animals were sedated in accordance with NIH Animal Welfare guidelines using ketamine and xylazine cocktail before organ perfusion with 50 ml of Tris-HCl buffered Saline (TBS) containing 50 mM Tris-HCl, 150 mM NaC1 and the pH adjusted to 7.4. Immediately after TBS,

we perfused with of 30 ml of 4% paraformaldehyde (PFA) in TBS. Tissues were collected, immersed in 30 ml of 4% PFA in TBS for 24 h at 4ºC, then in 30 ml of 0.5 M sucrose diluted in TBS at 4ºC for 48 h. The tissues were mounted in Tissue-Tek OCT Compound, frozen in a dry-ice/ethanol bath in a Cryomold (Tissue-Tek), immediately serial sectioned from 5 to 40 µm with a cryostat (Leica) and mounted on SuperFrost Plus glass slides (Thermo Fisher Scientific). Unprocessed specimen or mounted slides can also be stored at -80ºC.

***In situ* hybridization procedure**

Processing or wash steps were generally carried out by placing up to 20 slides in 75 ml glass Coplin jars (Electron Microcopy Sciences) filled with specified solutions and all wash steps were in 50 ml of the stated solution for 5 min at 25ºC, unless otherwise noted. Tissue sections mounted on glass slides were thawed and air-dried for 1 h at 25ºC and then incubated in a 75 ml solution containing 20 µg/ml proteinase K (Roche) in TBS, pH 7.4 for 20 min. Thereafter, the slide was washed two times in 75 ml TBS. Samples were fixed in 75 ml of 4% PFA in TBS for 10 min, washed with 0.2% (w/v) glycine in TBS, and washed two times in 75 ml TBS.

To remove residual phosphate from the TBS washes, slides processed with EDC fixation were incubated twice for 10 min in 75 ml of a freshly prepared solution containing 0.13 M 1-methylimidazole, 300 mM NaCl, pH 8.0 adjusted with HCl. To prepare 160 ml of imidazole buffer, add 1.6 ml of 1-methylimidazole to 130 ml water, adjust the pH by adding approximately 450 µl 12 M HCl to pH 8.0, then add 16 ml 3 M NaCl and water to a final volume of 160 ml. In the meantime, prepare a solution of 0.16 M l-ethyl-3-(3-dimethylaminopropyl) carbodiimide (EDC) (Sigma) by adding 176 µl EDC into 10 ml of 1-methylimidazole/NaCl (pH 8.0) solution,

and then readjust the pH of the EDC solution by further addition of approximately 100 µl 12 M HCl to pH 8.0. It is important for storage of commercial EDC to handle the reagent under anhydrous conditions and protect it with a layer of argon. Aqueous solutions containing EDC and/or 1-methylimidazole cannot be stored. Place slides in a humidified chamber and add 500 µl of EDC solution to each slide and incubated for 1 to 2 h at 25ºC. The slides were washed in 0.2% (w/v) glycine/TBS and then washed twice in TBS.

For inactivation of enzymes in tissues, e.g. alkaline phosphates and peroxidases, slides were acetylated by incubating for 30 min in a 75 ml solution of freshly prepared 0.1 M triethanolamine and 0.5% (v/v) acetic anhydride. Slides were then rinsed twice in TBS.

For pre-hybridization, the tissue sections on the slides were covered with 500 µl of hybridization buffer containing 50% formamide, 5x SSC, 5x Denhardt's solution (Applichem), 250 µg/ml yeast tRNA (Sigma), 500 µg/ml salmon sperm DNA (Sigma), 2% (w/v) Blocking Reagent (Roche), 0.1% 3-[(3-Cholamidopropyl) dimethylammonio]-1-propanesulfonate (CHAPs) (Sigma), 0.5% Tween at 25ºC for 2 h in a humidified chamber. The hybridization buffer was removed by tilting the slide.

For hybridization, 40 pmol of DIG-labeled LNA probe diluted in 100 µl of hybridization buffer were applied per section, and covered with coverslips (LifterSlips, Fisher) . The slides were incubated in a sealed humidified chamber for 16 h at a temperature 20ºC below the T_M of the experimentally determined miRNA/LNA probe duplex. Hybridization conditions were adjusted 20ºC below the LNA probe's experimentally determined T_M, taking into account that

the probe concentration for an ISH experiment is 40 nM compared to 1.5 μM required for optical T_M measurements.

The slides were immersed in 20 ml of 5x SSC at 25ºC so the coverslip can be removed and then washed twice in 75 ml of a solution containing 50% formamide, 1x SSC, and 0.1% Tween for 30 min at the same temperature as probe hybridization. Finally slides were washed in 75 ml 0.2x SSC for 15 min and once in 75 ml of 0.1% Tween in TBS.

To inactivate endogenous peroxidase activity, slides were incubated in 75 ml of 3% hydrogen peroxide in TBS with 0.1% Tween for 30 min, followed by three 1 min washes of TBS/0.1% Tween.

In preparation for probe detection, 500 μl of blocking solution containing 0.5% Blocking reagent (Roche), 10% heat inactivated goat serum, and 0.1% Tween 20 in TBS was applied to each slide for 1 h at 25ºC, then incubated in anti-DIG-FAB peroxidase (POD) (Roche) diluted 1:500 in blocking solution for 1 h at 25ºC. Slides were then washed as described below in preparation for the application of the various detection reagents.

Cy3 fluorescent detection system

The slides were washed twice in a solution containing 0.1% Tween 20, in TBS and 200 μl of TSA Plus Cy3 System working solution was applied onto to the sections for 10 min at 25ºC in the dark according to the manufacturer's protocol (PerkinElmer Life Sciences). The slides were then washed three times in TBS with a tilting rotator. The slides were mounted using 2 drops of Vectashield mounting medium with DAPI (Vector Laboratories) and samples processed for microscopy.

Alkaline phosphatase double amplification detection system

This detection method was adapted from studies by Lein et al.[145]. The slides were washed three times in 75 ml in TNT buffer, consisting of 0.1 M Tris-HCl, pH 7.5, 0.15 M NaCl, and 0.1% Tween 20. Thereafter, 250 µl of biotinylated tyramide solution from the Individual Indirect Tyramide Reagent kit (PerkinElmer Life Sciences) was applied to each slide for 30 min at 25ºC, according to the manufacturer's protocol. The slides were washed three times in 75 ml maleate buffer (0.09 M maleic acid, 0.175 M NaOH, 1 M NaCl, 0.5% Tween 20, pH 7.5). A 1:500 solution of 350 µl of NeutrAvidin-conjugated alkaline phosphatase (Thermo Scientific) in maleate buffer supplemented with 10 mg/ml blocking reagent (Roche) was applied to the slide for 40 min at 25ºC. Slides were then washed twice in 75 ml maleate buffer, and four times in 75 ml TMN buffer (0.1 M Tris base, pH 9.5, 0.05 M $MgCl_2$, 0.5 M NaCl, 0.5% Tween 20, 2 mM (-)-tetramisole hydrochloride). The formazan deposition was performed by applying 200 µl of a solution containing 0.375 mg/ml NBT (Roche) and 0.188 mg/ml BCIP (Roche) in TMN buffer. Upon deposition of the blue pigment, typically visible after 30 min, the slides were washed twice in 75 ml water, three times in 75 ml of 0.01 M Tris-HCl, pH 7.5, 0.5 M NaCl, 5 mM EDTA, 0.05% Tween 20, and incubated for 10 min in 75 ml of 4% aqueous paraformaldehyde solution. Finally, the slides were washed in 75 ml water and mounted using 2 drops of Vectashield mounting medium with DAPI (Vector Laboratories).

Immunohistochemistry and miRNA ISH co-staining

To assess whether miR-124 was localized specifically to neurons, brain sections were processed for double immunofluorescence staining to visualize the simultaneous localization of miR-124

(red; Cy3) and a primary antibody for NeuN (green; TRITC), a known neuron-specific nuclear protein. First we performed immunohistochemistry to label neuronal cells. Brain sections mounted on slides were rinsed three times for 5 min in 50 ml of TBS. Sections were incubated for 1 h in 500 µl of "working solution of M.O.M. Mouse Ig Blocking Reagent" (Vector Laboratories) at 25ºC, according to the manufacturers protocol. Sections were washed twice for 5 min in 50 ml of TBS, followed by incubation for 5 min in a "working solution of (M.O.M.) diluent" (Vector Laboratories) for 5 min at room temperature. The "working solution of (M.O.M.) diluent" was removed. To visualize neurons, we incubated the samples with a primary anti-NeuN-clone-A60-AlexaFluor488 conjugated antibody (Chemicon International, Temecula, CA) diluted 1:300 in a "working solution of M.O.M. diluent" (Vector Laboratories) for 1 h at 25ºC. Slides were then washed 3 times for 5 min in 50ml TBS. Slides were mounted using 2 drops of Vectashield mounting medium with DAPI (Vector Laboratories). Please note that the glass coverslips were not sealed, as the samples were later used for ISH to detect miR-124. After image acquisition, coverslips were removed by washes in 50 ml of TBS and the tissue sections were then processed for ISH for miR-124 (Cy3; red) by applying our miRNA ISH protocol described earlier. After miRNA-ISH, the sections were mounted using 2 drops of Vectashield mounting medium with DAPI (Vector Laboratories) and samples processed for microscopy. Photomicrographs of the nuclear staining are required to superimpose images for the immunohistochemistry and the miR-124 ISH. Images were combined to generate an overlay using Olympus Microsuite Five software.

Please note that the immunohistochemistry procedure for NeuN protein detection somewhat reduced the efficiency for miRNA detection; performing miRNA ISH before protein staining was not possible as EDC fixation interfered with protein immunohistochemistry.

Microscopy and image processing

Images were captured on an Olympus BX50 microscope equipped with a DP70 camera and Olympus DP controller software. For fluorescent imaging we used the following filter sets; U-MWU2 (Olympus) for DAPI, 41001 HQ (Chroma) for Fluro488, 49004 ET (Chroma) for Cy3. The images from both the immunohistochemistry and the ISH were captured using DP70 camera and processed using Olympus Microsuite Five software (Olympus).

Small RNA isolation from formalin-fixed tissue

Formalin-fixed brain tissues used for RNA extraction were cut into 1 mm sections and incubated with a 200 µl solution containing 20 µg/ml proteinase K (Roche) in TBS and incubated at 45ºC for 1 h. The samples were then processes for RNA isolation. Total RNA was isolated from 4% formaldehyde fixed tissue by using the commercial Trizol (Invitrogen) reagent. We added 1 ml of Trizol per 1 mm slice of brain. The mixture was immediately homogenized while kept on ice. Cells were homogenized using a Dounce glass homogenizer and then further mechanically homogenized using a Polytron homogenizer (Kinematica AG). Following tissue disruption, 1/10 volume of 3 M sodium acetate (pH 4.2) was added. The mixture was transferred to an Eppendorf tube and centrifuged for 15 min at 12,000g at 4ºC. The aqueous phase was transferred to a new tube without the white interphase. RNA was further extracted with 1/2 volume of acid-buffered phenol:chloroform:isoamyl alcohol (25:24:1) and centrifuged for 15 min at 4ºC at 12,000g.

Finally, we extracted the aqueous phase with 1/2 volume chloroform. The upper (aqueous) phase transferred to a new tube. We added 3 volumes of ethanol to precipitate the RNA and incubated the sample overnight at –20ºC in the freezer. The RNA pellet was collected by centrifugation for 15 min at 4 °C at 12,000g and the supernatant was removed. The pellet was then dissolved in 30 µl water and used for Northern blotting.

We were unable to isolate miR-124 from the formalin/EDC-treated tissue, presumably because miRNAs remained cross–linked to the protein matrix and the small RNAs were lost to the phenol- or inter-phase during RNA isolation.

Northern blotting

Northern blotting was performed as described[89] using Hybond-N+ membrane (Amersham GE healthcare), and the hybridization and wash steps were performed at 50°C. The oligodeoxynucleotide probes were 5'-labelled with [γ-^{32}P] ATP. The probe for miR-124 was 5' TTGGCATTCACCGCGTGCCTTA. To control for loading of the gel, 5S rRNA was detected by ethidium bromide staining of the polyacrylamide gel prior to transfer. Probe samples were recorded by phosphoimaging and quantified. Northern blotting images were quantitated using ImageJ software[171].

Small RNA library preparation and sequencing

The regulatory potency of miRNAs (miRNAs) depends on relative abundance and spatio-temporal expression patterning of miRNAs in a given species or local concentration within in a tissue. The Tuschl laboratory developed a small RNA cloning technique to characterize small interfering (siRNA) processing intermediates that were the molecular substrates for the RNA

interference (RNAi) pathway[169]. Further application of the technique lead to the identification of the majority of miRNAs expressed in fruitfly, zebrafish, mouse, human, and herpes viruses [86,96,122,133,185-188]. Methods for cloning and identifying small RNAs improved over the recent years (**Figure 9**) [90,187-189]. Using these optimized protocols, we prepared RNA extracted from dissected mouse brain regions and size-fractionated by a denaturing PAGE. miRNA cloning was performed as described previously[170]. The cDNA library was sequenced by 454 sequencing. MiRNA sequences were annotated as described[89] and obtained about 90,000 sequence clones.

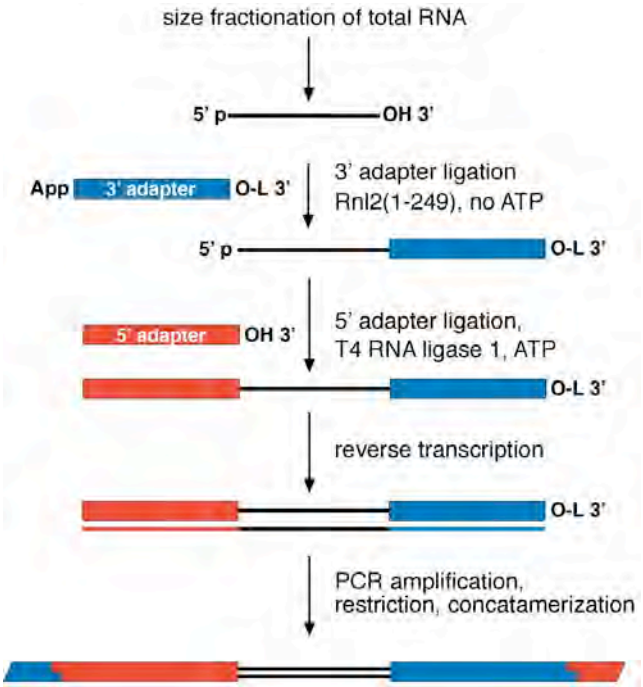

Figure 9. Small RNA cloning protocol [188]. Small RNAs are isolated by gel electrophoresis from total RNA or by immunoprecipitation using anti-Argonaute monoclonal antibodies. First, a chemically preadenylated 3' adapter oligonucleotide is ligated to the small RNAs. The ligase in this step can only accept pre-adenylated donor oligonucleotides and, in contrast to other ligases, has reduced activity to transfer the adenylate to the 5' phosphorylated input small RNAs, thereby minimizing losses of input material due to ligase-catalyzed circularization. The ligation products are gel-purified and the 5' adapter is ligated with regular RNA ligase in the presence of ATP. Because the 3' adapter is blocked with an aminolinker function at its 3' end, and the 5' adapter is not 5' phosphorylated, only intermolecular ligation reactions occur. The ligation product is again gel-purified, then reverse transcribed, PCR amplified, concatamerized and sequenced.

Chapter IV

Improved in situ hybridization method to detect microRNAs in mammalian tissue sections fixed with formaldehyde and EDC and Cyanogen Bromide under optimized hybridization conditions.

Summary of Chapter IV

MicroRNAs (miRNAs) are 20- to 23-nucleotide small regulatory RNAs are associated with many normal physiological process and associated with diseases such as cancer, neurological disorders, and cardiovascular diseases. Defining cell-type specific expression of miRNAs is critical for understanding the natural function of miRNAs and their role in pathology. The most widely used method for imaging messenger RNA and microRNA in tissue sections is *in situ* hybridization (ISH). We previously showed that conventional ISH using formaldehyde fixation can result in reversal of RNA crosslinks and subsequent loss of miRNAs during probe hybridization. Here in this protocol, we describe a fixation method to eliminate miRNA loss by introducing a permanent crosslink that immobilizes the miRNAs by condensing the miRNA 5' phosphate to protein amino groups using an additional treatment with 1-ethyl-3-(3-dimethylaminopropyl) carbodiimide (EDC) and or cyanogen bromide (BrCN). This modified miRNA ISH procedure requires 2 days to complete and is adaptable to existing ISH protocols by applying EDC and or BrCN treatment to samples previously fixed with formaldehyde. This ISH procedure can be automated, setting the stage for high throughput screening studies for large numbers of miRNAs in normal and disease tissues. The results from tissues crosslinked with formaldehyde–EDC and or formaldehyde–BrCN solution, yields miRNA ISH signals that are substantially more robust, when compared to conventional formaldehyde fixation alone.

Introduction

MicroRNAs (miRNAs) are important regulators of mRNA translation and stability in eukaryotes[52,54,190-194]. They participate in many biological processes including developmental timing, cell differentiation, stress response, and apoptosis[50,195-197], often in a tissue-specific manner. Recent investigations are assigning miRNAs to specific functions in given cell types, emphasizing the need to precisely define their endogenous expression. Association studies in human patient samples are linking miRNAs with diseases, the most studied examples being cancers[195,198], neurological disorders[155,172,199] and cardiovascular diseases[200]. To help clarify the role of miRNA in normal and disease phenotypes, identifying the spatial and temporal localization of miRNAs using ISH in tissues with diverse cell types is crucial[200].

Methods for imaging miRNAs in tissue sections

The most widely used procedure for imaging mRNA and miRNA in specific cell types is *in situ* hybridization (ISH) in tissues fixed with formalin. Whole-mount ISH for microRNAs in the zebra fish and mouse[142,201] set the foundation for miRNA ISH. In fresh-frozen tissue sections, miRNA ISH protocols were described[95,144,173-175] and results were shown in the brain[103] and eye[146]. Other groups used miRNA ISH to support disease association studies[176,177]. In our laboratory, miRNA ISH using formalin–fixed tissues often yielded inconsistent results, and other groups also reported that ISH for lower expressed miRNAs were challenging[146,147]. The technical limitations of conventional miRNA ISH led investigators to develop novel methods to monitor miRNA expression that include generating transgenic models expressing miRNA constructs with reporters[138], single cell detection using quantitative PCR[139], and profiling FACS sorted

hematological cells[89,140]. While useful, these methods are limited compared to ISH, as localization of miRNA location in the context of the natural tissue morphology will be needed for a broad range of studies.

Formaldehyde crosslinks are reverted under ISH conditions

We examined steps of the ISH protocol that may hamper miRNA detection, the most critical being defining the hybridization temperatures under the conditions of ISH, inadequate fixation and crosslinking of miRNAs, which results in loss of miRNAs during probe hybridization[147]. Conventional ISH is based on treating specimens with 10% formalin (3.7% formaldehyde), a universal fixative[178,202] used to inactivate, stabilize, and immobilize proteins and nucleic acids, which preserves tissue morphology. Formalin reacts with primary amino, imino and thiol groups present in proteins or nucleic acid bases forming N-methylol ($N\text{-}CH_2OH$) derivatives or Schiff-bases ($RN{=}CH_2$)[178,202]. The primary reaction products may undergo secondary reactions with amines, imines and reactive aromatic nuclei, such as tyrosine, yielding methylene–bridged condensation products of varying stability[178]. Formaldehyde reacts with nucleic acids by forming reversible crosslinks between nucleic acids and proteins. Crosslinks are biochemically unstable and partially revert when the ribonucleoprotein structures are exposed to elevated temperature, and or limited proteinase K treatment[147,179]. For most ISH procedures, formaldehyde–fixed tissues require exposure to proteinase K treatment and hybridization temperatures above 37ºC, which subsequently leads to loss of miRNA from the tissue section[147] and ultimately results in lower or no miRNA ISH signal.

Stable crosslinks with the miRNA 5' phosphate withstand hybridization conditions

To eliminate diffusion of the miRNA during hybridization, we introduced an irreversible fixation step of the miRNA 5' phosphate. Formaldehyde crosslinks at the nucleobases and leaves the miRNA 5' phosphate group unmodified[178] and available for condensation. The first reagent agent suitable for generating stable crosslinks at the miRNA 5' phosphate is thewater soluble 1-ethyl-3-(3-dimethylamino-propyl) carbodiimide (EDC), which reacts with phosphates and condenses it with aliphatic primary and secondary amino groups present in the protein matrix and results in a stable phosphoamidate linkage[181,203]. In combination with formaldehyde, EDC retains miRNAs under ISH conditions and substantially increases the miRNA ISH signal[147].

To optimize the formaldehyde–EDC–based miRNA ISH procedure, we determined the level of miRNA expression in the mouse brain by isolating RNA from 5 distinct brain regions, including the cerebral cortex, hippocampus, then profiled the miRNAs present using 454 deep sequencing[147]. The relative amount of miRNAs present in the tissue are represented as the clone count frequency. For our ISH experiments, we use DNA oligonuclotide probes with approximately one third of the nucleobases substituted with a locked nucleic acid (LNA) residues. Furthermore, we determined the optimal hybridization temperature for a probe set of 130 miRNA–LNA probes by measuring the UV absorption of the miRNA–LNA probe duplex in ISH buffer as a function of temperature. The melting profiles were recorded and we calculated the melting temperatures (T_M) for each miRNA–probe pair[147]. For our miRNA ISH experiments, we adjusted the hybridization temperature to be –20ºC below the experimentally determined T_M.

To validate this protocol, we examined formaldehyde–fixed fresh–frozen mouse brain tissue sections for expression of medium abundant miRNAs by hybridizing LNA probes targeting miR-129-3p (clone count frequency 0.35%)[147] and miR–130a (clone count frequency 0.12%), followed by detection using a sequence of tyramide signal amplification reactions with the fluorescent product being a Cyanine 3 (Cy3) precipitate (**Fig. 1a–d**). We observe robust detection of both miRNAs in formaldehyde–EDC fixed tissues (**Fig. 1a, c; left**), but the signal remained nearly blank in tissues fixed with formaldehyde alone (**Fig. 1b, d; left**). We applied the formaldehyde–EDC fixation in fresh–frozen mouse brain tissue sections to examine miRNAs expressed at various expression levels, and observe specific signal for the medium abundant miR–30b (clone count frequency 0.49%), and for the low abundant miR–145–5p (clone count frequency 0.05%) and miR–28–3p (clone count frequency 0.005%) (**Fig. 2 a–c**). miR–30b showed expression in distinct expression in the mouse cerebral cortex, hippocampus and cerebellum (**Fig. 2a**). For miR–28–3p, which is almost 100 fold less than miR–30b, we observe signal in the cerebellum (**Fig 2b**) and miR–145 showed robust staining in the cortex, yet absent in the superior colliculus (**Fig 2c**).

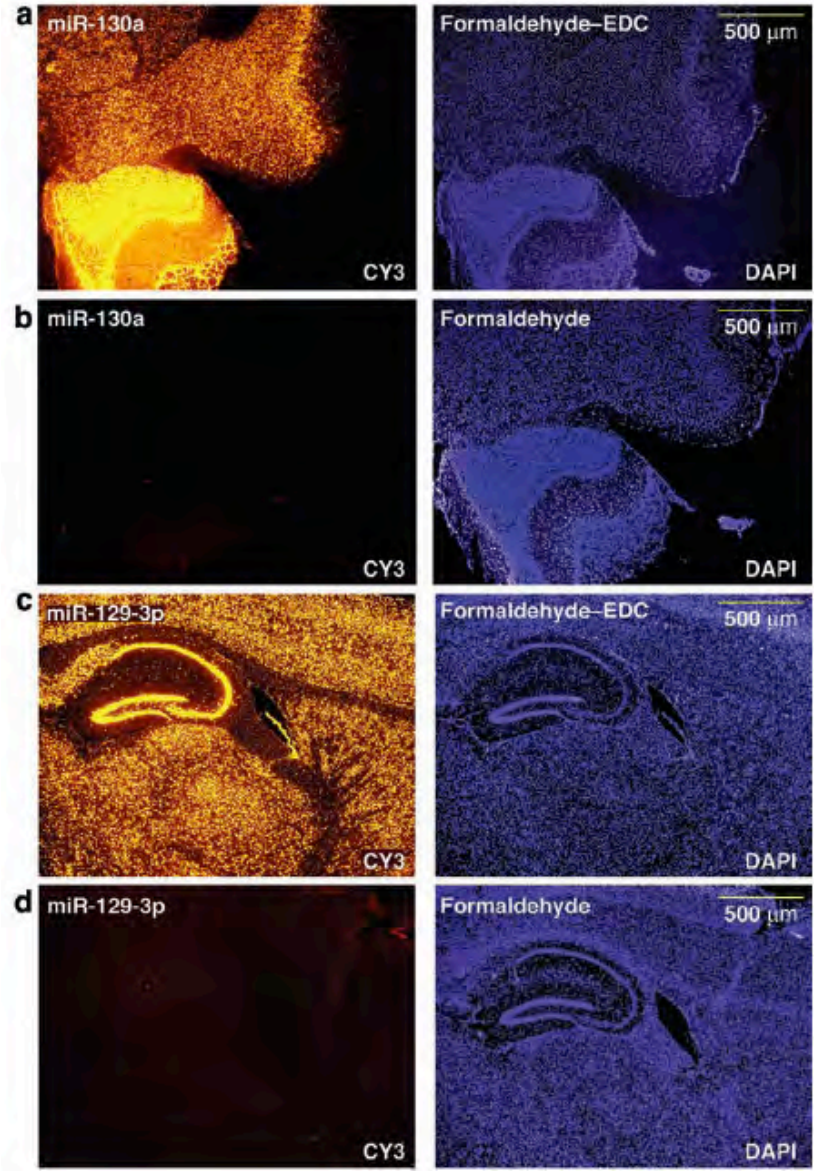

Figure 1: Tissues fixed with formaldehyde–EDC improves miRNA ISH signal for less abundant miRNAs. (**a**) Low–power fluorescent micrograph images showing medium expressed miR-130a (clone count frequency 0.12%) in regions of the olfactory bulb and cerebral cortex from mouse brain in tissues fixed formaldehyde–EDC (**a**, Cy3; orange, left) or formaldehyde alone (**b**, Cy3; orange, left). (**c**) Low–power fluorescent micrograph images of miR–129–3p (clone count frequency 0.35%) in the hippocampus and cerebral cortex from mouse brain tissues fixed with formaldehyde–EDC (**c**, Cy3; orange, left) or formaldehyde alone (**d**, Cy3; orange, left). Nuclei were stained (DAPI, **a–d**, blue; right). Scale bars 500 µm in **a–d**.

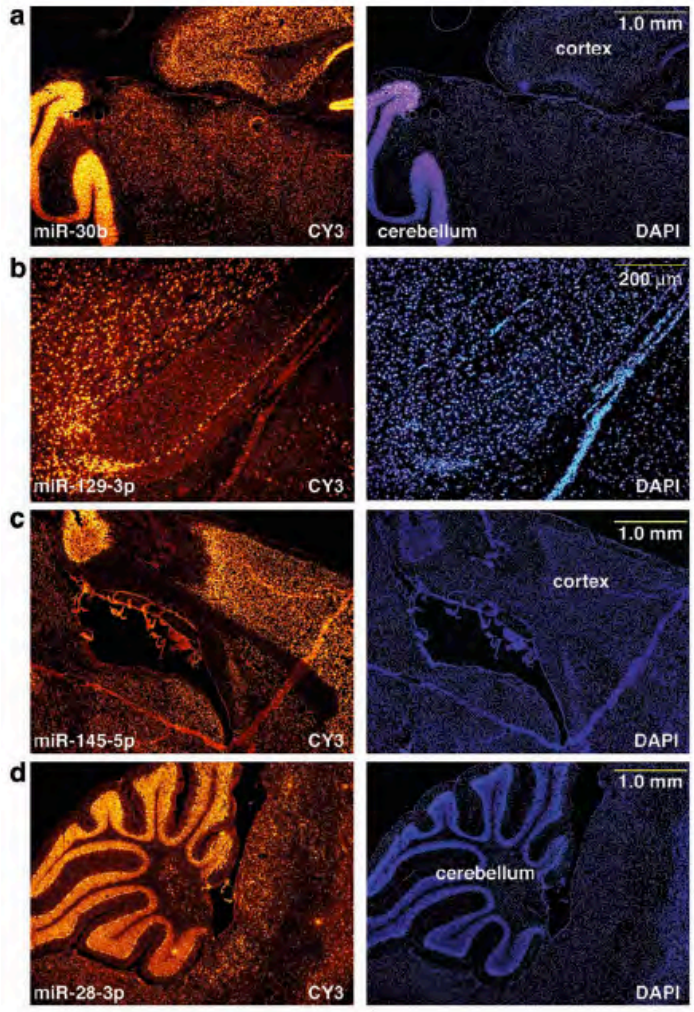

Figure 2: Detection of miRNAs expressed at various amounts in the mouse brain tissues fixed with formaldehyde–EDC. (a) Low–power fluorescent micrograph images of the medium expressed miR–30b (**a**, Cy3; orange, left) in the cerebellum, cerebral cortex and hippocampus. Low–power magnification micrograph images of miR–129–3p expression in a single cell layer (**b**, Cy3, left, arrows). (**c**) Fluorescent micrograph images show miR–145–5p expression in the cerebral cortex, without staining in the superior colliclus (**c**, Cy3, left, arrows), and the low abundant miR–28–3p shows expression in the cerebellum. Nuclei were stained (DAPI, blue; right, **a–d**). Scale bars 1.0 mm in a, **c–d**; 200 µm in **b**.

To determine if EDC–based ISH signal intensity is pH–dependent, we examined ISH signal for miR–129–3p in tissues treated with formaldehyde and then adjusted the pH of the EDC solution and observed a notably weaker signal for EDC solution at pH 5.5 and 6.0 (**Fig. 3a, b**), compared to EDC solution adjusted to pH 6.5 and above (**Fig. 3, c–h**). The most intense miRNA ISH signal occurred using EDC solution at pH 7.0–8.5 (**Fig. 3, d-g**) and the signal

became moderately less intense at pH 9.0 (**Fig. 3h**). To minimize the degree of pH drift and reduced crosslinking yields, we recommend working with EDC solution at pH 8.0 (**Fig. 3f**).

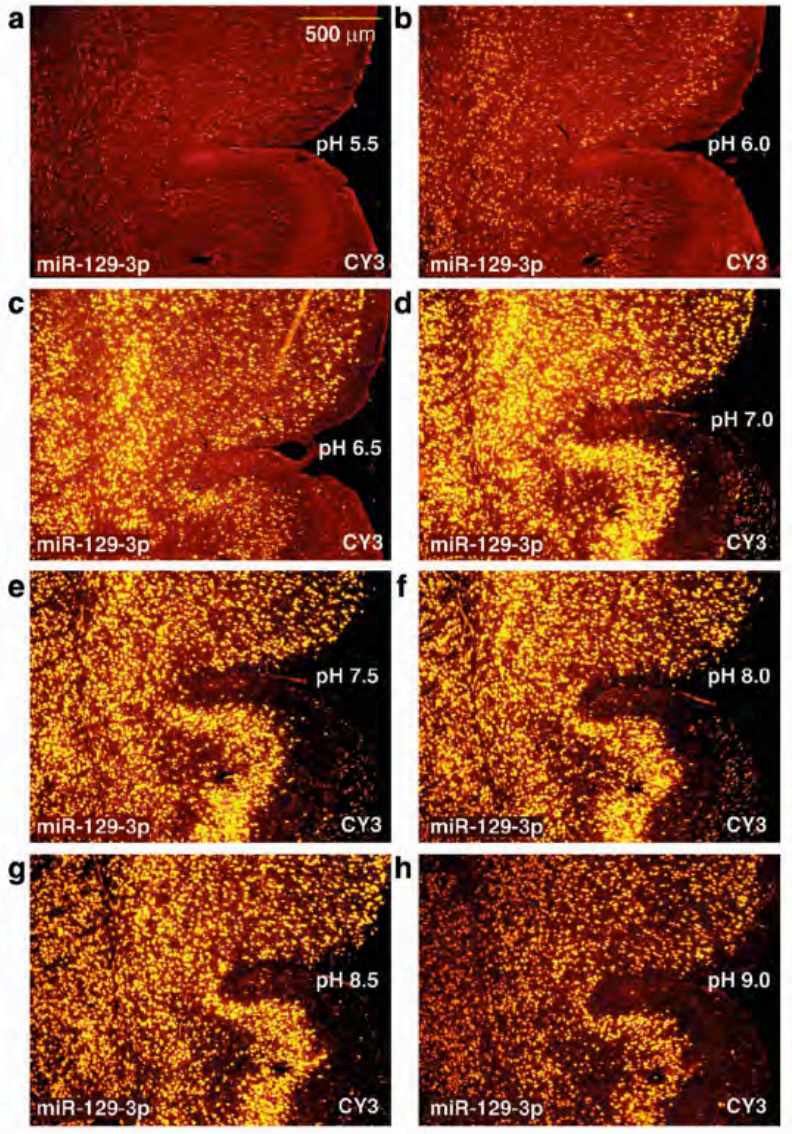

Figure 3: miRNA ISH signal intensity is EDC fixation pH dependent. (a) Low–power fluorescent micrograph images of mouse brain tissues fixed with formaldehyde and then EDC solution at pH 5.5 (**a**) and 6.0 (**b**) show reduced signal for miR–129–3p (**a–c**, Cy3; orange), compared to ISH signal for miR–129–3p in tissues fixed with EDC solution at pH 6.5 to 9.0 (**d–h**, Cy3; orange). Scale bars 500 μm in **a–h**.

We also evaluated an alternative method for permanently crosslinking the phosphate at the miRNA 5' end using the fixation reagent cyanogen bromide (BrCN), which also forms stable

phosphoamidate crosslinks by condensing phosphates to amino groups[204]. Using formaldehyde–fixed tissues, we applied 0.5 M BrCN in 0.16 M N-morpholinoethanesulfonate (MES)–buffer (initial MES buffer pH adjusted to 7.5) for 1 h. Formaldehyde–BrCN fixed tissues showed robust signal for miR-129-3p (**Fig. 4a**), while tissues fixed with formaldehyde alone show almost no staining (**Fig. 4b**), and the signal intensity of formaldehyde–BrCN tissues moderately improved the signal compared to formaldehyde–EDC (**Fig. 4a, c**). BrCN fixation alone showed no signal (data not shown). We examined the ISH signal strength as the BrCN solution pH varied (**Fig. 5 a–h**). At an initial MES buffer pH 5.5–9.0, we observed notably improved miRNA ISH signal for miR–129–3p (**Fig. 5 a–h)**. We settled on using BrCN at pH 7.5 (**Fig. 5e**). We also examined the dose dependence of BrCN (**Fig. 6a–h**) and the brightest signal for miR–129–3p occurred at 100 mM BrCN solution (**Fig. 6c**) diluted in 1 M MES solution (initial pH adjusted to 7.5). Advantages of the BrCN–formaldehyde fixation include faster reaction time, when compared to the 1-methylimidizole buffer for EDC, the MES buffer is more user friendly to handle and the MES buffer does not require handling under anhydrous conditions. However, BrCN is more toxic and needs to be handled with caution including proper management of cyanide waste.

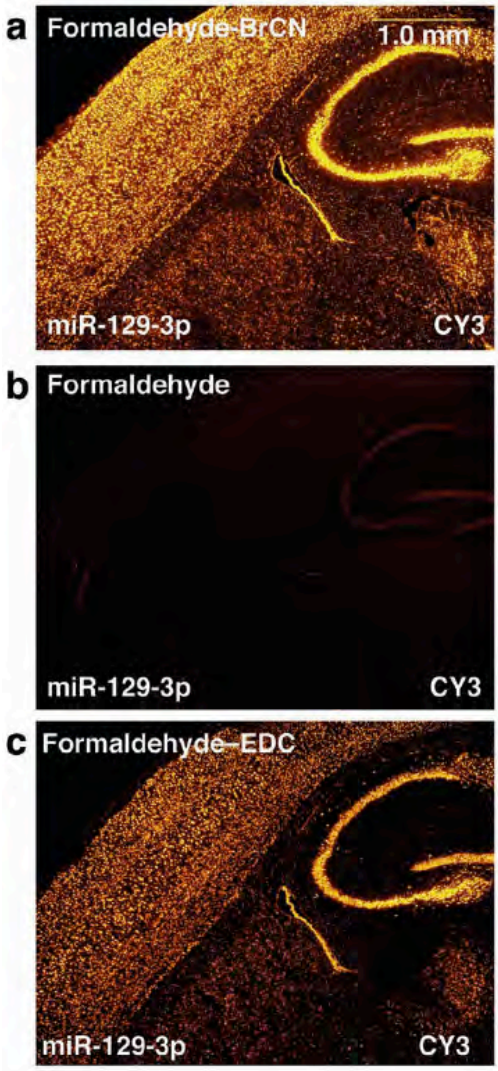

Figure 4: Fixation with formaldehyde–BrCN enhances miRNA ISH detection in tissues. Fluorescent micrograph images of the mouse cerebral cortex and hippocampus show expression of miR-129-3p (**a–c**, Cy3; orange) in tissue sections fixed with formaldehyde–BrCN fixation (**a**, Cy3; left), formaldehyde fixation (**b**, Cy3; left), and formaldehyde–EDC fixation (**c**, Cy3; left). Scale bars 1 mm in **a-c.**

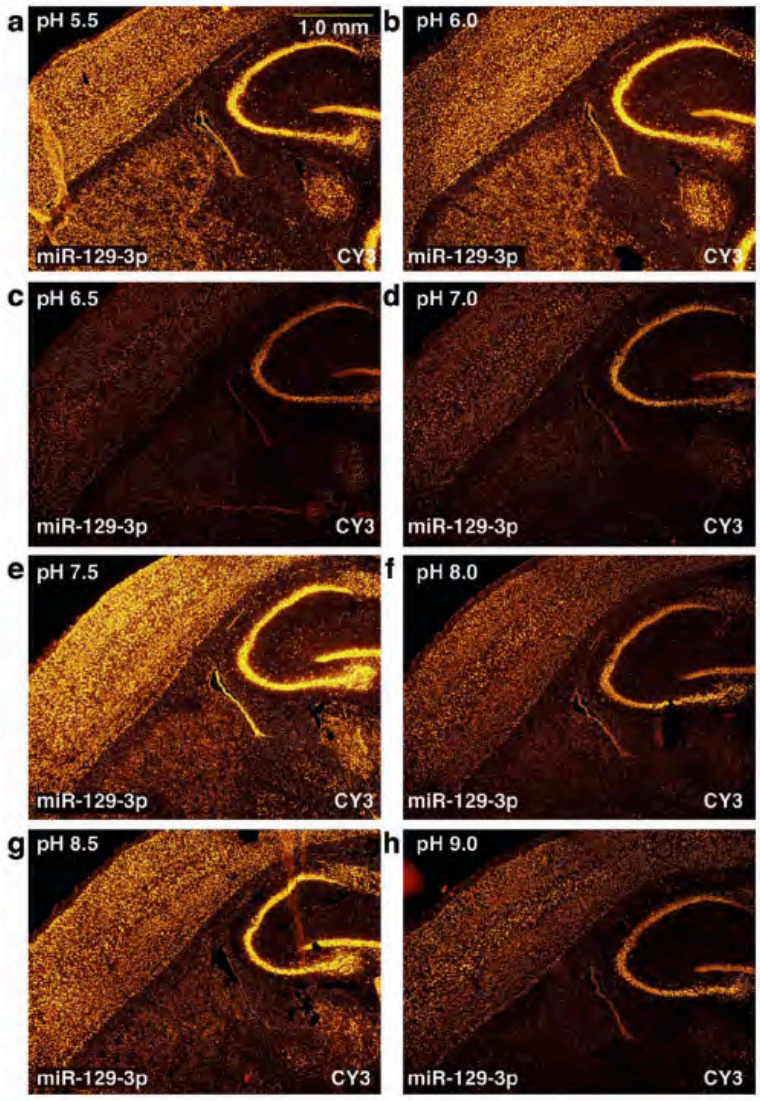

Figure 5: miRNA ISH signal strength for formaldehyde–BrCN tissue fixation is dependent on the BrCN solution pH. (a) Low–power fluorescent micrograph images of tissue sections of the mouse hippocampus and cerebral cortex from tissues fixed with formaldehyde–BrCN in MES buffer show expression of miR-129-3p (**a–h**, Cy3; orange). Images for miR–129–3p in tissues fixed with formaldehyde and subsequent BrCN in MES buffer adjusted to pH of pH 5.5–9.0 (**a-g**, Cy3; orange) with intense signal strength at pH 5.5, 6.0, 7.5, and 8.5 (**a-b, e, g**; Cy3; orange). Scale bars 1.0 mm in **a–h.**

Figure 6

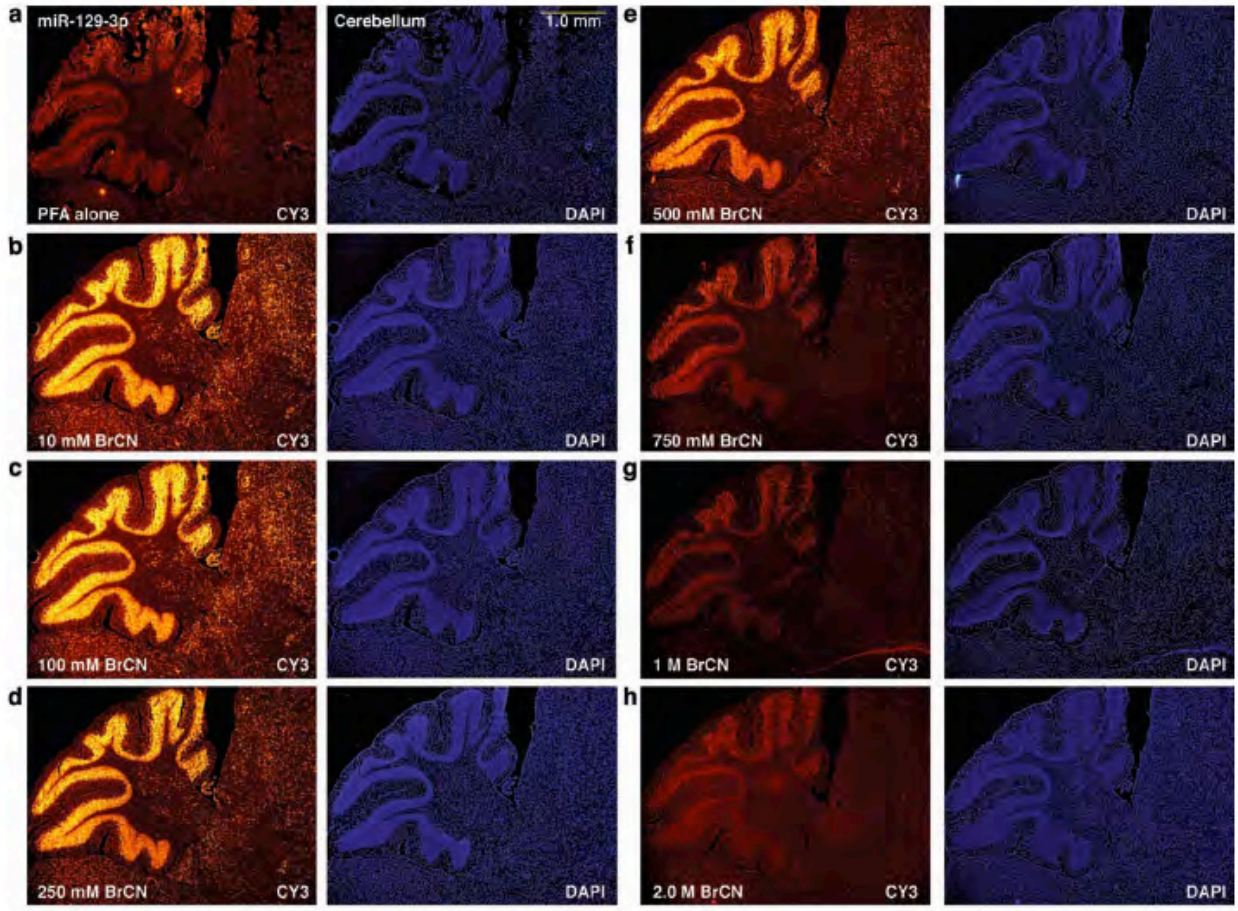

Figure 6: miRNA ISH signal strength for formaldehyde–BrCN tissue fixation is dose dependent. (a) Low–power fluorescent micrograph images of tissue sections of the mouse cerebellum from tissues fixed with formaldehyde–BrCN in MES buffer show expression of miR-129-3p (**a-h**, left, Cy3; orange). Images of tissues fixed with formaldehyde and subsequent BrCN at concentration of 10 mM to 500 mM show robust detection (**b-e**, left, Cy3; orange) with intense signal strength at 100 mM BrCN (**c**, rightCy3; orange). Nuclei were stained (DAPI, blue; right, **a–h**). Scale bars 1.0 mm in **a–h.**

To determine if applying the EDC and BrCN reagents in series results in results that are greater than either reagent alone. We tested tissues fixed with formaldehyde–EDC–BrCN and for

miR–129–3p the ISH signal was notably more intense than all other combinations (**Fig. 7 a–c**). These improvements may be due to synergistic mechanisms of action of the EDC and BrCN. In the presence of an N-morpholinoehanesulfonate (MES)–buffer, BrCN forms the condensed products considerably faster (1–3 min) than compared to the reaction rate of EDC in imidzole buffer (3–20 h)[204]. The rates of reactions suggest the mechanism of EDC and BrCN differ. The reaction efficiency for each reagent may depend on reacting groups or the adjacent nucleobases, suggesting a combination of formaldehyde–EDC–BrCN provides a wider coverage for miRNA varying in sequence, possibly improving the crosslinking efficiency for a diverse set of miRNAs.

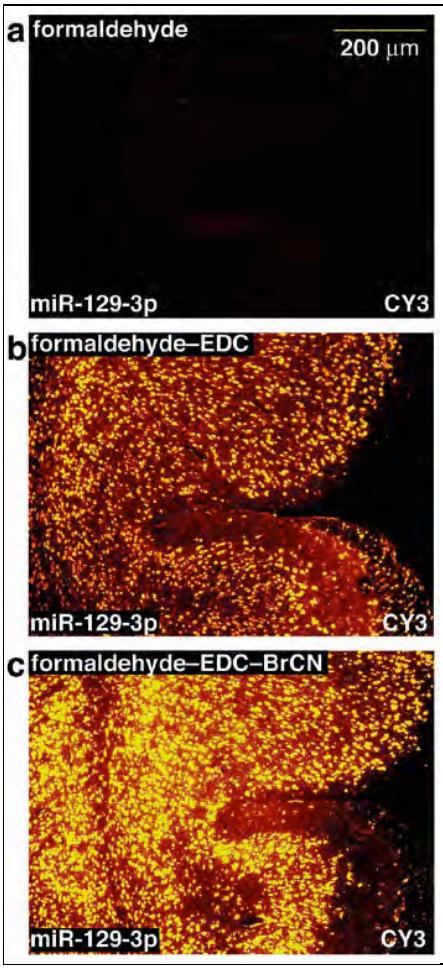

Figure 7: Fixation of with formaldehyde–EDC– BrCN improves microRNA detection in mammalian tissues. Fluorescent micrograph images of the mouse brain show expression of miR-129–3p (**a–c**, Cy3; orange) in tissue sections fixed with formaldehyde alone (**a**, Cy3; orange), formaldehyde–EDC solution diluted in 1–methylimidazole buffer at pH 7.5 (**c**, Cy3; orange) and formaldehyde–EDC–BrCN (**c**, Cy3; orange). Scale bars 200 µm in **a–c.**d

Application of miRNA ISH in other tissues

To broaden this method to other tissues, we conducted ISH in other tissues including the eye and liver. We fixed samples with formaldehyde–EDC–BrCN and then detected the miRNA using a series of enzymatic reactions with the product being a colorimetric precipitate of 5–bromo–4–chloro–3–indolyl phosphate (BCIP) and nitro blue tetrazolium (NBT). In the mouse eye, we were able to identify cell layer–specific staining for multiple miRNAs using this technique. While miR–124 (**Fig. 8a–b**) showed wide expression throughout the retina, let–7a expression displayed a more restricted expression pattern in ganglion cells, photoreceptor segments, and cells comprising the inner nuclear layer (**Fig. 8c–d**). In the mouse liver, we detected miR–122 and miR–26a (**Fig. 8e–f**) in hepatocytes and not the endothelium. In order to adapt this method to other samples or tissues, supplement existing ISH protocol by applying the formaldehyde–EDC or formaldehyde–BrCN fixation, or both combined.

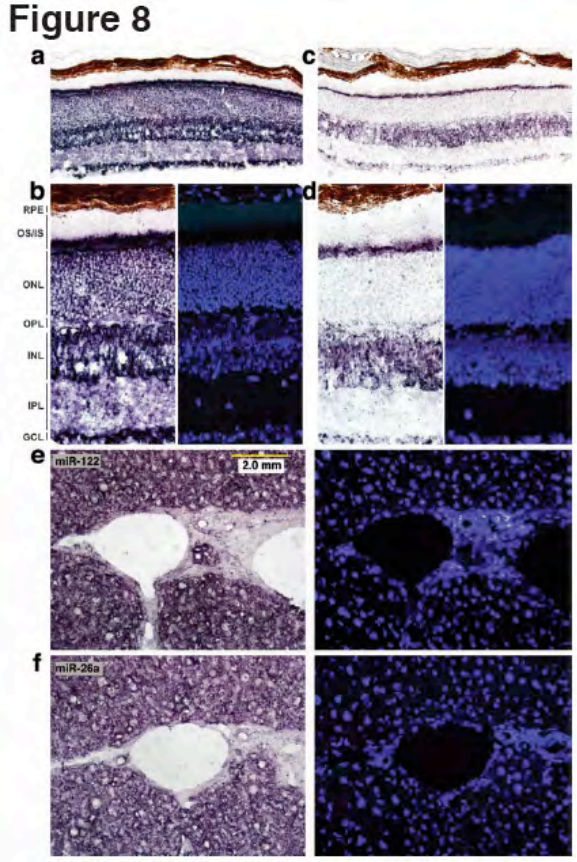

Figure 8: Detection of miRNAs in mouse eye and liver using alkaline phosphatase NBT/BCIP detection system. Low–power light microscopy images show staining of miR-124 in the mouse retina (**a–d**; Nitro blue tetrazolium chloride/5-Bromo–4-chloro–3–indolyl phosphate (NBT/BCIP); blue) and higher power images shown in **b** demonstrate staining in several layers of the retina (**b**, blue; retinal layers represented by; retinal pigment epithelium, RPE; photoreceptor outer and inner segment, OS/IS; outer nuclear layer, ONL; outer plexiform layer, OPL; inner nuclear layer, INL; inner plexiform layer, IPL; ganglion cell layer, GCL). (**c–d**) Low–power micrographs show specific staining of let–7a in the inner nuclear layer of the retina (**c**), and higher magnification images shown in d. Light microscopy micrographs show specific detection of miR–122 and miR–26a in hepatocytes using a pigment detection (**e–f**, NBT/BCIP; blue). Nuclei were stained (DAPI, blue; left, **b, d, e, f**). Scale bars 2.0 mm in **e–f.**

Automation of miRNA ISH protocol

To reduce the variability of the miRNA ISH procedure and to simultaneously process multiple samples in higher throughput, we automated the protocol on two mechanized platforms. First, we adapted the formaldehyde–EDC fixation procedure to the Ventana Molecular Discovery System, Discovery XT immunohistochemisty and *in situ* hybridization automated stainer. The tissue sections were processed on the Discovery XT, which automated the formaldehyde–EDC

fixation, probe hybridization, subsequent stringency washes and antibody staining, after which we manually applied a tyramide Cy3 detection system to obtain a positive signal for miR–124 (**Fig. 9a–b**). We also used a second high–throughput platform described by the Allen Institute for Brain Science[145]. Mouse brain tissue was manually fixed with formaldehyde–EDC–BrCN, then samples transferred to an automated platform developed on a Tecan liquid handling robot. The robot performed probe hybridization at 20ºC below the Tm, a series stringency washes and finally miRNA expression was detected with NBT/BCIP non-isotopic detection system. The slides were removed from the robot, cover–slipped and then images digitized and scanned on an automated high–throughput Aperio ScanScope(r) XT scanner. The miRNA ISH signal showed strong signal for miR–124 and let–7a (**Fig. 9c–f**), and were substantially more robust when compared to samples fixed with formaldehyde alone (data not shown).

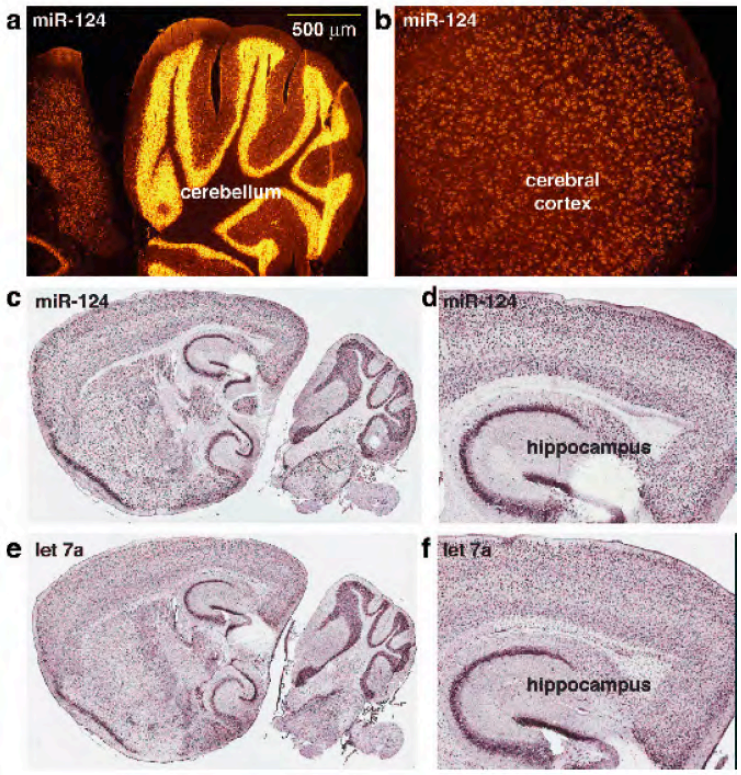

Figure 9: Automation of formaldehyde–EDC miRNA ISH protocol. Fluorescent micrograph images of the mouse cerebellum show expression of miR-124 (**a–b**, Cy3; orange) in tissue sections fixed with formaldehyde–EDC fixation (**a, top, b, left** Cy3;orange) after processing on a Ventana Discovery XT Automated Stainer. Light microcopy images show expression of miR–124 and let–7a at high and low power (**c, d**; alkaline phophatase NBT/BCIP; blue) and let–7a at high and lower magnification (**e, f** alkaline phophatase NBT/BCIP; blue).

In summary, the formaldehyde–EDC or formaldehyde–BrCN fixation prevents miRNA diffusion by generating a stable cross-link between the 5' miRNA phosphate and amino acid side chains, which substantially improves miRNA detection in tissues, most notably enabling detection of medium and lower abundant miRNAs. The advantage of formaldehyde–EDC or formaldehyde–BrCN, or formaldehyde–EDC–BrCN–based miRNA ISH is that fixation on the 5' end provides the probe with greater access to the miRNA target and less interference with probe hybridization, which facilitates detection. We show this method is useful in the mouse brain, liver, and eye tissue sections and that two detection systems are compatible with our approach.

Finally, automating the protocol allows the way for reliable high-throughput studies to map several hundred miRNAs in the brain and other organs, or for screening large tissue sets to associate miRNAs and disease.

Procedure

The protocol presented below has been optimized for the fresh-frozen mouse brain sections and a flow diagram outlining the procedure is presented (**Fig. 10**).

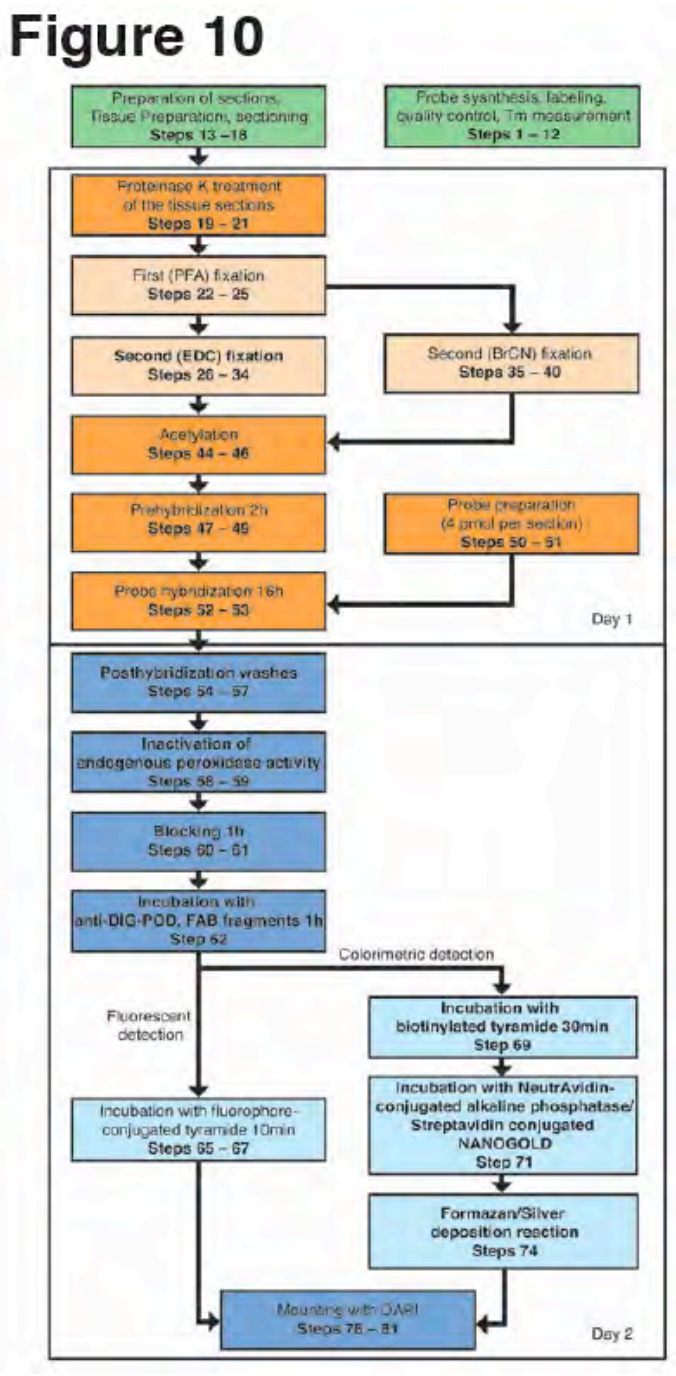

Designing and digoxigenin (DIG') labeling of probes

To design LNA–substituted DNA probes, obtain the miRNA sequence[89], then reverse complement the sequence, and replace approximately one third of the DNA nucleobases with an LNA base[142].

To decrease the probability that an oligonucleotide probe will from a hairpin with itself due

secondary structure, avoid substituting for LNA at positions of predicted secondary structure. A useful tool for predicting oligonucleotide secondary structure is freely available using mfold software (http://www.idtdna.com/Scitools/Applications/mFold/)[183]. Probes can be custom ordered from several commercial vendors using a 0.4 μM scale synthesis. The oligonucleotide probe must include a 3' amino modifier linker to enable digoxigenin conjugation.

We determine the LNA probe concentration by measuring the UV absorbance at 260 nm using an average absorbance coefficient of 11,000 $M^{-1}cm^{-1}$ per nucleotide. To conjugate the digoxigenin-label to the 3' end of the LNA probe, we use 30 nmol of the LNA that was dried in a concentrator and re-dissolve in 50 μl of 100 mM sodium carbonate buffer at pH 8.5. In a separate tube, we prepared 240 nmol of digoxigenin–3–O–methylcarbonyl–ε–aminocaproic acid–N–hydroxysuccinimide ester (Roche) dissolved in 50 μl anhydrous DMF. Mix 50 μl LNA probe solution with 50 μl of digoxigenin–3–O–methylcarbonyl–ε–aminocaproic acid–N–hydroxysuccinimide ester solution, then incubate the reaction for 16 h at 25ºC. The DIG-labeled probe is loaded on a 43 x 23 x 0.2 cm denaturing 18% PAGE gel (200 ml gel volume) with 8M urea, along with the unlabeled probe in an adjacent lane, then separate the products by electrophoresis for 6 h at 50 W. The product bands can be visualized by UV shadowing and the DIG–labeled probe shows reduced mobility compared to the starting material (**Fig. 11a)**. The typical yields are 80% of DIG labeled product, which is then excised and eluted from the gel slice by adding 3 volumes (w/v) of 0.3 M NaCl, incubated overnight, then precipitate with 3 volumes of ethanol and re-suspend in 100 μl water.

Quality control for DIG labeling of probes

DIG–labeling should be verified using an alkaline–phosphatase–based formazan blue detection system. Apply 1 pmol, 100 fmol and 10 fmol of the DIG–labeled LNA product on a positively charged nylon membrane followed by incubation of the membrane with anti–DIG antibody fragment conjugated to peroxidase antibody. Subsequent treatment with NBT/BCIP solution typically produces formazan blue deposition. In our experience, the reaction is completed within 10 min to 1 h, with the darkest staining for 1 pmol of LNA probe and less staining for lower amounts (**Fig. 11b**). Verification of LNA probe DIG labeling is a crucial quality control for ISH experiments.

Figure 11: 3' Labeling LNA probe with digoxigenin (DIG). 18% polyacrylamide gel after electrophoresis showing separation of 22–nt LNA probe targeting miR–129–3p labeled with DIG conjugated to the 3' end (**a, left, top band**) and the un–reacted probe below (**a, left, bottom band**), the unlabeled LNA probe (**a, right band**). 3' labeled LNA probe targeting miR–129–3p crosslinked to a H+ nylon membrane at 1 pmol, 100 fmol, and 10 fmol after reaction with NBT/BCIP substrate **(b).**

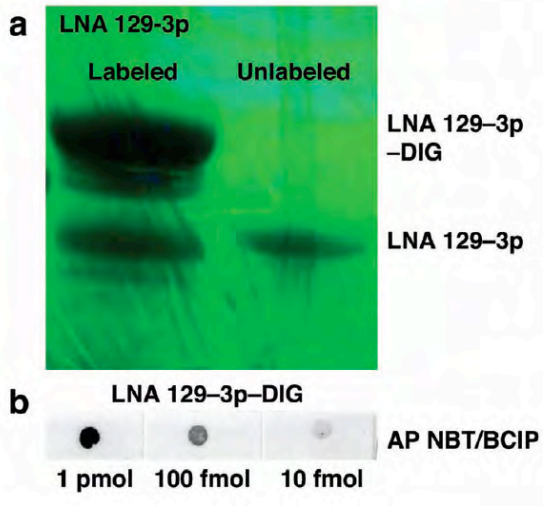

Designing ISH controls to assess specific miRNA staining

To differentiate miRNA signal from non-specific background staining due to the detection system or mishybridization of the probe, several controls and optimized hybridization conditions are necessary. We adjust the hybridization temperature to be approximately 20ºC below the

experimentally determined melting temperature (T_M)[147].

To rule out miRNA ISH signal derived from cross–hybridization, we conduct ISH experiments using serial sections. For the first tissue section, apply a probe that targets the mature miRNA. For the next serial section, use a probe that binds the opposing fragment in the miRNA duplex, known as the miRNA* sequence, or a probe that targets a cluster member miRNA, which exist in a polycistronic miRNA transcript. As for negative controls, a probe targeting a miRNA not expressed in the tissue of interest is ideal.

For maximum signal from miRNA ISH using the formaldehyde–EDC or formaldehyde–BrCN fixation method, it is imperative to refrain from using phosphate and carbonate–containing buffers prior to EDC fixation, as these buffers inhibit EDC or BrCN mediated condensation of the miRNA 5' phosphate and the amino group present in the tissue protein matrix. If phosphate–containing buffers are necessary, we recommend adequate removal of phosphate buffers by increasing the number of washes with imidizole buffer prior to EDC fixation or washes with MES buffer before BrCN application.

After fixation, a number of signal detection systems can be used to amplify or detect the miRNA–LNA signal. Our results were obtained using a tyramide signal amplification (TSA)–CY3 detection system that relies on an anti-DIG antibody conjugated to a peroxoidase enzyme. In our experience, the anti-DIG antibody activity is variable depending on the batch purchased from the vendor. For each lot of anti–DIG antibody, we evaluated the minimum concentration of antibody needed. For example, in these experiments we used the antibody using dilutions of 1:1000 and 1:500 to detect miR–129–3p in the mouse brain (**Fig. 12a**–**b**), however at antibody

dilutions of 1:250 and 1:100 the signal is not detected (**Fig. 12c–d**). We observed notable increases in signal intensity with negligible background staining (data not shown). These data suggest that antibody dilutions for detection are critical for optimizing miRNA ISH and in our experience. New batches of antibody require experiments to verify the optimal concentration.

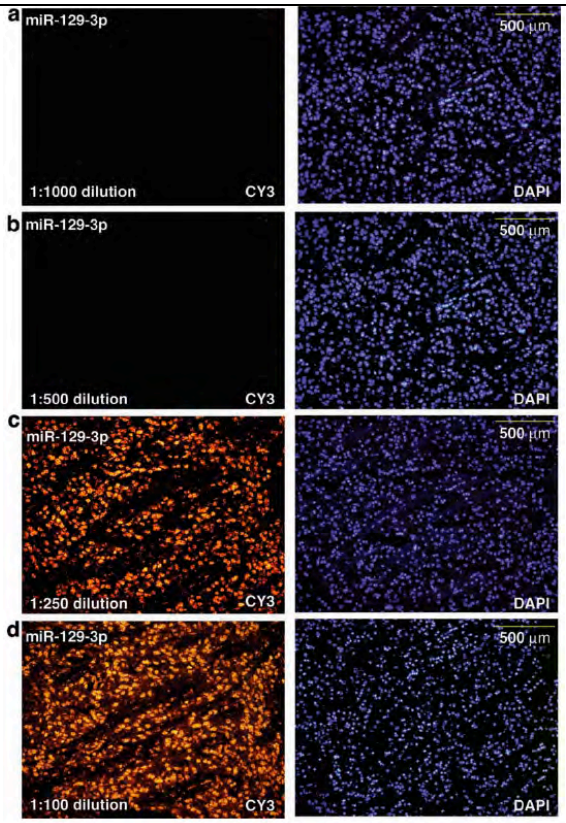

Figure 12: Dose curve for antibody concentration. (a) Low–power fluorescent micrograph images from the mouse brain showing miRNA ISH by applying dilutions of the Peroxidase (POD) detection antibody (**a–d**). Antibody diluted at 1:1000 and 1:500 show no signal for miR–129–3p (**a–b**, Cy3; orange) and ISH using antibody dilutions of 1:250 and 1:100 show staining (**c–d**, Cy3; orange). Scale bars 500 µm in **a-d.**

Methods and Materials

REAGENTS

All reagents use double distilled water (ddH2O).

Acetylation buffer CRITICAL STEP 5 min before use

873 µl of Triethanolamine ≥98% (Sigma cat. no. T1377–500ML).

375 µl Acetic anhydride ≥97.0% (Fisher cat. no. A10–500).

Fill to 75 ml with ddH_2O.

Alkaline phosphatase enzyme (Roche, Cat no 11093274910)

Antibody–blocking solution

0.1 g Blocking powder (heat gently in to solution)

1.0 ml heat inactivated goat serum (Sigma, cat. no. G9023–10ML)

20 µl Tween 20 (Sigma, cat. no. P1379-500 ml)

19 ml 1X TBS

Anti–Digoxigen–POD

Fab fragments 150 U/ml (Roche, cat. no. 11207733910)

Dilute Fab fragments in antibody blocking solution (1:100, however for each batch of antibody determine optimal concentration)

Blocking buffer (used for DIG labeling quality control)

1% Blocking reagent (Roche cat no. 11096176001)

dilute in maleic acid buffer

Cyanogen bromide (BrCN) solution, 1 ml CRITICAL STEP

10 µl of 5 M BrCN in acetonitrile (Sigma cat. no. 261610)

CRITICAL STEP Keep BrCN reagent under argon gas.

Dilute BrCN in 990 µl of MES buffer.

BrCN solution reacts quickly. Make BrCN solution immediately before use and discard unused solution. Discard BrCN reagent in a hazardous waste container.

Cryomold Standard (Sakura, cat. No. 4557)

Vectashield mounting medium for fluorescence with DAPI (Vector Laboratories, Inc., cat no H-1200)

DIG-labeled LNA probe stock

EDC buffer CRITICAL STEP

1.5 ml of 1–methylimidazole (Sigma Cat. No. 336092–1L). Keep under argon gas and protect from humidity.

15 ml of 3 M NaCl

100 ml dH2O

Adjust pH to 8.0 with HCl.

Fill to 150 mL with ddH_2O.

EDC solution CRITICAL STEP CAUTION

1 ml of 3 M NaCl

100 µl of 1-methylimidazole ≥99%

176 µl of EDC ≥97.0% (Sigma cat. no. 39391) Keep under argon gas and protect from humidity.

Adjust the pH to 8.0 with HCl.

Fill to 10 ml with ddH_2O.

Formamide wash buffer

50% Formamide (99% GC)

1X SSC

0.1% Tween 20

0.2% Glycine diluted in 1X TBS

Hybridization solution

In a siliconized tube, add 1 µl of 4 µM LNA probe stock diluted in 100 µl of hybridization buffer and mix.

(Approximately 1 µl of 4 µM LNA probe per tissue section.

Determining the optimal probe concentration is highly recommended.)

3% Hydrogen peroxide solution

5 ml of 30% Hydrogen Peroxide (Fisher, cat. no. H325–100)

45 ml of 1X TBS

0.1% Tween 20 (Sigma, cat. no. P1379-500 ml)

Individual Indirect Tyramide Reagent (PerkinElmer, cat. no. SAT700)

Dilute biotinyl tyramide reagent 1:50 in amplification diluent.

MES buffer, pH 7.5, for 30 ml

5.86 g of 2-(N-morphoino)ethanesufonic acid (MES) (Sigma cat. no.

M3671–250G)

20 ml of ddH_2O

600 µl of 1 M $MgCl_2$

1.5 ml of 3 M NaCl

Adjust pH to 7.5 with NaOH.

Adjust volume to 30 ml with ddH_2O.

Make immediately before use.

Discard unused solution.

4% Paraformaldehyde (PFA) in 1X TBS (16% Paraformaldehyde; Electron Microscopy Suites Cat. No. 15710) CAUTION

Pre-hybridization solution (store at –20ºC for up to 1 week)

10 ml Formamide 99% GC (Sigma cat. no. F7503–1L)

5.0 ml 20X SSC

2.0 ml 50X Denhardt's Reagent (Applichem cat. no. A3792,0050)

250 µl Baker's yeast tRNA 20 mg/ml (Sigma cat. no.

R8759–2KU), dilute stock powder with ddH_2O.

1.0 ml Salmon sperm DNA 10 mg/ml (Applichem, cat. no.

A2159,0001),), dilute stock powder with ddH_2O.

0.4 g Blocking reagent (Roche cat. no. 11096176001)

500 µl Chaps 100mM (Sigma cat. no. 198899-1ML-F)

100 µl Tween 20 (Sigma, cat. no. p1379-500 ml)

1150 µl dH_2O

Proteinase K (20 µg/ml) stock solution (Roche cat. no. 03115879001), diluted in water

NBT/BCIP stock solution (Roche, cat. no. 11 681 451 001)

Dilute NBT/BCIP stock in
0.1 M Tris–HCl
0.1 M NaCl
Adjusted pH to 9.5.

Nailpolish, clear

Obtain from local store

Neutravidin Alkaline Phosphatase conjugated 2 mg (Fisher Scientific, cat. no. PI–31002)

Neutravidin Alkaline Phosphatase conjugated blocking solution:

Dissolve 0.1 g Blocking powder in Maleate wash buffer.

Dilute Neutravidin 1:200 in blocking solution

Nitro blue tetrazolium chloride/5-Bromo–4-chloro–3–indolyl phosphate (NBT/BCIP Stock solution; Roche, cat. no. 11681451001)

Maleate wash buffer

10.45 g Maleic Acid

150 mM NaCl

0.05% Tween 20 (Sigma, cat. no. P1379-500 ml)

Maleic acid buffer

0.1 M Maleic Acid

0.15 M NaCl

Sigmacote (Sigma, cat. no. SL2–100mL)

Sodium carbonate (100 mM), pH adjusted to 8.5

20x SSC

175.3 g NaCl

88.2 g Sodium citrate

Adjust pH to 7.0 with NaOH.

Adjust volume to 1L with ddH_2O.

0.2X SSC Dilute 20X SSC to 0.2X SSC in ddH_2O.

0.5 M Sucrose in 1X TBS

TBS–Tween wash

1X TBS

0.1% Tween 20 (Sigma, cat. no. P1379-500 ml)

Tissue Tek O.C.T. compound (Sakura, cat. No. 4583)

TNT Buffer

10 mM Tris-HCl (pH 7.2)

150 mM NaCl

0.05% Tween 20 (Sigma, cat. no. P1379-500 ml)

TMN buffer (Prepare fresh before use)

100 mM Tris Base (pH 10.0)

500 mM NaCl

2 mM Tetramisole hydrochloride (Sigma, cat. no. T1512–10g)

0.05% Tween 20

Adjust pH to 9.5 with 5 M NaOH

1X Tris Buffered Saline (TBS) pH 7.4

10 ml of 1 M Tris-HCl (pH 7.4)

20 ml of 5 M NaCl

970 ml dH_2O

TSA–Plus Cyanine 3 System (PerkinElmer, cat. no. NEL744B001KT) working solution

Dilute cyanine 3 amplification reagent 1:50 in 1X amplification diluent.

Sodium Tris EDTA solution

500 mM NaCl

10 mM Tris HCl (pH 8.0)

5 mM EDTA

0.05% Tween 20

Vectashield DAPI + Mounting Media (Vector Laboratories, cat. no. H-1200)

REAGENT SETUP

TMN buffer, EDC buffer, EDC solution, MES buffer, and BrCN solution should be prepared fresh immediately prior to use. EDC stored at –20°C. BrCN in acetonitrile stored at 4ºC. CAUTION. CRITICAL STEP. EDC or BrCN reagent is disabled by humidity and must be kept under inert conditions by flushing the syringe with argon gas prior to withdrawing the EDC. CRITICAL STEP.

Equipment

Cryomold

Coplin jars (Electron Microcopy Sciences, cat. no. 70312–20)

Cryostat (Leica CM3050 S)

Cy3 filter (Chroma, cat. no. 49004 ET)

DAPI filter (Olympus, cat. no. U–MWU2)

27 1/2 gauge sterile needle

LifterSlips (Fisher, cat. no. 22–035–804)

InSlide Out Hybridization Oven (Boekel, cat. no. 241000)

Olympus BX51 microscope with DP70 camera

Olympus DP controller software

Olympus MicroSuite Five imaging software (http://www.olympusamerica.com)

Positively charged nylon transfer membrane (GE Healthcare, cat no RNP303B)

1.5 ml siliconized tubes (Bio Plas Inc, cat no 4165SL)

Stainless Steel Humidified Slide Rack (Aluminum tray and insert; Boekel, cat. no. C2403973, and C2403754 respectively)

1 ml sterile syringe

Stratalinker

SuperFrost Plus glass slides (Thermo Fisher Scientific, cat no 1255015)

Super PAP pen (Beckman Coulter cat. no. IM3580)

EQUIPMENT SETUP

Humidified Chamber

1 Humidified slide racks should be soaked with clean water prior to EDC or BrCN fixation, hybridization, antibody blocking steps, and detection.

Argon gas for EDC withdrawal.

Argon gas is used to layer the reagent with an inert gas such as argon. Store to exclude humidity as humidity leads to inactivation of the reagent.

Siliconize coverslips (LifterSlips) for hybridization

A Siliconize the LifterSlips by adding one drop (approximately 50 µl) of Sigmacote.

B Spread the Sigmacote evenly over the coverslip using a tissue or Kimwipe.

C Rinse with 5 ml ddH_2O then rinse with 5 ml 100% ethanol.

DIG labeling of the LNA probe

1 To 3'–digoxigenin–label the LNA probe, dry an aliquot of 30 nmol of the LNA probe in an Eppendorf tube using an Eppendorf concentrator.

2 Redissolve the LNA probe in 50 µl of 100 mM sodium carbonate buffer at pH 8.5.

3 In a separate tube, dissolve 240 nmol of digoxigenin-3–o–methylcarbonyl–ε–aminocaproic acid–N–hydroxysuccinimide ester (Roche) in 50 µl anhydrous DMF.

4 Mix solution prepared in step 2 with solution from step 3, then incubate the mixture for 16 h at 25ºC.

5 Separate the DIG–labeled probes on a 43 x 23 x 0.2 cm denaturing 18% PAGE gel (200 ml gel volume) for 6 h at 50 W in 1X TBE running buffer. The DIG labeled probe will show reduced mobility compared to the starting material (**Fig. 11a**).

6 Visualize the product bands by UV shadowing, excise the upper band (**Fig. 11a**) and place the gel slice in a 1.5 ml siliconized tube. The expected yield of a labeling reaction is 80%.

7 To elute the DIG-labeled LNA from the gel slice and add 3 volumes (w/v) of 0.3 M NaCl, incubate samples at 4ºC for 16 hr while rotating at 300 rpm. Then ethanol precipitate the solution by adding 3 volumes (v/v) of 100% cold ethanol. Incubate for 1 h at –20ºC, centrifuge at 12,000g, remove the supernatant and dry the pellet, then resuspend in 100 µl of ddH_2O.

Quality controlling DIG–labeled probes

8 To examine the efficiency of DIG–labeling, obtain a positively charged nylon transfer membrane and apply 1 pmol, 100 fmol and 10 fmol of DIG–labeled probe on to the membrane. Allow the membrane to dry for 10 min at 25ºC.

9 Expose the nylon membrane to UV crosslinking at 254 nm using 1200 J (UV stratalinker 2400, Stratagene).

10 Equilibrate the membrane by applying 1 ml of maleic acid buffer per 15 spotted DIG–labeled probes, for 10 seconds at 25ºC.

11 Remove the maleic acid buffer, and apply 1 ml of blocking buffer for 30 min at 25ºC.

12 Discard the blocking buffer and incubate the membrane with 1 ml of anti–DIG–AP Fab fragments (1:10,000 dilution in antibody blocking buffer) conjugated to alkaline phosphatase enzyme for 30 min at 25ºC.

13 Wash twice with maleate buffer for 15 min each at 25ºC.

14 Apply 20 µl of NBT/BCIP stock solution (Roche, cat no 11681451001) per 980 µl of 0.1 M Tris–HCl in 0.1 M NaCl, pH adjusted to 9.5. Apply 1 ml of this solution to the membrane and incubate for 10 min to 1 hr at 25ºC.

15 Formazan Blue deposition is observed between 10 min to 1 h for all amounts spotted and a positive reaction is shown (**Fig. 11b**).

Tissue preparation and processing

16 Sedate and anesthetize animals in accordance with NIH Animal Welfare guidelines using ketamine and xylazine cocktail. Perfuse animal with 50 ml of 1X TBS at pH 7.4, followed by 40 ml of 4% paraformaldehyde (PFA) pepared in 1X TBS.

17 Dissect organs and tissues of interest.

18 Immediately immerse the sample in 30 ml of 4% PFA in 1X TBS in a 50 ml Falcon tube for 16 h at 4ºC.

19 Transfer the specimen to a new 50 ml falcon tube containing 30 ml of 0.5 M sucrose diluted in 1X TBS and incubate the sample for 48 h at 4ºC.

Mounting Tissue Sections

20 Mount tissues in OCT Compound in a Cryomold, and position the immersed sample as desired. Then immediately freeze in dry–ice–ethanol bath. Liquid nitrogen is not a recommended method for flash freezing samples.

21 This step can be performed by using option A or option B, depending on the timing of the sectioning. PAUSE POINT

A. Immediately section the tissues at 5–40 µm using a cryostat or microtome, then mount sections on SuperFrost Plus glass slides.

B. Unprocessed specimen or mounted slides can be stored for up to four months at –80ºC.

Proteinase K treatment

22 Thaw and air–dry tissue mounted slides for 1 h at 25ºC.

23 Draw a hydrophobic barrier encircling the tissue section using a Super PAP Pen, PAP Pen, or nail polish, then allow barrier to dry before continuing.

24 Incubate the tissue-mounted slides in a coplin jar containing 75 ml of 1X TBS with 37.5 µl of 20 µg/ml proteinase K stock solution for 20 min at 25ºC. Avoid using phosphate–containing buffers, such as phosphate buffered saline (PBS), prior to the EDC or BrCN fixation step, as this interferes with EDC and BrCN fixation.

Formaldehyde tissue fixation

25 Wash slides twice in 75 ml of 1X TBS for 5 min at 25ºC.

26 Fix tissue sections in 40 ml of 4% formaldehyde diluted in 1X TBS for 10 min at 25ºC.

CRITICAL STEP Prepare fresh formaldehyde for each experiment.

27 Wash the slides in 0.2% (w/v) glycine diluted in 1X TBS for 5 min at 25ºC.

28 Wash twice with 1X TBS for 5 min at 25ºC.

Option A, Fixation of tissues with EDC

29 Prepare 150 ml of EDC buffer as described in *Reagents* section and prepare a humidified chamber.

30 CRITICIAL STEP Avoid using phosphate buffered saline before fixation. Using buffers containing phosphates interferes with EDC and BrCN fixation and should not be used.

31 This step can be performed by using fixation option A (EDC) or option B (BrCN), depending on preference for fixative.

32 Incubate slides in 75 ml of freshly prepared EDC buffer for 10 min at 25ºC. CRITICAL STEP. Check pH of EDC buffer (pH 8.0) before use.

33 Repeat wash step and prepare EDC solution during second incubation.

CRITICAL STEP Store EDC at –20ºC. Handle the reagent under anhydrous conditions by protecting the stock EDC reagent with a layer of argon. EDC is liable in aqueous solutions therefore apply EDC solution to the slides quickly. Aqueous solutions containing EDC and/or 1–methylimidazole cannot be stored and unused EDC solution should be discarded. CAUTION EDC should be handled according to the MSDS guidelines.

34 Check pH of EDC solution (pH 8.0) before use. EDC reactivity is dependant on pH. CRITICAL STEP

35 In a humidified chamber, place slides face up in a slide rack. Remove EDC wash buffer by tilting the slide and decanting the solution.

36 Add 500 µl of EDC solution to each slide and incubate samples for at least 1 h (up to 2 h) at 25ºC in a sealed humidified chamber.

37 Decant EDC solution into a hazardous waste container. EDC reagent is hazardous. See MSDS for details in handing and disposing of the reagent. CAUTION

Option B, Tissue fixation with BrCN

38 In a humidified chamber, place slides face up in a slide rack. Remove wash buffers by tilting the slide and decanting the solution.

39 Apply 1 ml of freshly prepared MES buffer to the slides for 10 min at 25ºC. Check pH of MES buffer (pH 7.5) before use. Note, checking the initial pH of the MES buffer is crucial as fluctuations in pH reduce signal intensity. CRITICAL STEP

40 Repeat wash step and prepare BrCN solution immediately following the second incubation.

CRITICAL STEP Store BrCN at 4ºC. Handle the reagent under anhydrous conditions by protecting the stock BrCN solution with a layer of argon. After adding BrCN to the MES buffer, apply the BrCN solution to the slides quickly. Aqueous solutions containing BrCN cannot be stored. Discard the remaining reagent. CAUTION BrCN should be handled according to the MSDS guidelines.

41 Immediately add BrCN solution. CRITICAL STEP BrCN in MES buffer reacts rapidly, and applying the solution to the slides quickly is crucial.

42 Add 1 ml of BrCN solution to each slide and incubate samples for 20 min to 1 h at 25ºC in a sealed humidified chamber. Repeat step 39.

43 BrCN reagent is hazardous. Decant BrCN solution into a hazardous waste container. See MSDS for details in handing and disposing of the reagent. CAUTION

For formaldehyde–EDC–BrCN fixation, follow steps 22–43.

Wash steps after fixation

44 For the remainder of the protocol, use either 1X TBS or phosphate buffer saline (PBS, pH 7.4) to wash slides after fixation.

45 Wash the slides with 75 ml of 0.2% (w/v) glycine diluted in 1X TBS for 5 min at 25ºC.

46 Wash the samples twice with 75 ml of 1X TBS for 5 min at 25ºC.

Acetylation for inactivation of enzymes in tissues

47 Prepare fresh acetylation buffer immediately before use and mix vigorously by shaking.

48 Incubate slides in 75 ml of acetylation buffer for 30 min at 25ºC. (OPTIONAL Place a small magnetic stir bar at the bottom of the coplin jar to continuously mix the solution during the incubation.)

49 Rinse slides twice in 75 ml of 1X TBS for 5 min at 25ºC.

Pre–hybridization and hybridization of probe and microRNA

50 Place the slides with the tissue side up on a slide rack in a humidified chamber.

51 Add 500 µl of freshly prepared pre–hybridization solution to each slide within the hydrophobic barrier. Incubate slides in a sealed humidified chamber for 1–4 h at 25ºC.

52 Remove pre–hybridization buffer by tilting the slide and decant the solution.

Preparing the probe and Hybridization

53 Select the desired probes and pre–heat hybridization oven to the appropriate hybridization temperature, approximately 20ºC below the T_M.

54 In a siliconized 1.5 ml tube, mix 100 µl of hybridization buffer, with 1 µl of 4 µM LNA probe directly into the buffer. For typical mouse brain sections we use 1 µl of 4 µM LNA probe per tissue section.

55 Add 100 µl hybridization solution to each slide and gently place the coverslip (siliconized LifterSlips) over the tissue sections. Avoid forming bubbles below the coverslip. When testing more than one probe, handle the slides carefully to prevent cross contamination between probes.

56 Incubate the slides in a sealed humidified chamber for 16 h at the hybridization temperature, typically which is 20ºC below the T_M of the experimentally determined miRNA–LNA probe duplex.

Post–hybridization stringency washes

CRITICAL STEP When working with more than one probe, assign one Coplin jar for each probe. This will help prevent cross–contamination during the wash steps.

57 Prepare a small container, (e.g. lid of a pipette tips box). Immerse the slides in 20 ml of 5X SSC at 25ºC to remove the coverslip.

58 Wash the samples two times in a Coplin jar filled with 75 ml of 50% formamide–1X SSC–0.1% Tween 20 for 30 min at respective hybridization temperature.

59 Wash the samples in 75 ml of 0.2X SSC for 15 min at 25 ºC.

60 Rinse the samples in 75 ml of TBS–Tween Wash for 5 min at 25 ºC.

Inactivation of endogenous peroxidase activity

61 Incubate the slides in 75 ml of 3% hydrogen peroxide solution for 30 min at 25 ºC.

CRITICAL STEP Hydrogen peroxide is used to block endogenous peroxidases before the Anti–Digoxigen–POD antibody is added and expired hydrogen peroxide can lead to high background levels.

62 Wash the slides three times in 75 ml of TBS–Tween Wash for 5 min at 25 ºC.

Anti–DIG detection and Peroxidase conjugation

63 Place the slides horizontally, face up in a humidified slide rack and add 500 µl of antibody blocking solution to each slide within the hydrophobic barrier. Incubate for 1 h at 25ºC.

64 Remove antibody–blocking solution by tilting the slides and decant the solution.

65 Dilute the Anti–Digoxigen–POD, FAB fragments in antibody blocking solution, and add 500 µl to each slide within the hydrophobic barrier. Incubate for 1 h at 25ºC.

66 Wash the slides as described below.

67 This step can be performed by using option A or option B, depending on preference of the detection. For fluorescent detection use option A, for tissues not amenable to fluorescent detection, use option B.

A. Cy3 fluorescent detection system

68 Wash the slides two times in 75 ml of TBS–Tween Wash for 15 min at 25 ºC.

69 Place the slides with the tissue side face up in a humidified slide rack and add 200 µl of TSA Plus Cy3 System working solution onto to the sections for 10 min at 25ºC in the dark.

70 Wash the slides three times in 75 ml of TBS–Tween Wash for 5 min at 25 ºC on a tilting rotator, proceed to step 78.

B. Alkaline phosphatase detection system

71 Wash the slides three times in 75 ml of TNT buffer for 5 min at 25 ºC.

72 Place the slides face up in a humidified slide rack and add 250 µl of the Individual Indirect Tyramide Reagent kit working solution to each slide and incubate for 30 min at 25ºC.

73 Washed the slides three times in 75 ml of maleate wash buffer for 5 min at 25 ºC.

74 Place the slides horizontally, face up in a humidified slide rack and apply a 1:200 dilution of NeutrAvidin–conjugated alkaline phosphatase in maleate buffer supplemented with 10 mg/ml blocking reagent. Apply 500 µl to each slide for 40 min at 25ºC.

75 Wash the slides two times in 75 ml of maleate buffer for 5 min at 25 ºC

76 Wash the slides four times in 75 ml of TMN buffer for 5 min at 25 ºC

77 Dilute 200 µl of NBT/BCIP stock solution in 10 ml TMN buffer. Place the slides face up in a humidified slide rack and add 250 µl of the solution to each slide for 30 min at 25ºC.

While incubating, protect the samples from light. Note: the time to form Formazan Blue deposits (blue color) may vary between samples. Typically the reaction finishes after 30 min.

78 Immerse the slides two times in 75 ml of water upon completion of the reaction for 20 sec at 25ºC.

79 Wash the slides three times in 75 ml of Sodium Tris EDTA solution for 5 min at 25 ºC.

80 Incubate slides in 80 ml of 4% formaldehyde solution for 10 min at 25 ºC.

Mounting slides for microscopy

81 Mount the slides using 2 drops of Vectashield mounting medium with DAPI.

82 Carefully place a glass coverslip over the tissue sections.

83 Seal glass coverslip by covering the edges the coverslip with clear nail polish and allow to air dry.

84 Store samples and protect from light.

Microscopy

85 Images were captured on an Olympus BX50 microscope equipped with a DP70 camera and Olympus DP controller software.

TIMING

Step 1–15, probe preparation: four to several days

Steps 16–21, tissue preparation and processing, mounting tissue sections: 3 d

Steps 22–24, proteinase K treatment 1 h 20 min

Steps 25–28, tissue fixation formaldehyde: 40 min

Steps 29–37, tissue fixation with EDC:1 h 20 min

Steps 38–43, tissue fixation with BrCN: 30 min

Steps 44–49, wash steps and acetylation: 40 min

Step 50–51, prehybridization: 1–4 h

Step 52–56, hybridization: 16 h

Steps 57–60, post-hybridization stringency washes: 1 h 25 min

Steps 61–62, inactivation of endogenous peroxidases: 33 min

Steps 63–67, anti–DIG detection and Peroxidase conjugation: 1 h

Steps 68–70, Cy3 fluorescent detection system: 55 min

Steps 71–80, alkaline phosphatase detection system: 3 h 5 min

Steps 81–83, mounting slides for microscopy: 5 min

Steps 84, microscopy: 30 min to 2 h

Troubleshooting

Here we present common pitfalls and areas of the miRNA ISH protocol that can be adjusted to optimize the signal. Troubleshooting suggestions are presented in the table below.

Problem	Possible reason	Solution
Tissue detaches from slide during ISH procedure.	• Drying time insufficient. • Glass slides need special coating to hold on to tissue.	• Increase drying time. • Use Superfrost Plus microscopy slides. • Apply substrates such as poly–L lysine or gelatin to coat microscopy slide.
High background levels in the blank and test samples.	• Endogenously expressed peroxidase enzymes present and were not adequately inhibited. • Concentration of the POD–antibody is too high. • Tissue folds due to cryostat sectioning or ISH procedure and intense staining present in folded regions.	• Increase acetylation time to inhibit endogenous peroxidase activity. • Check the activity of hydrogen peroxide as this reagent expires and loses its activity. Also increase hydrogen peroxide concentration. • Conduct a dose curve to determine the minimal amount of antibody necessary. • Optimize the time and concentration of TSA reagent. • For alkaline phosphatase NBT/BCIP detection, use and optimize the dose of levamisole to inhibit endogenous alkaline phosphatase activity. • To avoid folds in the tissue while using the cryostat, adjust the cryostat temperature to improve sectioning. • Tissue folding can solved by altering the coating of the glass slides
No signal	• miRNA is not expressed. • miRNA has been lost to diffusion prior to EDC fixation. • Insufficient DIG labeling of the probe. • Probe may have secondary structure and poorly hybridizes. • Melting temperature of the probe–miRNA is inaccurate. • EDC reagent may have been exposed to air, and unreactive. The shelf life of the EDC reagent is approximately 1 week after initial use. • The concentration of the antibody used for detection is too	• Check miRNA cloning expression atlas to verify miRNA is expressed in the tissue of interest. • At temperatures above 37ºC, formaldehyde crosslinks are susceptible to reversion and subsequent miRNA diffusion, keeping samples stored at –80ºC greatly reduces the rate of crosslink reversion. • Verify the LNA probe is properly DIG labeled using a dot blot and the detection system described. • LNA probe may not be optimal for hybridization. Alter the positions of the LNA residues, which greatly enhance the ISH signal.

	low. • Using solutions that contain phosphates or carbonate, such as PBS, inhibit EDC or BrCN crosslinking.	• For miRNA with secondary structure, increasing the concentration of the probe, however adequate controls are necessary to rule out cross–hybridization. • Conduct miRNA–LNA probe melting temperature experiment as described[147]. • Replace EDC reagent with a new vial. • Conduct a dose curve for antibody. • Substitute phosphate buffers for TBS buffers, as TBS does not interfere with EDC or BrCN fixation.
LNA probe does not hybridize or DIG labeling is not verified.	•DIG labeling inefficient. •Probe or miRNA contains significant. secondary structure and poorly hybridizes. •Repeated freezing and thawing of the probe damages the reagent.	• Test probe using a dot blot and if test is negative, perform DIG' labeling again. • Change the position of the LNA residue and avoid inserting at positions of predicted secondary structure. • Store LNA probe in aliquots to prevent repeated freezing and thawing.

Conclusion

We present the results of a typical miRNA ISH experiments in **Fig. 1–5**. For highly abundant miRNAs, we observed a moderate improvement of the miRNA ISH signal in tissues fixed with formaldehyde–EDC, when compared to the formaldehyde alone[147]. For the medium and low abundant miRNAs, using the formaldehyde–EDC fixation results in substantial improvement of the miRNA ISH signal (**Fig. 1 a, c**), when compared samples fixed with formaldehyde alone (**Fig. 1 b, d**). In our experience, a successful miRNA ISH experiments using formaldehyde–EDC fixed tissues depend on the adequate crosslinking of miRNA using EDC buffer at an optimized pH (**Fig. 3a–h**) and accurately determining the hybridization conditions[147]. In summary, this EDC–based miRNA ISH protocol provides a sensitive method for detecting miRNAs in the brain, eye, and liver, and should be easily adapted to other tissue types.

Appendix

Supplementary tables and charts

Supplementary Table 1 List of miRNA, LNA probes and star sequence probes used in this study, as well as melting profiles of miRNA/LNA probe pair.

miRNA	Sequence (5' to 3')	LNA probe	Sequence (5' to 3')[†]	Transcription unit	Exiqon T_M (ºC)[††]	Exp T_M (ºC)	T_M(up) –T_M(down) (ºC) [†††]	ISH confirmed
mmu-miR-21	UAGCUUAUCAGACUGAUGUUGA	LNA-21	TC[A]AC[A]TC[A]GTCT[G]AT[A]AGC[T]A	cluster-mmu-mir-21(1)	63.0	64.5	1.2	Y
mmu-let-7i	UGAGGUAGUAGUUUGUGCUGUU	LNA-let-7i	AA[C]AG[C]AC[A]A[A]CT[A]CTA[C]C[T]CA	cluster-mmu-mir-let-7i(1)	69.0	69.8	1.3	Y
mmu-miR-101a	UACAGUACUGUGAUAACUGAA	LNA-101a	T[T]C[A]G[T]T[A]T[C]ACA[G]TA[C]TGTA	cluster-mmu-mir-101a(1)	63.0	66.6	0.2	Y
mmu-miR-133a	UUUGGUCCCCUUCAACCAGCUG	LNA-133a	C[A]GC[T]GG[T]TG[A]AGG[G]G[A]CCA[A]A	cluster-mmu-mir-1-2(2), cluster-mmu-mir-1-1(2)	75.0	79.8	0.9	Y
mmu-miR-1	UGGAAUGUAAAGAAGUAUGUAU	LNA-1	ATA[C]ATA[C]T[T]C[T]TTA[C]AT[T]C[C]A	cluster-mmu-mir-1-1(2), cluster-mmu-mir-1-2(2)	61.1	77.6	1.9	Y
mmu-miR-124	UAAGGCACGCGGUGAAUGCC	LNA-124	GGCA[T][T]C[A]CCGCGTGCC[T][T][A]	cluster-mmu-mir-124-1(1), cluster-mmu-mir-124-2(1), cluster-mmu-mir-124-3(1)	75.0	67.5	1.1	Y
mmu-miR-126	UCGUACCGUGAGUAAUAAUGCG	LNA-126	C[G]CG[T]ACC[A]A[A][A]GT[A]AT[A]ATG	cluster-mmu-mir-126(1)	65.0	60.6	0.5	
mmu-miR-126*	UCGUACCGUGAGUAAUAAUGCG	LNA-126*	CGCA[T]TAT[T]AC[T]C[A]CGG[T][A]CGA	cluster-mmu-mir-126(1)	66.0	71.4	1.0	Y
mmu-miR-136	ACUCCAUUUGUUUUGAUGAUGG	LNA-136	CCATC[A][T]C[A]A[A][A]CA[A]ATGG[A]G[T]	cluster-mmu-mir-127(13)	65.0	58.4	0.2	
mmu-miR-434-5p	GCUCGACUCAUGGUUUGAACCA	LNA-434-5p	TGG[T]TCA[A]ACCA[T]GA[G]TC[G]AGC	cluster-mmu-mir-127(13)	68.0	63.9	0.9	Y
mmu-miR-370	GCCUGCUGGGGUGGAACCUGGU	LNA-370	A[C]CA[G]GT[T]CC[A]CCCC[A]GC[A]GGC	cluster-mmu-mir-127(13)	82.0	80.1	1.0	Y
mmu-miR-431	UGUCUUGCAGGCCGUCAUGCA	LNA-431	TGCA[T]G[A]C[G]G[C]CTGCA[A]G[A]C[A]	cluster-mmu-mir-127(13)	79.0	77.1	0.8	
mmu-miR-673-3p	UCCGGGGCUGAGUUCUGUGCACC	LNA-673-3p	GG[T]GC[A]CA[G]AA[C]TC[A]GC[C]CC[G]GA	cluster-mmu-mir-127(13)	83.0	80.8	0.2	
mmu-miR-341	UCGGUCGAUCGGUCGGUCGGU	LNA-341	A[C]CG[A]CCGA[C]CG[A]TCG[A]CC[G]A	cluster-mmu-mir-127(13)	79.0	73.7	0.6	
mmu-miR-770-5p	AGCACCACGUGUCUGGGCCACG	LNA-770-5p	CGTG[G]CC[C]AG[A]CACG[T]GG[T]G[C]T	cluster-mmu-mir-127(13)	81.0	83.0	3.3	
mmu-miR-770-3p	CGUGGGCCUGACGUGGAGCUGG	LNA-770-3p	C[C]AG[C]TC[C]ACGT[C]AG[G]CC[C]ACG	cluster-mmu-mir-127(13)	81.0	85.1	0.1	
mmu-miR-128a/128b	UCACAGUGAACCGGUCUCUUU	LNA-128a	A[A]AG[A]GA[C]CG[G]TTC[A]CT[G]TGA	cluster-mmu-mir-128a(1), cluster-mmu-mir-128b(1)	69.0	70.4	0.8	Y
mmu-miR-129	CUUUUUGCGGUCUGGGCUUGC	LNA-129	G[C]A[A]GC[C]CA[G]AC[C]GC[A]AA[A]AG	cluster-mmu-mir-129-1(2), cluster-mmu-mir-129-2(1)	76.0	74.0	2.2	Y
mmu-miR-130a	CAGUGCAAUGUUAAAAGGGCAU	LNA-130a	ATGCCC[T]TT[T]A[A]C[A]T[T]GCAC[T]G	cluster-mmu-mir-130a(1)	65.0	64.5	0.1	Y
mmu-miR-132	UAACAGUCUACAGCCAUGGUCG	LNA-132	C[G]ACCA[T]GG[C]TGT[A]GA[C]TGT[T]A	cluster-mmu-mir-132(2)	71.0	65.9	7.6	Y
mmu-miR-379	UGGUAGACUAUGGAACGUAGG	LNA-379	CCTACG[T]TCC[A]TAG[T]CT[A]CC[A]	cluster-mmu-mir-134(33)	63.0	59.9	0.4	
mmu-miR-300	UAUGCAAGGGCAAGCUCUCUUC	LNA-300	GAA[G]AG[A]G[C]TTGC[C]CT[T]GCA[T]A	cluster-mmu-mir-134(33)	71.0	75.8	1.3	
mmu-miR-410	AAUAUAACACAGAUGGCCUGU	LNA-410	ACAG[G]C[C]A[T]CTGT[G]T[T]A[T]A[T]T	cluster-mmu-mir-134(33)	66.0	72.1	1.4	Y
mmu-miR-134	UGUGACUGGUUGACCAGAGGGG	LNA-134	C[C]CC[T]CTGG[T]CA[A]CCAG[T]CA[C]A	cluster-mmu-mir-134(33)	74.0	74.3	1.5	Y
mmu-miR-485	AGAGGCUGGCCGUGAUGAAUUC	LNA-485	G[A]AT[T]CA[T]CA[C]GG[C]CA[G]CC[T]CT	cluster-mmu-mir-134(33)	74.0	77.5	1.5	
mmu-miR-382	GAAGUUGUUCGUGGUGGAUUCG	LNA-382	CG[A]AT[C]CA[C]CACG[A]AC[A]AC[T]TC	cluster-mmu-mir-134(33)	69.0	66.9	2.0	
mmu-miR-381	UAUACAAGGGCAAGCUCUCUGU	LNA-381	ACAGAG[A]GCTTG[C]C[C]TTGTA[T]A	cluster-mmu-mir-134(33)	66.0	65.7	1.1	
mmu-miR-411	UAGUAGACCGUAUAGCGUACG	LNA-411	CGT[A]CGC[T]A[T]ACGGT[C]TA[C]TA	cluster-mmu-mir-134(33)	64.0	66.5	1.4	
mmu-miR-376b	AUCAUAGAGGAACAUCCACUU	LNA-376b	AA[G]TGGA[T]G[T]T[C]CTC[T]A[T]G[A]T	cluster-mmu-mir-134(33)	65.0	69.9	1.5	
mmu-miR-32	UAUUGCACAUUACUAAGUUGCA	LNA-32	TGCA[A]CT[T]A[G]TA[A]T[G]TGCAA[T]A	cluster-mmu-mir-32(1)	61.0	56.3	0.8	
mmu-miR-135a	UAUGGCUUUUUAUUCCUAUGUGA	LNA-135a	T[C]AC[A]TAGGA[A]TA[A]A[A]A[G]CC[A]TA	cluster-mmu-mir-135a-1(2),	62.0	55.3	0.3	

				cluster-mmu-mir-135a-2(1)				
mmu-let-7g	UGAGGUAGUAGUUUGUACAGUU	LNA-let-7g	AA[C]TGTA[C]A[A]ACTAC[T]AC[C]T[C]A	cluster-mmu-mir-135a-1(3)	64.0	62.4	1.4	Y
mmu-miR-135b	UAUGGCUUUUCAUUCCUAUGUGA	LNA-135b	T[C]ACATA[G]G[A]ATG[A]AA[A]GC[C]A[T]A	cluster-mmu-mir-135b(1)	68.0	62.5	0.9	Y
mmu-miR-139	UCUACAGUGCACGUGUCUCCAG	LNA-139	CTG[G]AG[A]CA[C]GT[G]CA[C]TG[T]A[G]A	cluster-mmu-mir-139(1)	76.0	75.9	1.2	
mmu-miR-140	CAGUGGUUUUACCCUAUGGUAG	LNA-140	C[T]ACC[A]T[A]GGGT[A]AA[A]CC[A]C[T]G	cluster-mmu-mir-140(1)	67.0	65.1	1.1	Y
mmu-miR-140*	UACCACAGGGUAGAACCACGG	LNA-140*	C[C]GT[G]GT[T]CTACC[C]TG[T]GGTA	cluster-mmu-mir-140(1)	72.0			Y
mmu-miR-141	UAACACUGUCUGGUAAAGAUGG	LNA-141	CCA[T]CT[T]TA[C]C[A]GA[C]AG[T]G[T]TA	cluster-mmu-mir-141(2)	67.0	69.2	1.2	
mmu-miR-200c	UAAUACUGCCGGGUAAUGAUGGA	LNA-200c	TCC[A]TC[A]TTAC[C]CGGC[A]GTA[T]TA	cluster-mmu-mir-141(2)	66.0	58.8	0.1	
mmu-miR-142-5p	CAUAAAGUAGAAAGCACUACU	LNA-142-5p	AGTAG[T]G[C]T[T]TCTACT[T]TA[T]G	cluster-mmu-mir-142(1)	58.0	57.7	0.6	
mmu-miR-142-3p	UGUAGUGUUUCCUACUUUAUGGA	LNA-142-3p	T[C]CA[T]AA[A]GTAG[G]AA[A]C[A]CTACA	cluster-mmu-mir-142(1)	63.0	59.7	0.8	
mmu-miR-143	UGAGAUGAAGCACUGUAGCUCU	LNA-143	[A]GAGC[T][A]C[A]G[T]GCT[T]C[A][T]C[T]C[A]	cluster-mmu-mir-143(2)	73.0	78.5	0.3	Y
mmu-miR-145	GUCCAGUUUUCCCAGGAAUCCCU	LNA-145	AGG[G]AT[T]CCT[G]GG[A]AA[A]CT[G]G[A]C	cluster-mmu-mir-143(2)	76.0	74.7	0.8	
mmu-miR-144	UACAGUAUAGAUGAUGUACU	LNA-144	A[G]TACA[T]C[A]T[C]TA[T]A[C]TG[T]A	cluster-mmu-mir-144(2)	59.0	65.7	1.4	
mmu-miR-451	AAACCGUUACCAUUACUGAGUU	LNA-451	A[A]C[T]CA[G]TA[A]TG[G]TA[A]CG[G]T[T]T	cluster-mmu-mir-144(2)	63.0	62.9	1.7	
mmu-miR-146a	UGAGAACUGAAUUCCAUGGGUU	LNA-146a	AA[C]CC[A]T[G]GAAT[T]CA[G]TTCT[C]A	cluster-mmu-mir-146a(1)	68.0	68.9	1.2	
mmu-miR-152	UCAGUGCAUGACAGAACUUGG	LNA-152	C[C]A[A]G[T]T[C]T[G]TCA[T]G[C]A[C]TGA	cluster-mmu-mir-152(1)	73.0	76.0	1.2	
mmu-miR-153	UUGCAUAGUCACAAAAGUGAUC	LNA-153	G[A]TCAC[T]TT[T]GTGA[C]TA[T]G[C]AA	cluster-mmu-mir-153(1)	73.0	61.0	1.1	Y
mmu-miR-15a	UAGCAGCACAUAAUGGUUUGUG	LNA-15a	CACA[A]AC[C]AT[T]ATGTG[C]TG[C]TA	cluster-mmu-mir-15a(4)	64.0	61.0	1.4	Y
mmu-miR-16	UAGCAGCACGUAAAUAUUGGCG	LNA-16	CG[C]CAA[T]AT[T]T[A]CG[T]GC[T]G[C]TAT	cluster-mmu-mir-15a(2),	65.0	71.2	1.1	Y
				cluster-mmu-mir-15b(2)				
mmu-miR-17	CAAAGUGCUUACAGUGCAGGUAG	LNA-17	C[T]AC[C]TGC[A]CT[G]TA[A]GCA[C]TT[T]G	cluster-mmu-mir-17(6)	69.0	70.1	1.1	
mmu-miR-181b	AACAUUCAUUGCUGUCGGUGGGU	LNA-181b	A[C]CC[A]CC[G]ACA[G]CA[A]TG[A]AT[G]TT	cluster-mmu-mir-181a-2(2),	73.0	69.0	1.5	
				cluster-mmu-mir-181a-1(2)				
mmu-miR-500	AAUGCACCUGGGCAAGGGUUCA	LNA-500	TG[A]AC[C]CT[T]G[C]CC[A]GG[T]G[C]A[T]T	cluster-mmu-mir-188(5)	80.0	87.3	0.2	
mmu-miR-188-5p	CAUCCCUUGCAUGGUGGAGGG	LNA-188-5p	CCCT[C]C[A]CC[A]TG[C]AAGGGA[T]G	cluster-mmu-mir-188(5)	73.0	69.2	1.0	
mmu-miR-191	CAACGGAAUCCCAAAAGCAGCUG	LNA-191	CAG[C]TG[C]TT[T]TGG[G]AT[T]CCGT[T]G	cluster-mmu-mir-191(2)	70.0	72.9	1.1	Y
mmu-miR-425	AAUGACACGAUCACUCCCGUUGA	LNA-425	TC[A]ACG[G]GAG[T]G[A]TCGTGTCA[T]T	cluster-mmu-mir-191(2)	70.0	64.3	1.0	
mmu-miR-497	CAGCAGCACACUGUGGUUUGUA	LNA-497	T[A]CA[A]AC[C]ACAGT[G]TG[C]TGCTG	cluster-mmu-mir-195(2)	69.0	63.3	0.8	Y
mmu-miR-200a	UAACACUGUCUGGUAACGAUGU	LNA-200a	ACA[T]C[G]T[T]A[C]C[A]G[A]CAGTGTT[A]	cluster-mmu-mir-200a(3)	68.0	70.0	0.7	
mmu-miR-200b	UAAUACUGCCUGGUAAUGAUGA	LNA-200b	T[C]A[T]CA[T]TAC[C]AG[G]CAGTAT[T]A	cluster-mmu-mir-200a(3)	63.0	54.7	0.4	
mmu-miR-204	UUCCCUUUGUCAUCCUAUGCCU	LNA-204	AG[G]CA[T]AG[G]ATG[A]CA[A]AG[G]G[A]A	cluster-mmu-mir-204(1)	68.7	68.7	1.0	
mmu-miR-205	UCCUUCAUUCCACCGGAGUCUG	LNA-205	C[A]G[A]CTCCGG[T]GGA[A][T]G[A][A]GG[A]	cluster-mmu-mir-205(1)	75.0	70.1	1.2	
mmu-miR-216a	UAAUCUCAGCUGGCAACUGUGA	LNA-216a	T[C]ACAGT[T]G[C]C[A]GCTG[A]G[A]T[T]A	cluster-mmu-mir-216a(3)	71.0	70.0	1.1	
mmu-miR-217	UACUGCAUCAGGAACUGACUGGA	LNA-217	T[C]CA[G]TCA[G]TT[C]CTG[A]TG[C]AG[T]A	cluster-mmu-mir-216a(3)	72.0	70.4	0.6	
mmu-miR-218	UUGUGCUUGAUCUAACCAUGU	LNA-218	A[C]A[T]GGT[T]A[G]A[T]CA[A]GCAC[A]A	cluster-mmu-mir-218-1(1),	69.0	66.3	1.2	
				cluster-mmu-mir-218-2(1)				
mmu-miR-22	AAGCUGCCAGUUGAAGAACUGU	LNA-22	[A]CAGTT[C]TT[C]AACTG[G]CA[G]C[T]T	cluster-mmu-mir-22(1)	66.0	65.2	0.1	Y
mmu-miR-222	AGCUACAUCUGGCUACUGGGU	LNA-222	A[C]CC[A]G[T]AGC[C]A[G]A[T]G[T]A[G]CT	cluster-mmu-mir-221(2)	78.0	73.7	0.9	
mmu-miR-27b	UUCACAGUGGCUAAGUUCUGC	LNA-27b	GCAG[A]A[C]T[T]A[G]C[C]ACTGTG[A]A	cluster-mmu-mir-23a(6)	69.0	68.0	1.2	
mmu-miR-23b	AUCACAUUGCCAGGGAUUACC	LNA-23b	GGTAA[T]CCCTG[G]CAA[T]G[T]GAT	cluster-mmu-mir-23a(6)	66.0	68.0	1.2	
mmu-miR-27a	UUCACAGUGGCUAAGUUCCGC	LNA-27a	GCGG[A]ACT[T]AGCCACTGTG[A]A	cluster-mmu-mir-23a(6)	65.0	61.9	1.3	Y
mmu-miR-23a	AUCACAUUGCCAGGGAUUUCC	LNA-23a	GG[A]AA[T]CCC[T]G[G]CA[A]TGTG[A]T	cluster-mmu-mir-23a(6)	68.0	68.8	0.7	

mmu-miR-93	CAAAGUGCUGUUCGUGCAGGUAG	LNA-93	C[T]A[C]CTGC[A]CG[A]A[C]AGC[A]CT[T]TG	cluster-mmu-mir-25(3)	72.0	71.4	1.1	
mmu-miR-26a	UUCAAGUAAUCCAGGAUAGGCU	LNA-26a	[A][G]CC[T]A[T]CC[T]GG[A]TT[A]C[T]T[G][A]A	cluster-mmu-mir-26a-1(1), cluster-mmu-mir-26a-2(1), cluster-mmu-mir-26a-3(1)	69.0	74.4	1.2	Y
mmu-miR-26b	UUCAAGUAAUUCAGGAUAGGU	LNA-26b	A[C]C[T]A[T]C[C]T[G]AATT[A]CTT[G]AA	cluster-mmu-mir-26b(1)	64.0	76.0	1.1	Y
mmu-miR-28*	CACUAGAUUGUGAGCUGCUGGA	LNA-28*	TC[C]AG[C]AG[C]TCACAA[T]C[T]AGTG	cluster-mmu-mir-28(1)	69.0	65.9	1.1	
mmu-miR-28	AAGGAGCUCACAGUCUAUUGAG	LNA-28	CTCAA[T]A[G]A[C]TGTGAGC[T]C[C]TT	cluster-mmu-mir-28(1)	65.0	70.1	1.2	Y
mmu-miR-298	GGCAGAGGAGGGCUGUUCUUCCC	LNA-298	GGG[A]A[G]A[A]C[A]GCCC[T]C[C]T[C]T[G]CC	cluster-mmu-mir-296(2)	78.0	83.5	3.9	
mmu-miR-296-3p	GAGGGUUGGGUGGAGGCUCUCC	LNA-296-3p	GGAG[A]G[C]CTCC[A]CC[C]AA[C]CC[T]C	cluster-mmu-mir-296(2)	78.0	80.6	3.0	
mmu-miR-467a	UAAGUGCCUGCAUGUAUAUGCG	LNA-467a	CGCA[T]AT[A]CA[T]GCAGG[C]ACTTA	cluster-mmu-mir-297a-1(46)	66.0	60.7	0.4	Y
mmu-miR-29a	UAGCACCAUCUGAAAUCGGUUA	LNA-29a	T[A]ACC[G]ATT[T]CA[G]A[T]GGTG[C]TA	cluster-mmu-mir-29a(4)	68.0	68.1	1.0	Y
mmu-miR-29b	UAGCACCAUUUGAAAUCAGUGUU	LNA-29b	A[A]CACT[G][A]TT[T]C[A]A[A][T]GGTGC[T]A	cluster-mmu-mir-29a(2), cluster-mmu-mir-29b-2(2)	68.0	64.2	0.6	
mmu-miR-29c	UAGCACCAUUUGAAAUCGGUUA	LNA-29c	T[A]ACCG[A]TT[T]CA[A]A[T]GGTG[C]TA	cluster-mmu-mir-29a(4)	64.0	60.2	0.8	
mmu-miR-30a	UGUAAACAUCCUCGACUGGAAG	LNA-30a	C[T]TCC[A]G[T]CG[A]GG[A]TGTT[T]AC[A]	cluster-mmu-mir-30a(4)	68.0	67.4	0.6	Y
mmu-miR-30c	UGUAAACAUCCUACACUCUCAGC	LNA-30c	GC[T]G[A]G[A]GTGTAG[G]ATG[T]T[T]ACA	cluster-mmu-mir-30c-1(2), cluster-mmu-mir-30a(2)	68.0	67.4	1.2	
mmu-miR-30e*	CUUUCAGUCGGAUGUUUACAGC	LNA-30e*	G[C]TG[T]AA[A]CA[T]CC[G]ACTG[A]AAG	cluster-mmu-mir-30a(4)	67.0	63.2	1.8	
mmu-miR-30e	UGUAAACAUCCUUGACUGGAAG	LNA-30e	CTTCC[A]G[T]CA[A]GG[A]T[G]TT[T]AC[A]	cluster-mmu-mir-30a(4)	66.0	67.4	0.1	
mmu-miR-30d	UGUAAACAUCCCCGACUGGAAG	LNA-30d	C[T]TCC[A]G[T]C[G]GGG[A]TG[T]T[T]ACA	cluster-mmu-mir-30b(2)	66.0	75.2	1.6	Y
mmu-miR-322	CAGCAGCAAUUCAUGUUUUGGA	LNA-322	TTCA[A]AA[C]ATGAA[T]TG[C]TG[C]TG	cluster-mmu-mir-322(7)	63.0	53.2	1.4	
mmu-miR-384-5p	UGUAAACAAUUCCUAGGCAAUGU	LNA-384-5p	ACA[T]T[G]C[C]T[A]G[G]AA[T]TGTTT[A]CA	cluster-mmu-mir-325(2)	66.0	68.9	1.2	
mmu-miR-384-3p	AUUCCUAGAAAUUGUUCACAAU	LNA-384-3p	ATTG[T]GA[A]CAAT[T]T[C]T[A]G[G]A[A]T	cluster-mmu-mir-325(2)	66.0	62.5	1.0	
mmu-miR-335	UCAAGAGCAAUAACGAAAAAUGU	LNA-335	ACA[T]T[T]T[T]CGT[T]AT[T]GCT[C]T[T]GA	cluster-mmu-mir-335(1)	62.0	65.9	1.2	
mmu-miR-34c	AGGCAGUGUAGUUAGCUGAUUGC	LNA-34c	GCAA[T]C[A]GCTA[A]CT[A]CA[C]TG[C]CT	cluster-mmu-mir-34b(2)	70.0	67.4	1.1	
mmu-miR-378	ACUGGACUUGGAGUCAGAAGG	LNA-378	CC[T]T[C]T[G]ACT[C]C[A]A[G]TC[C]A[G]T	cluster-mmu-mir-378(1)	72.0	77.0	2.3	
mmu-miR-488	UUGAAAGGCUGUUUCUUGGUCU	LNA-488	A[G]ACCA[A]GAAA[C]AGC[C]TTTC[A]A	cluster-mmu-mir-488(1)	66.0	56.9	1.1	
mmu-miR-672	UGAGGUUGGUGUACUGUGUGUGA	LNA-672	TC[A]C[A]C[A]CA[G]T[A]CA[C]C[A]A[C]C[T]CA	cluster-mmu-mir-672(1)	75.0	77.2	1.2	
mmu-miR-708*	CAACUAGACUGUGAGCUUCUAG	LNA-708*	CTAGA[A]G[C]T[C]A[C]A[G]TCTAGT[T]G	cluster-mmu-mir-708(1)	66.0	69.2	1.3	
mmu-miR-708	AAGGAGCUUACAAUCUAGCUGGG	LNA-708	C[C]CAGCTA[G]A[T]TG[T]AAGCTC[C]TT	cluster-mmu-mir-708(1)	67.0	63.3	0.8	
mmu-miR-744	UGCGGGGCUAGGGCUAACAGCA	LNA-744	TGC[T]GT[T]AGC[C]CT[A]GC[C]CC[G]CA	cluster-mmu-mir-744(1)	79.0	81.2	1.0	Y
mmu-miR-7a	UGGAAGACUAGUGAUUUUGUUGU	LNA-7a	AC[A]ACA[A]AA[T]CA[C]T[A]GT[C]TT[C]CA	cluster-mmu-mir-7a-1(1), cluster-mmu-mir-7a-2(1)	66.0	64.5	1.3	Y
mmu-miR-872	AAGGUUACUUGUUAGUUCAGG	LNA-872	CC[T]G[A]A[C]T[A][A]CAAG[T]A[A]CCTT	cluster-mmu-mir-872(1)	64.0	65.0	0.5	Y
mmu-miR-874	CUGCCCUGGCCCGAGGGACCGA	LNA-874	T[C]GG[T]CCCT[C]GGGCC[A]GGG[C]AG	cluster-mmu-mir-874(1)	82.0	85.0	1.2	
mmu-miR-877	GUAGAGGAGAUGGCGCAGGG	LNA-877	CC[C]TG[C]G[C]CA[T]CT[C]CT[C]T[A]C	cluster-mmu-mir-877-1(2)	77.0	82.5	0.8	
mmu-miR-879	AGAGGCUUAUAGCUCUAAGCC	LNA-879	GGC[T]TA[G]A[G]C[T]A[T]AA[G]CCT[C]T	cluster-mmu-mir-879(1)	67.0	69.1	1.8	
mmu-miR-9	UCUUUGGUUAUCUAGCUGUAUGA	LNA-9	[T]C[A][T][A]C[A]GCT[A]G[A]T[A][A]CC[A][A]AG[A]	cluster-mmu-mir-9-1(1), cluster-mmu-mir-9-2(1)	70.0	69.8	1.2	Y
mmu-miR-9*	AUAAAGCUAGAUAACCGAAAGU	LNA-9*	AC[T]T[T]C[G]GTT[A]TC[T]A[G]CT[T]T[A]T	cluster-mmu-mir-9-1(3)	63.0	70.8	0.5	Y
mmu-let-7a	UGAGGUAGUAGGUUGUAUAGUU	LNA-let-7a	A[A]CT[A]TA[C]AA[C]CTA[C]TA[C]C[T]CA	cluster-mmu-mir-let-7a-1(3), cluster-mmu-mir-100(3)	66.0	66.4	1.1	Y

mmu-let-7d	AGAGGUAGUAGGUUGCAUAGUU	LNA-let-7d	AA[C]TATG[C]AA[C]CTA[C]TA[C]CT[C]T	cluster-mmu-mir-98(13)	67.0	69.7	1.1	Y
mmu-let-7f	UGAGGUAGUAGAUUGUAUAGUU	LNA-let-7f	A[A][C]TATA[C]AAT[C]TA[C]TA[C]C[T][C]A	cluster-mmu-mir-let-7a-1(3), cluster-mmu-mir-98(2)	64.0	67.2	1.0	Y
mmu-let-7b	UGAGGUAGUAGGUUGUGUGGUU	LNA-let-7b	A[A]CC[A]CA[C]AA[C]CT[A]CT[A]CC[T]CA	cluster-mmu-mir-98(13)	71.0	69.0	0.2	Y
mmu-miR-99a	AACCCGUAGAUCCGAUCUUGUG	LNA-99a	C[A]C[A]AGA[T]C[G][G][A]TCT[A]CG[G]G[T]T	cluster-mmu-mir-98(13)	76.0	77.0	1.1	Y
mmu-miR-125b	UCCCUGAGACCCUAACUUGUGA	LNA-125b	[T]C[A]C[A]AG[T]T[A]GGG[T]CTC[A]GGGA	cluster-mmu-mir-100(3), cluster-mmu-mir-99a(3)	70.0	72.8	0.7	
mmu-let-7c	UGAGGUAGUAGGUUGUAUGGUU	LNA-let-7c	[A][A]CC[A]TAC[A][A]CCTAC[T][A]CC[T]C[A]	cluster-mmu-mir-99a(3), cluster-mmu-mir-let-7b(2)	65.0	67.2	0.9	Y
mmu-miR-99b	CACCCGUAGAACCGACCUUGCG	LNA-99b	C[G]CA[A]GG[T]CG[G]TT[C]TACG[G]G[T]G	cluster-mmu-mir-99b(3)	78.0	76.8	0.9	Y
mmu-miR-125a	UCCCUGAGACCCUUUAACCUGUGA	LNA-125a	T[C]ACAG[G]T[T]A[A]AG[G]GTCTCAG[G]GA	cluster-mmu-mir-99b(3)	72.0	68.8	0.9	
mmu-let-7e	UGAGGUAGGAGGUUGUAUAGUU	LNA-let-7e	AA[C]T[A]TA[C]A[A]CC[T]C[C]TACC[T]CA	cluster-mmu-mir-99b(3)	66.0	73.1	0.5	Y
mmu-miR-7b	UGGAAGACUUGUGAUUUUGUUGU	LNA-7b	AC[A]AC[A]AA[A]TC[A]CAAGT[C]TTC[C]A	cluster-mmu-mir-7b(1)	64.0	55.8	0.4	
mmu-miR-149	UCUGGCUCCGUGUCUUCACUCCC	LNA-149	GGG[A]GTGAA[G]ACACG[G]AG[C]CA[G]A	cluster-mmu-mir-149(1)	76.0	67.4	0.5	
mmu-miR-223	UGUCAGUUUGUCAAAUACCCCA	LNA-223	TG[G]GGTA[T]T[T]GACAA[A]C[T]GA[C]A	cluster-mmu-mir-223(1)	68.0	64.3	0.1	
mmu-miR-133b	UUUGGUCCCCUUCAACCAGCUA	LNA-133b	TA[G]CT[G]GT[T]GA[A]GGG[G]ACCA[A]A	cluster-mmu-mir-133b(2)	72.0	76.8	1.2	
mmu-miR-203	GUGAAAUGUUUAGGACCACUAG	LNA-203	C[T]AGT[G]GT[C]CTAAACA[T]TT[C]A[C]	cluster-mmu-mir-203(1)	65.0	63.6	0.1	
mmu-miR-671	UCCGGUUCUCAGGGCUCCACC	LNA-671	GG[T]GG[A]GCCCTG[A]G[A]A[C]CGG[A]	cluster-mmu-mir-671(1)	78.0	77.3	0.6	
mmu-miR-122	UGGAGUGUGACAAUGGUGUUUG	LNA-122	CA[A]ACA[C]C[A]TTGT[C]AC[A]C[T]C[C]A	cluster-mmu-mir-122(1)	71.0	73.0	1.1	Y
mmu-miR-486	UCCUGUACUGAGCUGCCCCGAG	LNA-486	C[T]CGGGGC[A]GCTC[A]GTA[C]AGG[A]	cluster-mmu-mir-486(1)	74.0	67.9	0.9	
mmu-miR-455	GCAGUCCACGGGCAUAUACAC	LNA-455	GT[G]TA[T]AT[G]CCC[G]TGGA[C]T[G]C	cluster-mmu-mir-455(1)	71.0	72.7	0.9	
mmu-miR-551b	GCGACCCAUACUUGGUUUCAG	LNA-551b	CT[G]AA[A]CCAA[G]T[A]TGGGT[C]GC	cluster-mmu-mir-551b(1)	68.0	66.1	0.5	
mmu-miR-449b	AGGCAGUGUUGUUAGCUGGC	LNA-449b	ACCAGCT[A]AC[A]AT[A]C[A]CTGC[C]A	cluster-mmu-mir-449a(2)	68.0	61.8	0.4	
mmu-miR-107	AGCAGCAUUGUACAGGGCUAUCA	LNA-107	TGA[T]AGCC[C]TG[T]A[C]AA[T]GCTG[C]T	cluster-mmu-mir-107(1)	71.0	71.6	0.4	
mmu-miR-10a	UACCCUGUAGAUCCGAAUUUGUG	LNA-10a	CACA[A]AT[T]CG[G]ATCTAC[A]GGGTA	cluster-mmu-mir-10a(1)	63.0	60.4	0.2	

† LNA-modified DNA positions are marked in square brackets.

†† Exiqon T_M (ºC) was calculated with 50 mM salt concentration and 1.5 µM total oligo (target + probe) concentration.

††† Difference between the melting temperature of denaturation (up) and melting temperature of renaturation (down).

Table Supplementary Table 2. List of miRNA clone counts and frequencies from mouse cerebellum, prefrontal cortex, parietal cortex and hypothalamus.

miRNA profiles were derived from 454 sequencing of small RNA cDNA libraries prepared from size-fractionated total RNA. Mouse miRNA precursors were mapped to the genome. Host transcripts were identified and the unigene ID together with the name and an identifier. Furthermore it is indicated whether the miRNA gene is expressed in the cerebellum, prefrontal cortex, parietal cortex or hypothalamus.

*"Summation of clone counts" represents the summation of clone counts derived from the five regions of mouse brain analyzed.

	Summation of clone counts*		Cerebellum		Prefrontal_Cortex		Hypothalamus		Cortex_parietal		Hippocampus		Amygdala	
Name	Clone count	Clone fraction	Clone count	Clone fraction	Clone count	Clone fraction	Clone count	Clone fraction	Clone count	Clone fraction	Clone count	Clone fraction	Clone count	Clone fraction
mmu-miR-124	8352	8.8049	2871	16.9831	577	5.2897	656	4.2016	2187	13.2233	1396	9.3266	665	4.3269
mmu-miR-9	8214	8.7207	2296	13.5818	774	7.0957	843	5.3993	1842	11.1373	1477	9.8677	982	6.3895
mmu-miR-125b	5410	6.1228	474	2.8039	935	8.5717	1300	8.3264	833	5.0366	965	6.4471	903	5.8755
mmu-miR-128	3904	4.7548	288	1.7036	818	7.4991	370	2.3698	1170	7.0742	470	3.1400	788	5.1272
mmu-let-7c	3780	4.1315	944	5.5841	441	4.0429	604	3.8686	499	3.0171	655	4.3760	637	4.1447
mmu-miR-127	3224	3.9207	177	1.0470	478	4.3821	955	6.1167	334	2.0195	352	2.3517	928	6.0381
mmu-miR-29a	3461	3.5374	551	3.2594	358	3.2820	547	3.5035	897	5.4235	767	5.1243	341	2.2188
mmu-miR-26a	3167	3.2824	1290	7.6309	192	1.7602	257	1.6461	692	4.1840	553	3.6945	183	1.1907
mmu-let-7a	2507	2.7691	580	3.4309	252	2.3102	501	3.2089	277	1.6748	402	2.6857	495	3.2208
mmu-miR-138	1939	2.2542	81	0.4791	324	2.9703	211	1.3514	291	1.7595	308	2.0577	724	4.7108
mmu-let-7f	1811	1.9427	368	2.1769	247	2.2644	326	2.0880	263	1.5902	362	2.4185	245	1.5941
mmu-let-7g	1690	1.9362	455	2.6915	198	1.8152	331	2.1200	220	1.3302	221	1.4765	265	1.7243
mmu-miR-101a	1623	1.9048	344	2.0349	175	1.6043	278	1.7806	229	1.3846	179	1.1959	418	2.7198
mmu-let-7b	1629	1.7229	367	2.1710	181	1.6593	223	1.4283	229	1.3846	326	2.1780	303	1.9715
mmu-miR-125a	1429	1.6668	326	1.9284	208	1.9069	293	1.8766	198	1.1972	185	1.2360	219	1.4249
mmu-miR-29b	1511	1.5569	86	0.5087	107	0.9809	440	2.8182	306	1.8502	322	2.1513	250	1.6267
mmu-let-7d	1359	1.4923	339	2.0053	126	1.1551	219	1.4027	191	1.1548	216	1.4431	268	1.7438
mmu-let-7i	1208	1.3880	275	1.6267	177	1.6227	156	0.9992	161	0.9735	175	1.1692	264	1.7177
mmu-miR-103	1166	1.3461	117	0.6921	204	1.8702	267	1.7101	130	0.7860	191	1.2761	257	1.6722
mmu-miR-30c	1262	1.3278	315	1.8634	132	1.2101	161	1.0312	304	1.8381	243	1.6235	107	0.6962
mmu-miR-7a	852	1.0556	10	0.0592	25	0.2292	505	3.2345	18	0.1088	41	0.2739	253	1.6462
mmu-miR-24	907	1.0509	130	0.7690	156	1.4301	113	0.7238	207	1.2516	135	0.9019	166	1.0801
mmu-miR-181a	844	0.9655	147	0.8696	139	1.2743	139	0.8903	175	1.0581	131	0.8752	113	0.7352
mmu-miR-22	819	0.9500	58	0.3431	128	1.1735	148	0.9479	152	0.9190	123	0.8218	210	1.3664
mmu-miR-29c	903	0.9094	158	0.9346	81	0.7426	161	1.0312	218	1.3181	205	1.3696	80	0.5205
mmu-miR-99a	778	0.8984	98	0.5797	135	1.2376	171	1.0952	103	0.6228	124	0.8284	147	0.9565
mmu-miR-30d	787	0.8614	300	1.7746	95	0.8709	76	0.4868	120	0.7256	127	0.8485	69	0.4490
mmu-miR-221	665	0.8303	31	0.1834	166	1.5218	76	0.4868	83	0.5018	85	0.5679	224	1.4575
mmu-miR-30a	777	0.8186	246	1.4552	81	0.7426	61	0.3907	166	1.0037	146	0.9754	77	0.5010
mmu-miR-30e	801	0.7941	185	1.0944	76	0.6967	75	0.4804	168	1.0158	192	1.2827	105	0.6832
mmu-miR-126-3p	693	0.7897	85	0.5028	86	0.7884	110	0.7045	126	0.7618	103	0.6881	183	1.1907
mmu-let-7e	643	0.7176	106	0.6270	81	0.7426	138	0.8839	69	0.4172	108	0.7215	141	0.9174
mmu-miR-222	568	0.7154	25	0.1479	129	1.1826	77	0.4932	78	0.4716	62	0.4142	197	1.2818
mmu-miR-132	630	0.6993	19	0.1124	135	1.2376	73	0.4676	155	0.9372	134	0.8952	114	0.7418
mmu-miR-143	497	0.6208	57	0.3372	98	0.8984	81	0.5188	93	0.5623	47	0.3140	121	0.7873
mmu-miR-136-5p	528	0.5869	54	0.3194	33	0.3025	152	0.9735	116	0.7014	75	0.5011	98	0.6376
mmu-miR-21	539	0.5866	83	0.4910	41	0.3759	103	0.6597	97	0.5865	89	0.5946	126	0.8198
mmu-miR-218	595	0.5743	86	0.5087	50	0.4584	53	0.3395	162	0.9795	154	1.0289	90	0.5856
mmu-miR-101b	471	0.5472	56	0.3313	68	0.6234	96	0.6149	67	0.4051	67	0.4476	117	0.7613
mmu-miR-126-5p	432	0.5267	30	0.1775	54	0.4950	63	0.4035	80	0.4837	40	0.2672	165	1.0736
mmu-miR-136-3p	433	0.5034	40	0.2366	38	0.3484	125	0.8006	72	0.4353	51	0.3407	107	0.6962
mmu-miR-16	486	0.4996	170	1.0056	30	0.2750	45	0.2882	102	0.6167	91	0.6080	48	0.3123
mmu-miR-30b	460	0.4905	148	0.8755	41	0.3759	56	0.3587	106	0.6409	78	0.5211	31	0.2017
mmu-miR-338	422	0.4637	35	0.2070	54	0.4950	98	0.6277	71	0.4293	78	0.5211	86	0.5596
mmu-miR-27b	459	0.4278	66	0.3904	36	0.3300	41	0.2626	146	0.8828	128	0.8552	42	0.2733
mmu-miR-137	451	0.4154	5	0.0296	46	0.4217	83	0.5316	111	0.6711	141	0.9420	65	0.4229
mmu-miR-191	365	0.4012	46	0.2721	44	0.4034	78	0.4996	61	0.3688	65	0.4343	71	0.4620
mmu-miR-153	408	0.3982	25	0.1479	31	0.2842	89	0.5700	99	0.5986	104	0.6948	60	0.3904
mmu-miR-33	307	0.3920	18	0.1065	64	0.5867	56	0.3587	49	0.2963	26	0.1737	94	0.6116
mmu-miR-7b	324	0.3904	2	0.0118	14	0.1283	201	1.2874	6	0.0363	26	0.1737	75	0.4880
mmu-miR-135a	343	0.3636	28	0.1656	26	0.2384	151	0.9671	33	0.1995	67	0.4476	38	0.2473
mmu-miR-129-3p	294	0.3528	39	0.2307	35	0.3209	97	0.6213	30	0.1814	30	0.2004	63	0.4099
mmu-miR-434-3p	338	0.3465	43	0.2544	33	0.3025	81	0.5188	71	0.4293	75	0.5011	35	0.2277

mmu-miR-23b	329	0.3437	55	0.3253	34	0.3117	44	0.2818	58	0.3507	69	0.4610	69	0.4490
mmu-miR-328	262	0.3221	18	0.1065	52	0.4767	75	0.4804	27	0.1633	31	0.2071	59	0.3839
mmu-miR-300	284	0.3144	22	0.1301	53	0.4859	63	0.4035	44	0.2660	58	0.3875	44	0.2863
mmu-miR-100	253	0.3051	31	0.1834	48	0.4400	70	0.4483	32	0.1935	32	0.2138	40	0.2603
mmu-miR-376a	259	0.2872	13	0.0769	17	0.1558	91	0.5828	38	0.2298	40	0.2672	60	0.3904
mmu-miR-34a	249	0.2713	75	0.4437	15	0.1375	41	0.2626	73	0.4414	34	0.2272	11	0.0716
mmu-miR-376b-5p	222	0.2665	12	0.0710	16	0.1467	71	0.4547	22	0.1330	20	0.1336	81	0.5270
mmu-miR-26b	253	0.2598	105	0.6211	16	0.1467	23	0.1473	42	0.2539	47	0.3140	20	0.1301
mmu-miR-497	220	0.2526	119	0.7039	20	0.1834	18	0.1153	28	0.1693	21	0.1403	14	0.0911
mmu-miR-139	231	0.2413	8	0.0473	26	0.2384	29	0.1857	43	0.2600	52	0.3474	73	0.4750
mmu-miR-204	231	0.2402	124	0.7335	3	0.0275	35	0.2242	12	0.0726	35	0.2338	22	0.1431
mmu-miR-181b	213	0.2334	29	0.1715	20	0.1834	51	0.3267	34	0.2056	36	0.2405	43	0.2798
mmu-miR-23a	201	0.2325	18	0.1065	33	0.3025	27	0.1729	53	0.3205	30	0.2004	40	0.2603
mmu-miR-99b	185	0.2320	35	0.2070	50	0.4584	30	0.1921	21	0.1270	22	0.1470	27	0.1757
mmu-miR-382	178	0.2311	6	0.0355	36	0.3300	63	0.4035	9	0.0544	13	0.0869	51	0.3318
mmu-miR-107	187	0.2266	14	0.0828	33	0.3025	48	0.3074	19	0.1149	23	0.1537	50	0.3253
mmu-miR-434-5p	190	0.2232	17	0.1006	26	0.2384	42	0.2690	27	0.1633	25	0.1670	53	0.3449
mmu-miR-376b-3p	193	0.2092	7	0.0414	23	0.2109	58	0.3715	30	0.1814	38	0.2539	37	0.2407
mmu-miR-381	212	0.2008	33	0.1952	19	0.1742	37	0.2370	41	0.2479	59	0.3942	23	0.1497
mmu-miR-151-5p	169	0.1978	11	0.0651	39	0.3575	36	0.2306	20	0.1209	30	0.2004	33	0.2147
mmu-miR-27a	183	0.1891	23	0.1361	24	0.2200	25	0.1601	57	0.3446	41	0.2739	13	0.0846
mmu-miR-219-5p	222	0.1888	19	0.1124	5	0.0458	51	0.3267	49	0.2963	73	0.4877	25	0.1627
mmu-miR-744	154	0.1850	8	0.0473	16	0.1467	79	0.5060	6	0.0363	16	0.1069	29	0.1887
mmu-miR-708-5p	154	0.1708	3	0.0177	24	0.2200	20	0.1281	28	0.1693	30	0.2004	49	0.3188
mmu-miR-369-3p	145	0.1688	7	0.0414	19	0.1742	38	0.2434	26	0.1572	20	0.1336	35	0.2277
mmu-miR-219-3p	161	0.1685	21	0.1242	18	0.1650	43	0.2754	18	0.1088	35	0.2338	26	0.1692
mmu-miR-34c	158	0.1606	8	0.0473	28	0.2567	41	0.2626	9	0.0544	44	0.2940	28	0.1822
mmu-miR-383	129	0.1599	0	0.0000	38	0.3484	32	0.2050	16	0.0967	20	0.1336	23	0.1497
mmu-miR-129-5p	128	0.1585	16	0.0946	32	0.2934	23	0.1473	21	0.1270	16	0.1069	20	0.1301
mmu-miR-379	135	0.1560	17	0.1006	19	0.1742	45	0.2882	9	0.0544	20	0.1336	25	0.1627
mmu-miR-148a	123	0.1526	8	0.0473	15	0.1375	49	0.3138	5	0.0302	10	0.0668	36	0.2342
mmu-miR-341	135	0.1519	6	0.0355	15	0.1375	54	0.3459	14	0.0846	22	0.1470	24	0.1562
mmu-miR-378	125	0.1506	26	0.1538	17	0.1558	19	0.1217	8	0.0484	13	0.0869	42	0.2733
mmu-miR-185	114	0.1499	5	0.0296	23	0.2109	33	0.2114	18	0.1088	6	0.0401	29	0.1887
mmu-miR-149	124	0.1433	17	0.1006	11	0.1008	44	0.2818	16	0.0967	15	0.1002	21	0.1366
mmu-miR-370-3p	97	0.1417	0	0.0000	43	0.3942	18	0.1153	6	0.0363	5	0.0334	25	0.1627
mmu-miR-411	134	0.1411	20	0.1183	12	0.1100	29	0.1857	31	0.1874	26	0.1737	16	0.1041
mmu-miR-598	136	0.1370	25	0.1479	7	0.0642	45	0.2882	9	0.0544	30	0.2004	20	0.1301
mmu-miR-195	107	0.1252	81	0.4791	4	0.0367	2	0.0128	15	0.0907	4	0.0267	1	0.0065
mmu-miR-541	102	0.1219	4	0.0237	20	0.1834	31	0.1986	9	0.0544	15	0.1002	23	0.1497
mmu-miR-652	112	0.1219	23	0.1361	8	0.0733	33	0.2114	14	0.0846	18	0.1203	16	0.1041
mmu-miR-130a	100	0.1177	21	0.1242	4	0.0367	29	0.1857	12	0.0726	8	0.0534	26	0.1692
mmu-miR-140-3p	104	0.1177	13	0.0769	20	0.1834	15	0.0961	19	0.1149	19	0.1269	18	0.1171
mmu-miR-150	112	0.1174	18	0.1065	7	0.0642	21	0.1345	24	0.1451	21	0.1403	21	0.1366
mmu-miR-433	119	0.1169	5	0.0296	11	0.1008	38	0.2434	9	0.0544	32	0.2138	24	0.1562
mmu-miR-15a	109	0.1147	18	0.1065	15	0.1375	10	0.0640	17	0.1028	24	0.1603	25	0.1627
mmu-miR-330-5p	105	0.1091	11	0.0651	10	0.0917	27	0.1729	12	0.0726	23	0.1537	22	0.1431
mmu-miR-320	85	0.1074	25	0.1479	16	0.1467	20	0.1281	6	0.0363	6	0.0401	12	0.0781
mmu-miR-674-5p	75	0.0991	5	0.0296	20	0.1834	10	0.0640	6	0.0363	6	0.0401	28	0.1822
mmu-miR-335-5p	74	0.0953	5	0.0296	18	0.1650	17	0.1089	6	0.0363	7	0.0468	21	0.1366
mmu-miR-344	84	0.0925	9	0.0532	9	0.0825	17	0.1089	7	0.0423	15	0.1002	27	0.1757
mmu-miR-301a	88	0.0923	14	0.0828	5	0.0458	36	0.2306	4	0.0242	17	0.1136	12	0.0781
mmu-miR-324-5p	74	0.0914	9	0.0532	14	0.1283	15	0.0961	6	0.0363	8	0.0534	22	0.1431
mmu-miR-98	88	0.0901	10	0.0592	8	0.0733	23	0.1473	11	0.0665	20	0.1336	16	0.1041
mmu-miR-181d	72	0.0892	12	0.0710	6	0.0550	17	0.1089	8	0.0484	4	0.0267	25	0.1627
mmu-miR-331	72	0.0891	5	0.0296	14	0.1283	16	0.1025	8	0.0484	8	0.0534	21	0.1366
mmu-miR-495	86	0.0886	6	0.0355	6	0.0550	19	0.1217	22	0.1330	18	0.1203	15	0.0976
mmu-miR-93	79	0.0866	7	0.0414	16	0.1467	15	0.0961	16	0.0967	17	0.1136	8	0.0521
mmu-miR-140-5p	77	0.0849	18	0.1065	5	0.0458	15	0.0961	13	0.0786	11	0.0735	15	0.0976
mmu-miR-873-5p	66	0.0828	0	0.0000	11	0.1008	11	0.0705	10	0.0605	6	0.0401	28	0.1822
mmu-miR-135b	76	0.0825	8	0.0473	4	0.0367	26	0.1665	16	0.0967	12	0.0802	10	0.0651
mmu-miR-384-3p	75	0.0806	11	0.0651	7	0.0642	24	0.1537	8	0.0484	14	0.0935	11	0.0716
mmu-miR-186	72	0.0792	5	0.0296	11	0.1008	12	0.0769	14	0.0846	14	0.0935	16	0.1041
mmu-miR-487b	67	0.0790	3	0.0177	10	0.0917	16	0.1025	12	0.0726	9	0.0601	17	0.1106
mmu-miR-148b	88	0.0789	10	0.0592	8	0.0733	11	0.0705	22	0.1330	28	0.1871	9	0.0586
mmu-miR-384-5p	81	0.0778	9	0.0532	6	0.0550	15	0.0961	23	0.1391	21	0.1403	7	0.0455
mmu-miR-369-5p	58	0.0744	1	0.0059	7	0.0642	13	0.0833	6	0.0363	3	0.0200	28	0.1822
mmu-miR-106b	67	0.0734	13	0.0769	12	0.1100	10	0.0640	16	0.0967	13	0.0869	3	0.0195
mmu-miR-582	58	0.0733	7	0.0414	11	0.1008	12	0.0769	5	0.0302	5	0.0334	18	0.1171

mmu-miR-484	64	0.0730	30	0.1775	6	0.0550	5	0.0320	8	0.0484	7	0.0468	8	0.0521
mmu-miR-326	60	0.0729	0	0.0000	10	0.0917	26	0.1665	9	0.0544	7	0.0468	8	0.0521
mmu-miR-181c	60	0.0717	19	0.1124	2	0.0183	16	0.1025	11	0.0665	3	0.0200	9	0.0586
mmu-miR-330-3p	59	0.0711	0	0.0000	11	0.1008	18	0.1153	8	0.0484	8	0.0534	14	0.0911
mmu-miR-340	66	0.0680	19	0.1124	2	0.0183	9	0.0576	24	0.1451	11	0.0735	1	0.0065
mmu-miR-770-3p	54	0.0664	0	0.0000	4	0.0367	24	0.1537	3	0.0181	4	0.0267	19	0.1236
mmu-miR-770-5p	62	0.0663	0	0.0000	2	0.0183	33	0.2114	5	0.0302	11	0.0735	11	0.0716
mmu-miR-361	60	0.0661	15	0.0887	6	0.0550	7	0.0448	17	0.1028	9	0.0601	6	0.0390
mmu-miR-410	71	0.0655	8	0.0473	2	0.0183	18	0.1153	7	0.0423	20	0.1336	16	0.1041
mmu-miR-872	54	0.0649	3	0.0177	5	0.0458	14	0.0897	10	0.0605	5	0.0334	17	0.1106
mmu-miR-551b	60	0.0596	0	0.0000	1	0.0092	15	0.0961	19	0.1149	13	0.0869	12	0.0781
mmu-miR-194	55	0.0574	27	0.1597	3	0.0275	3	0.0192	9	0.0544	9	0.0601	4	0.0260
mmu-miR-676	45	0.0571	0	0.0000	8	0.0733	8	0.0512	4	0.0242	4	0.0267	21	0.1366
mmu-miR-145-5p	48	0.0551	8	0.0473	5	0.0458	5	0.0320	13	0.0786	6	0.0401	11	0.0716
mmu-miR-219	56	0.0531	5	0.0296	1	0.0092	16	0.1025	13	0.0786	14	0.0935	7	0.0455
mmu-miR-708-3p	40	0.0501	0	0.0000	7	0.0642	12	0.0769	3	0.0181	4	0.0267	14	0.0911
mmu-miR-665	40	0.0495	2	0.0118	5	0.0458	10	0.0640	9	0.0544	3	0.0200	11	0.0716
mmu-miR-337-5p	37	0.0466	3	0.0177	6	0.0550	8	0.0512	4	0.0242	3	0.0200	13	0.0846
mmu-miR-212-3p	35	0.0461	1	0.0059	13	0.1192	5	0.0320	10	0.0605	4	0.0267	2	0.0130
mmu-miR-485-5p	33	0.0457	1	0.0059	11	0.1008	8	0.0512	2	0.0121	2	0.0134	9	0.0586
mmu-miR-154-5p	45	0.0451	2	0.0118	0	0.0000	13	0.0833	14	0.0846	9	0.0601	7	0.0455
mmu-miR-874	36	0.0447	4	0.0237	8	0.0733	8	0.0512	6	0.0363	4	0.0267	6	0.0390
mmu-miR-329-5p	34	0.0446	0	0.0000	7	0.0642	6	0.0384	7	0.0423	2	0.0134	12	0.0781
mmu-miR-380-3p	39	0.0438	2	0.0118	4	0.0367	17	0.1089	7	0.0423	6	0.0401	3	0.0195
mmu-miR-19b	46	0.0437	8	0.0473	7	0.0642	5	0.0320	7	0.0423	14	0.0935	5	0.0325
mmu-miR-190	40	0.0430	5	0.0296	3	0.0275	8	0.0512	8	0.0484	7	0.0468	9	0.0586
mmu-miR-25	39	0.0419	8	0.0473	6	0.0550	10	0.0640	5	0.0302	8	0.0534	2	0.0130
mmu-miR-206	35	0.0416	33	0.1952	0	0.0000	0	0.0000	0	0.0000	0	0.0000	2	0.0130
mmu-miR-409-5p	31	0.0407	0	0.0000	7	0.0642	5	0.0320	7	0.0423	2	0.0134	10	0.0651
mmu-miR-339	33	0.0397	3	0.0177	3	0.0275	12	0.0769	4	0.0242	3	0.0200	8	0.0521
mmu-miR-151-3p	31	0.0395	4	0.0237	8	0.0733	5	0.0320	7	0.0423	3	0.0200	4	0.0260
mmu-miR-323	32	0.0390	4	0.0237	4	0.0367	7	0.0448	3	0.0181	3	0.0200	11	0.0716
mmu-miR-17	31	0.0375	2	0.0118	4	0.0367	7	0.0448	8	0.0484	3	0.0200	7	0.0455
mmu-miR-543	34	0.0367	0	0.0000	4	0.0367	15	0.0961	3	0.0181	7	0.0468	5	0.0325
mmu-miR-187	42	0.0363	8	0.0473	0	0.0000	4	0.0256	5	0.0302	13	0.0869	12	0.0781
mmu-miR-409-3p	23	0.0346	0	0.0000	9	0.0825	5	0.0320	0	0.0000	0	0.0000	9	0.0586
mmu-miR-134	31	0.0344	3	0.0177	3	0.0275	13	0.0833	5	0.0302	5	0.0334	2	0.0130
mmu-miR-152	31	0.0341	5	0.0296	5	0.0458	4	0.0256	5	0.0302	6	0.0401	6	0.0390
mmu-miR-370-5p	23	0.0339	0	0.0000	8	0.0733	7	0.0448	2	0.0121	0	0.0000	6	0.0390
mmu-miR-34b	52	0.0330	7	0.0414	1	0.0092	11	0.0705	3	0.0181	26	0.1737	4	0.0260
mmu-miR-532-5p	30	0.0322	6	0.0355	4	0.0367	7	0.0448	3	0.0181	6	0.0401	4	0.0260
mmu-miR-154-3p	25	0.0320	1	0.0059	7	0.0642	8	0.0512	1	0.0060	3	0.0200	5	0.0325
mmu-miR-345-5p	30	0.0311	6	0.0355	2	0.0183	7	0.0448	4	0.0242	6	0.0401	5	0.0325
mmu-miR-376c	24	0.0308	1	0.0059	3	0.0275	9	0.0576	5	0.0302	1	0.0067	5	0.0325
mmu-miR-322	27	0.0302	1	0.0059	2	0.0183	3	0.0192	7	0.0423	4	0.0267	10	0.0651
mmu-miR-146b	31	0.0295	4	0.0237	6	0.0550	5	0.0320	5	0.0302	10	0.0668	1	0.0065
mmu-miR-92b	31	0.0277	3	0.0177	2	0.0183	5	0.0320	3	0.0181	10	0.0668	8	0.0521
mmu-miR-324-3p	21	0.0271	1	0.0059	3	0.0275	4	0.0256	4	0.0242	1	0.0067	8	0.0521
mmu-miR-212-5p	20	0.0270	0	0.0000	5	0.0458	3	0.0192	4	0.0242	1	0.0067	7	0.0455
mmu-miR-500	23	0.0264	2	0.0118	2	0.0183	10	0.0640	3	0.0181	3	0.0200	3	0.0195
mmu-miR-377	24	0.0262	2	0.0118	4	0.0367	6	0.0384	3	0.0181	5	0.0334	4	0.0260
mmu-miR-1	24	0.0254	0	0.0000	1	0.0092	6	0.0384	11	0.0665	4	0.0267	2	0.0130
mmu-miR-142-3p	28	0.0252	1	0.0059	2	0.0183	9	0.0576	3	0.0181	9	0.0601	4	0.0260
mmu-miR-210	18	0.0248	0	0.0000	3	0.0275	2	0.0128	2	0.0121	0	0.0000	11	0.0716
mmu-miR-20a	22	0.0243	3	0.0177	3	0.0275	7	0.0448	2	0.0121	4	0.0267	3	0.0195
mmu-miR-805	22	0.0238	0	0.0000	4	0.0367	3	0.0192	4	0.0242	5	0.0334	6	0.0390
mmu-miR-92a	24	0.0238	0	0.0000	4	0.0367	3	0.0192	4	0.0242	7	0.0468	6	0.0390
mmu-miR-488	22	0.0233	0	0.0000	6	0.0550	2	0.0128	7	0.0423	6	0.0401	1	0.0065
mmu-miR-146a	18	0.0232	0	0.0000	3	0.0275	5	0.0320	5	0.0302	1	0.0067	4	0.0260
mmu-miR-19a	15	0.0222	1	0.0059	8	0.0733	1	0.0064	1	0.0060	1	0.0067	3	0.0195
mmu-miR-199a-3p	16	0.0213	1	0.0059	4	0.0367	3	0.0192	2	0.0121	1	0.0067	5	0.0325
mmu-miR-425	21	0.0211	1	0.0059	2	0.0183	5	0.0320	6	0.0363	5	0.0334	2	0.0130
mmu-miR-345-3p	16	0.0210	5	0.0296	4	0.0367	3	0.0192	0	0.0000	1	0.0067	3	0.0195
mmu-miR-486	16	0.0210	4	0.0237	4	0.0367	6	0.0384	1	0.0060	1	0.0067	0	0.0000
mmu-miR-145-3p	15	0.0205	3	0.0177	3	0.0275	3	0.0192	2	0.0121	0	0.0000	4	0.0260
mmu-miR-672	15	0.0203	0	0.0000	2	0.0183	8	0.0512	1	0.0060	0	0.0000	4	0.0260
mmu-miR-423-3p	19	0.0200	0	0.0000	6	0.0550	3	0.0192	0	0.0000	6	0.0401	4	0.0260
mmu-miR-346	25	0.0195	0	0.0000	1	0.0092	6	0.0384	5	0.0302	10	0.0668	3	0.0195
mmu-miR-192	15	0.0189	8	0.0473	1	0.0092	4	0.0256	1	0.0060	0	0.0000	1	0.0065

mmu-miR-380-5p	16	0.0188	1	0.0059	2	0.0183	7	0.0448	2	0.0121	2	0.0134	2	0.0130
mmu-miR-296-3p	14	0.0185	1	0.0059	1	0.0092	6	0.0384	0	0.0000	0	0.0000	6	0.0390
mmu-miR-329-3p	16	0.0180	0	0.0000	3	0.0275	1	0.0064	5	0.0302	3	0.0200	4	0.0260
mmu-miR-496	15	0.0175	2	0.0118	2	0.0183	3	0.0192	2	0.0121	2	0.0134	4	0.0260
mmu-miR-666-5p	13	0.0171	0	0.0000	1	0.0092	5	0.0320	3	0.0181	0	0.0000	4	0.0260
mmu-miR-335-3p	14	0.0171	0	0.0000	1	0.0092	1	0.0064	4	0.0242	1	0.0067	7	0.0455
mmu-miR-540-5p	17	0.0170	1	0.0059	1	0.0092	1	0.0064	3	0.0181	4	0.0267	7	0.0455
mmu-miR-133a	17	0.0161	5	0.0296	0	0.0000	4	0.0256	2	0.0121	4	0.0267	2	0.0130
mmu-miR-32	11	0.0160	1	0.0059	4	0.0367	2	0.0128	3	0.0181	0	0.0000	1	0.0065
mmu-miR-667-3p	13	0.0158	1	0.0059	1	0.0092	8	0.0512	1	0.0060	1	0.0067	1	0.0065
mmu-miR-674-3p	16	0.0157	0	0.0000	3	0.0275	2	0.0128	2	0.0121	5	0.0334	4	0.0260
mmu-miR-431	15	0.0153	1	0.0059	0	0.0000	2	0.0128	2	0.0121	3	0.0200	7	0.0455
mmu-miR-142-5p	12	0.0151	2	0.0118	2	0.0183	1	0.0064	0	0.0000	1	0.0067	6	0.0390
mmu-miR-879	11	0.0147	0	0.0000	1	0.0092	5	0.0320	1	0.0060	0	0.0000	4	0.0260
mmu-miR-873-3p	12	0.0146	0	0.0000	1	0.0092	6	0.0384	1	0.0060	1	0.0067	3	0.0195
mmu-miR-540-3p	10	0.0145	0	0.0000	3	0.0275	3	0.0192	1	0.0060	0	0.0000	3	0.0195
mmu-miR-199a-5p	12	0.0141	1	0.0059	0	0.0000	3	0.0192	0	0.0000	1	0.0067	7	0.0455
mmu-miR-668	12	0.0138	0	0.0000	2	0.0183	3	0.0192	2	0.0121	2	0.0134	3	0.0195
mmu-miR-374	11	0.0131	2	0.0118	1	0.0092	2	0.0128	2	0.0121	1	0.0067	3	0.0195
mmu-miR-28-5p	13	0.0129	5	0.0296	1	0.0092	3	0.0192	0	0.0000	3	0.0200	1	0.0065
mmu-miR-1224-5p	10	0.0127	0	0.0000	0	0.0000	2	0.0128	3	0.0181	0	0.0000	5	0.0325
mmu-miR-490	8	0.0125	0	0.0000	4	0.0367	2	0.0128	0	0.0000	0	0.0000	2	0.0130
mmu-miR-375	8	0.0123	2	0.0118	4	0.0367	1	0.0064	0	0.0000	0	0.0000	1	0.0065
mmu-miR-298	9	0.0121	0	0.0000	1	0.0092	6	0.0384	0	0.0000	0	0.0000	2	0.0130
mmu-miR-203	10	0.0119	2	0.0118	1	0.0092	2	0.0128	1	0.0060	1	0.0067	3	0.0195
mmu-miR-296-5p	10	0.0115	0	0.0000	0	0.0000	8	0.0512	0	0.0000	1	0.0067	1	0.0065
mmu-miR-467a	9	0.0113	0	0.0000	2	0.0183	4	0.0256	1	0.0060	1	0.0067	1	0.0065
mmu-miR-467b	9	0.0113	0	0.0000	2	0.0183	4	0.0256	1	0.0060	1	0.0067	1	0.0065
mmu-miR-299-5p	12	0.0113	1	0.0059	0	0.0000	6	0.0384	2	0.0121	3	0.0200	0	0.0000
mmu-miR-667-5p	7	0.0112	0	0.0000	4	0.0367	3	0.0192	0	0.0000	0	0.0000	0	0.0000
mmu-miR-193b	9	0.0107	0	0.0000	3	0.0275	2	0.0128	0	0.0000	2	0.0134	2	0.0130
mmu-miR-351	7	0.0106	0	0.0000	3	0.0275	0	0.0000	1	0.0060	0	0.0000	3	0.0195
mmu-miR-764	8	0.0103	0	0.0000	0	0.0000	3	0.0192	0	0.0000	0	0.0000	5	0.0325
mmu-miR-15b	10	0.0102	0	0.0000	0	0.0000	4	0.0256	1	0.0060	2	0.0134	3	0.0195
mmu-miR-532-3p	9	0.0102	0	0.0000	0	0.0000	3	0.0192	2	0.0121	1	0.0067	3	0.0195
mmu-miR-760	9	0.0101	0	0.0000	2	0.0183	3	0.0192	0	0.0000	2	0.0134	2	0.0130
mmu-miR-592	8	0.0101	0	0.0000	0	0.0000	4	0.0256	3	0.0181	0	0.0000	1	0.0065
mmu-miR-199b	7	0.0100	0	0.0000	2	0.0183	2	0.0128	1	0.0060	0	0.0000	2	0.0130
mmu-miR-337-3p	12	0.0100	1	0.0059	0	0.0000	2	0.0128	3	0.0181	4	0.0267	2	0.0130
mmu-miR-362-5p	7	0.0094	0	0.0000	3	0.0275	2	0.0128	0	0.0000	1	0.0067	1	0.0065
mmu-miR-362-3p	10	0.0093	1	0.0059	1	0.0092	2	0.0128	2	0.0121	3	0.0200	1	0.0065
mmu-miR-671-5p	8	0.0090	0	0.0000	0	0.0000	6	0.0384	0	0.0000	1	0.0067	1	0.0065
mmu-miR-485-3p	10	0.0090	0	0.0000	0	0.0000	7	0.0448	0	0.0000	3	0.0200	0	0.0000
mmu-miR-188	7	0.0085	4	0.0237	0	0.0000	1	0.0064	1	0.0060	0	0.0000	1	0.0065
mmu-miR-700-5p	7	0.0084	5	0.0296	0	0.0000	1	0.0064	1	0.0060	0	0.0000	0	0.0000
mmu-miR-501-3p	6	0.0075	0	0.0000	2	0.0183	1	0.0064	1	0.0060	1	0.0067	1	0.0065
mmu-miR-421	6	0.0074	1	0.0059	0	0.0000	0	0.0000	3	0.0181	0	0.0000	2	0.0130
mmu-miR-350	9	0.0073	1	0.0059	2	0.0183	1	0.0064	1	0.0060	4	0.0267	0	0.0000
mmu-miR-666-3p	5	0.0070	0	0.0000	1	0.0092	1	0.0064	0	0.0000	0	0.0000	3	0.0195
mmu-miR-455-3p	5	0.0069	1	0.0059	1	0.0092	2	0.0128	0	0.0000	0	0.0000	1	0.0065
mmu-miR-1224-3p	5	0.0064	0	0.0000	0	0.0000	4	0.0256	0	0.0000	0	0.0000	1	0.0065
mmu-miR-18a	7	0.0063	0	0.0000	0	0.0000	4	0.0256	1	0.0060	2	0.0134	0	0.0000
mmu-miR-325-5p	5	0.0062	2	0.0118	0	0.0000	0	0.0000	1	0.0060	0	0.0000	2	0.0130
mmu-miR-215	4	0.0062	1	0.0059	2	0.0183	0	0.0000	0	0.0000	0	0.0000	1	0.0065
mmu-miR-574-3p	5	0.0061	3	0.0177	0	0.0000	2	0.0128	0	0.0000	0	0.0000	0	0.0000
mmu-miR-423-5p	4	0.0057	0	0.0000	1	0.0092	2	0.0128	0	0.0000	0	0.0000	1	0.0065
mmu-miR-539	5	0.0055	1	0.0059	1	0.0092	1	0.0064	1	0.0060	1	0.0067	0	0.0000
mmu-miR-130b	6	0.0052	0	0.0000	0	0.0000	1	0.0064	0	0.0000	2	0.0134	3	0.0195
mmu-miR-503	5	0.0052	0	0.0000	0	0.0000	2	0.0128	0	0.0000	1	0.0067	2	0.0130
mmu-miR-28-3p	4	0.0051	0	0.0000	0	0.0000	1	0.0064	1	0.0060	0	0.0000	2	0.0130
mmu-miR-669a-5p	4	0.0051	0	0.0000	0	0.0000	2	0.0128	1	0.0060	0	0.0000	1	0.0065
mmu-miR-544-5p	4	0.0050	0	0.0000	0	0.0000	2	0.0128	2	0.0121	0	0.0000	0	0.0000
mmu-miR-700-3p	4	0.0050	1	0.0059	0	0.0000	2	0.0128	1	0.0060	0	0.0000	0	0.0000
mmu-miR-325-3p	4	0.0049	2	0.0118	0	0.0000	2	0.0128	0	0.0000	0	0.0000	0	0.0000
mmu-miR-544-3p	5	0.0049	0	0.0000	0	0.0000	1	0.0064	3	0.0181	1	0.0067	0	0.0000
mmu-miR-720	4	0.0049	0	0.0000	2	0.0183	0	0.0000	1	0.0060	1	0.0067	0	0.0000
mmu-miR-365	5	0.0044	0	0.0000	1	0.0092	1	0.0064	0	0.0000	2	0.0134	1	0.0065
mmu-miR-412-5p	3	0.0044	0	0.0000	1	0.0092	2	0.0128	0	0.0000	0	0.0000	0	0.0000
mmu-miR-299-3p	5	0.0039	0	0.0000	0	0.0000	0	0.0000	0	0.0000	2	0.0134	3	0.0195

mmu-miR-877-3p	3	0.0039	0	0.0000	0	0.0000	2	0.0128	0	0.0000	0	0.0000	1	0.0065
mmu-miR-448-3p	3	0.0038	0	0.0000	0	0.0000	3	0.0192	0	0.0000	0	0.0000	0	0.0000
mmu-miR-494	3	0.0038	0	0.0000	0	0.0000	3	0.0192	0	0.0000	0	0.0000	0	0.0000
mmu-miR-455-5p	3	0.0038	1	0.0059	0	0.0000	0	0.0000	0	0.0000	0	0.0000	2	0.0130
mmu-miR-542-5p	3	0.0038	1	0.0059	0	0.0000	0	0.0000	0	0.0000	0	0.0000	2	0.0130
mmu-miR-669a	3	0.0038	0	0.0000	0	0.0000	2	0.0128	1	0.0060	0	0.0000	0	0.0000
mmu-miR-467c	4	0.0037	2	0.0118	0	0.0000	0	0.0000	0	0.0000	1	0.0067	1	0.0065
mmu-miR-133b	3	0.0035	3	0.0177	0	0.0000	0	0.0000	0	0.0000	0	0.0000	0	0.0000
mmu-miR-182	3	0.0035	3	0.0177	0	0.0000	0	0.0000	0	0.0000	0	0.0000	0	0.0000
mmu-miR-449a	2	0.0030	1	0.0059	1	0.0092	0	0.0000	0	0.0000	0	0.0000	0	0.0000
mmu-miR-223	2	0.0026	0	0.0000	0	0.0000	0	0.0000	0	0.0000	0	0.0000	2	0.0130
mmu-miR-31	2	0.0026	0	0.0000	0	0.0000	0	0.0000	0	0.0000	0	0.0000	2	0.0130
mmu-miR-448-5p	2	0.0026	0	0.0000	0	0.0000	0	0.0000	0	0.0000	0	0.0000	2	0.0130
mmu-miR-297c	2	0.0026	0	0.0000	0	0.0000	1	0.0064	0	0.0000	0	0.0000	1	0.0065
mmu-miR-504	3	0.0026	0	0.0000	0	0.0000	1	0.0064	0	0.0000	1	0.0067	1	0.0065
mmu-miR-216b	2	0.0026	0	0.0000	0	0.0000	2	0.0128	0	0.0000	0	0.0000	0	0.0000
mmu-miR-217-5p	2	0.0026	0	0.0000	0	0.0000	2	0.0128	0	0.0000	0	0.0000	0	0.0000
mmu-miR-466a-5p	2	0.0026	0	0.0000	0	0.0000	2	0.0128	0	0.0000	0	0.0000	0	0.0000
mmu-miR-758	3	0.0026	0	0.0000	0	0.0000	2	0.0128	0	0.0000	1	0.0067	0	0.0000
mmu-miR-491	2	0.0025	0	0.0000	0	0.0000	1	0.0064	1	0.0060	0	0.0000	0	0.0000
mmu-miR-301b	4	0.0024	0	0.0000	0	0.0000	0	0.0000	2	0.0121	2	0.0134	0	0.0000
mmu-miR-429	2	0.0024	0	0.0000	0	0.0000	0	0.0000	2	0.0121	0	0.0000	0	0.0000
mmu-miR-297a	2	0.0024	1	0.0059	0	0.0000	0	0.0000	1	0.0060	0	0.0000	0	0.0000
mmu-miR-10a	3	0.0024	2	0.0118	0	0.0000	0	0.0000	0	0.0000	1	0.0067	0	0.0000
mmu-miR-501-5p	2	0.0024	2	0.0118	0	0.0000	0	0.0000	0	0.0000	0	0.0000	0	0.0000
mmu-miR-184	1	0.0018	0	0.0000	1	0.0092	0	0.0000	0	0.0000	0	0.0000	0	0.0000
mmu-miR-291a-5p	1	0.0018	0	0.0000	1	0.0092	0	0.0000	0	0.0000	0	0.0000	0	0.0000
mmu-miR-291b-5p	1	0.0018	0	0.0000	1	0.0092	0	0.0000	0	0.0000	0	0.0000	0	0.0000
mmu-miR-327	1	0.0018	0	0.0000	1	0.0092	0	0.0000	0	0.0000	0	0.0000	0	0.0000
mmu-miR-465c-5p	1	0.0018	0	0.0000	1	0.0092	0	0.0000	0	0.0000	0	0.0000	0	0.0000
mmu-miR-669a-3p	1	0.0018	0	0.0000	1	0.0092	0	0.0000	0	0.0000	0	0.0000	0	0.0000
mmu-miR-673-5p	2	0.0018	0	0.0000	1	0.0092	0	0.0000	0	0.0000	1	0.0067	0	0.0000
mmu-miR-742	1	0.0018	0	0.0000	1	0.0092	0	0.0000	0	0.0000	0	0.0000	0	0.0000
mmu-miR-183	1	0.0013	0	0.0000	0	0.0000	0	0.0000	0	0.0000	0	0.0000	1	0.0065
mmu-miR-452	1	0.0013	0	0.0000	0	0.0000	0	0.0000	0	0.0000	0	0.0000	1	0.0065
mmu-miR-499	1	0.0013	0	0.0000	0	0.0000	0	0.0000	0	0.0000	0	0.0000	1	0.0065
mmu-miR-654	1	0.0013	0	0.0000	0	0.0000	0	0.0000	0	0.0000	0	0.0000	1	0.0065
mmu-miR-669c	1	0.0013	0	0.0000	0	0.0000	0	0.0000	0	0.0000	0	0.0000	1	0.0065
mmu-miR-671-3p	2	0.0013	0	0.0000	0	0.0000	0	0.0000	0	0.0000	1	0.0067	1	0.0065
mmu-miR-122	3	0.0013	0	0.0000	0	0.0000	1	0.0064	0	0.0000	2	0.0134	0	0.0000
mmu-miR-200c	1	0.0013	0	0.0000	0	0.0000	1	0.0064	0	0.0000	0	0.0000	0	0.0000
mmu-miR-216a	2	0.0013	0	0.0000	0	0.0000	1	0.0064	0	0.0000	1	0.0067	0	0.0000
mmu-miR-217-3p	1	0.0013	0	0.0000	0	0.0000	1	0.0064	0	0.0000	0	0.0000	0	0.0000
mmu-miR-293	1	0.0013	0	0.0000	0	0.0000	1	0.0064	0	0.0000	0	0.0000	0	0.0000
mmu-miR-412-3p	1	0.0013	0	0.0000	0	0.0000	1	0.0064	0	0.0000	0	0.0000	0	0.0000
mmu-miR-449c	1	0.0013	0	0.0000	0	0.0000	1	0.0064	0	0.0000	0	0.0000	0	0.0000
mmu-miR-466b-3p	1	0.0013	0	0.0000	0	0.0000	1	0.0064	0	0.0000	0	0.0000	0	0.0000
mmu-miR-466d-5p	1	0.0013	0	0.0000	0	0.0000	1	0.0064	0	0.0000	0	0.0000	0	0.0000
mmu-miR-466f-3p	1	0.0013	0	0.0000	0	0.0000	1	0.0064	0	0.0000	0	0.0000	0	0.0000
mmu-miR-467d	1	0.0013	0	0.0000	0	0.0000	1	0.0064	0	0.0000	0	0.0000	0	0.0000
mmu-miR-483	1	0.0013	0	0.0000	0	0.0000	1	0.0064	0	0.0000	0	0.0000	0	0.0000
mmu-miR-505-5p	1	0.0013	0	0.0000	0	0.0000	1	0.0064	0	0.0000	0	0.0000	0	0.0000
mmu-miR-653	1	0.0013	0	0.0000	0	0.0000	1	0.0064	0	0.0000	0	0.0000	0	0.0000
mmu-miR-669b	1	0.0013	0	0.0000	0	0.0000	1	0.0064	0	0.0000	0	0.0000	0	0.0000
mmu-miR-877-5p	1	0.0013	0	0.0000	0	0.0000	1	0.0064	0	0.0000	0	0.0000	0	0.0000
mmu-miR-193	1	0.0012	0	0.0000	0	0.0000	0	0.0000	1	0.0060	0	0.0000	0	0.0000
mmu-miR-200a	1	0.0012	0	0.0000	0	0.0000	0	0.0000	1	0.0060	0	0.0000	0	0.0000
mmu-miR-20b	2	0.0012	0	0.0000	0	0.0000	0	0.0000	1	0.0060	1	0.0067	0	0.0000
mmu-miR-670	2	0.0012	0	0.0000	0	0.0000	0	0.0000	1	0.0060	1	0.0067	0	0.0000
mmu-miR-802	1	0.0012	0	0.0000	0	0.0000	0	0.0000	1	0.0060	0	0.0000	0	0.0000
mmu-miR-211	1	0.0012	1	0.0059	0	0.0000	0	0.0000	0	0.0000	0	0.0000	0	0.0000
mmu-miR-467e	1	0.0012	1	0.0059	0	0.0000	0	0.0000	0	0.0000	0	0.0000	0	0.0000
mmu-miR-615-3p	1	0.0012	1	0.0059	0	0.0000	0	0.0000	0	0.0000	0	0.0000	0	0.0000
mmu-miR-96	1	0.0012	1	0.0059	0	0.0000	0	0.0000	0	0.0000	0	0.0000	0	0.0000
mmu-miR-155	1	0.0000	0	0.0000	0	0.0000	0	0.0000	0	0.0000	1	0.0067	0	0.0000
mmu-miR-466a-3p	0	0.0000	0	0.0000	0	0.0000	0	0.0000	0	0.0000	0	0.0000	0	0.0000
mmu-miR-466d-3p	1	0.0000	0	0.0000	0	0.0000	0	0.0000	0	0.0000	1	0.0067	0	0.0000
mmu-miR-466e-3p	0	0.0000	0	0.0000	0	0.0000	0	0.0000	0	0.0000	0	0.0000	0	0.0000
mmu-miR-880	1	0.0000	0	0.0000	0	0.0000	0	0.0000	0	0.0000	1	0.0067	0	0.0000

sum	90302	100	16905	100	10908	100	15613	100	16539	100	14968	100	15369	100	

Supplementary Table 3. List of miRNA, mismatch (MM) LNA probes and sequence used in this study; melting profiles for miRNA/LNA probe pairs also presented

LNA probe	LNA probe sequence (5' to 3') [Φ]	Exp T_M (ºC)	Exiqon T_M (ºC)[Ψ]
LNA-124	GGCA[T][T]C[A]CCGCGTGCC[T][T][A]	67.5	75.0
LNA-124/C3A	GG**A**A[T][T]C[A]CCGCGTGCC[T][T][A]	66.4	72.0
LNA-124/C9A	GGCA[T][T]C[A]**A**CGCGTGCC[T][T][A]	58.0	73.0
LNA-124/T19A	GGCA[T][T]C[A]CCGCGTGCC[T][**A**][A]	66.8	73.0
LNA-124/C9AC10A	GGCA[T][T]C[A]**AA**GCGTGCC[T][T][A]	52.9	70.0

[Φ] LNA-modified DNA positions are marked in square brackets. Mismatch bases are in bold and underlined.

[Ψ] Exiqon T_M (ºC) was calculated with 50 mM salt concentration and 1.5 µM total oligo (target + probe) concentration.

References

[1] Merzenich, M. M., Nelson, R. J., Stryker, M. P. et al., Somatosensory cortical map changes following digit amputation in adult monkeysJ Comp Neurol 224 (4), 591 (1984).

[2] Robertson, D. and Irvine, D. R., Plasticity of frequency organization in auditory cortex of guinea pigs with partial unilateral deafnessJ Comp Neurol 282 (3), 456 (1989).

[3] Gilbert, C. D. and Wiesel, T. N., Receptive field dynamics in adult primary visual cortexNature 356 (6365), 150 (1992).

[4] Darian-Smith, C. and Gilbert, C. D., Topographic reorganization in the striate cortex of the adult cat and monkey is cortically mediatedJ Neurosci 15 (3 Pt 1), 1631 (1995).

[5] Darian-Smith, C. and Gilbert, C. D., Axonal sprouting accompanies functional reorganization in adult cat striate cortexNature 368 (6473), 737 (1994).

[6] Baker, C. I., Peli, E., Knouf, N., and Kanwisher, N. G., Reorganization of visual processing in macular degenerationJ Neurosci 25 (3), 614 (2005).

[7] Gilbert, C. D., Hirsch, J. A., and Wiesel, T. N., Lateral interactions in visual cortexCold Spring Harb Symp Quant Biol 55, 663 (1990).

[8] Schmid, L. M., Rosa, M. G., Calford, M. B., and Ambler, J. S., Visuotopic reorganization in the primary visual cortex of adult cats following monocular and binocular retinal lesionsCereb Cortex 6 (3), 388 (1996).

[9] Calford, M. B., Schmid, L. M., and Rosa, M. G., Monocular focal retinal lesions induce short-term topographic plasticity in adult cat visual cortexProc Biol Sci 266 (1418), 499 (1999).

[10] Heinen, S. J. and Skavenski, A. A., Recovery of visual responses in foveal V1 neurons following bilateral foveal lesions in adult monkeyExp Brain Res 83 (3), 670 (1991).

[11] Das, A. and Gilbert, C. D., Long-range horizontal connections and their role in cortical reorganization revealed by optical recording of cat primary visual cortexNature 375 (6534), 780 (1995).

[12] Kossut, M., Experience-dependent changes in function and anatomy of adult barrel cortexExperimental brain research. Experimentelle Hirnforschung 123 (1-2), 110 (1998).

[13] Ghosh, A. and Greenberg, M. E., Distinct roles for bFGF and NT-3 in the regulation of cortical neurogenesisNeuron 15 (1), 89 (1995).

[14] Cohen-Cory, S. and Fraser, S. E., Effects of brain-derived neurotrophic factor on optic axon branching and remodelling in vivoNature 378 (6553), 192 (1995).

[15] Okamura, K., Phillips, M. D., Tyler, D. M. et al., The regulatory activity of microRNA* species has substantial influence on microRNA and 3' UTR evolutionNature structural & molecular biology 15 (4), 354 (2008).

[16] Cabelli, R. J., Hohn, A., and Shatz, C. J., Inhibition of ocular dominance column formation by infusion of NT-4/5 or BDNFScience 267 (5204), 1662 (1995).

[17] Zweifel, L. S., Kuruvilla, R., and Ginty, D. D., Functions and mechanisms of retrograde neurotrophin signallingNat Rev Neurosci 6 (8), 615 (2005).

[18] Cohen, S. and Levi-Montalcini, R., Purification and properties of a nerve growth-promoting factor isolated from mouse sarcoma 180Cancer Res 17 (1), 15 (1957).

[19] Lewin, G. R. and Barde, Y. A., Physiology of the neurotrophinsAnnu Rev Neurosci 19, 289 (1996).

[20] Lu, B., Pang, P. T., and Woo, N. H., The yin and yang of neurotrophin actionNat Rev Neurosci 6 (8), 603 (2005).

[21] Campenot, R. B., Local control of neurite development by nerve growth factorProc Natl Acad Sci U S A 74 (10), 4516 (1977).

[22] Lohof, A. M., Ip, N. Y., and Poo, M. M., Potentiation of developing neuromuscular synapses by the neurotrophins NT-3 and BDNFNature 363 (6427), 350 (1993).

[23] Kang, H., Jia, L. Z., Suh, K. Y. et al., Determinants of BDNF-induced hippocampal synaptic plasticity: role of the Trk B receptor and the kinetics of neurotrophin deliveryLearn Mem 3 (2-3), 188 (1996).

[24] Maffei, L., Berardi, N., Domenici, L. et al., Nerve growth factor (NGF) prevents the shift in ocular dominance distribution of visual cortical neurons in monocularly deprived ratsJ Neurosci 12 (12), 4651 (1992).

[25] Lindholm, D., Castren, E., Berzaghi, M. et al., Activity-dependent and hormonal regulation of neurotrophin mRNA levels in the brain--implications for neuronal plasticityJ Neurobiol 25 (11), 1362 (1994).

[26] Patterson, S. L., Grover, L. M., Schwartzkroin, P. A., and Bothwell, M., Neurotrophin expression in rat hippocampal slices: a stimulus paradigm inducing LTP in CA1 evokes increases in BDNF and NT-3 mRNAsNeuron 9 (6), 1081 (1992).

[27] Castren, E., Zafra, F., Thoenen, H., and Lindholm, D., Light regulates expression of brain-derived neurotrophic factor mRNA in rat visual cortexProc Natl Acad Sci U S A 89 (20), 9444 (1992).

[28] Thoenen, H., Neurotrophins and neuronal plasticityScience 270 (5236), 593 (1995).

[29] Berardi, N., Cellerino, A., Domenici, L. et al., Monoclonal antibodies to nerve growth factor affect the postnatal development of the visual systemProc Natl Acad Sci U S A 91 (2), 684 (1994).

[30] Gianfranceschi, L., Siciliano, R., Walls, J. et al., Visual cortex is rescued from the effects of dark rearing by overexpression of BDNFProc Natl Acad Sci U S A 100 (21), 12486 (2003).

[31] Ip, N. Y., Wiegand, S. J., Morse, J., and Rudge, J. S., Injury-induced regulation of ciliary neurotrophic factor mRNA in the adult rat brainEur J Neurosci 5 (1), 25 (1993).

[32] Huang, Z. J., Kirkwood, A., Pizzorusso, T. et al., BDNF regulates the maturation of inhibition and the critical period of plasticity in mouse visual cortexCell 98 (6), 739 (1999).

[33] Lein, E. S. and Shatz, C. J., Rapid regulation of brain-derived neurotrophic factor mRNA within eye-specific circuits during ocular dominance column formationJ Neurosci 20 (4), 1470 (2000).

[34] Lein, E. S., Hohn, A., and Shatz, C. J., Dynamic regulation of BDNF and NT-3 expression during visual system developmentJ Comp Neurol 420 (1), 1 (2000).

[35] Obata, S., Obata, J., Das, A., and Gilbert, C. D., Molecular correlates of topographic reorganization in primary visual cortex following retinal lesionsCereb Cortex 9 (3), 238 (1999).

[36] Kaplitt, M. G. and Pfaff, D. W., Viral Vectors for Gene Delivery and Expression in the CNSMethods 10 (3), 343 (1996).

[37] Kaplitt, M. G., Leone, P., Samulski, R. J. et al., Long-term gene expression and phenotypic correction using adeno-associated virus vectors in the mammalian brainNat Genet 8 (2), 148 (1994).

[38] Erles, K., Sebokova, P., and Schlehofer, J. R., Update on the prevalence of serum antibodies (IgG and IgM) to adeno-associated virus (AAV)J Med Virol 59 (3), 406 (1999).

[39] Stilwell, J. L. and Samulski, R. J., Role of viral vectors and virion shells in cellular gene expressionMol Ther 9 (3), 337 (2004).

[40] Nakai, H., Yant, S. R., Storm, T. A. et al., Extrachromosomal recombinant adeno-associated virus vector genomes are primarily responsible for stable liver transduction in vivoJ Virol 75 (15), 6969 (2001).

[41] Burger, C., Gorbatyuk, O. S., Velardo, M. J. et al., Recombinant AAV viral vectors pseudotyped with viral capsids from serotypes 1, 2, and 5 display differential efficiency and cell tropism after delivery to different regions of the central nervous systemMol Ther 10 (2), 302 (2004).

[42] Klein, R. L., Hamby, M. E., Gong, Y. et al., Dose and promoter effects of adeno-associated viral vector for green fluorescent protein expression in the rat brainExp Neurol 176 (1), 66 (2002).

[43] Loeb, J. E., Cordier, W. S., Harris, M. E. et al., Enhanced expression of transgenes from adeno-associated virus vectors with the woodchuck hepatitis virus posttranscriptional regulatory element: implications for gene therapyHum Gene Ther 10 (14), 2295 (1999).

[44] Farazi, T. A., Juranek, S. A., and Tuschl, T., The growing catalog of small RNAs and their association with distinct Argonaute/Piwi family membersDevelopment (Cambridge, England) 135 (7), 1201 (2008).

[45] Griffiths-Jones, S., The microRNA RegistryNucleic Acids Res. 32 (1), D109 (2004).

[46] Cullen, B. R., Transcription and processing of human microRNA precursorsMol. Cell 16 (6), 861 (2004).

[47] Gregory, R. I. and Shiekhattar, R., MicroRNA biogenesis and cancerCancer Res. 65 (9), 3509 (2005).

[48] Kim, V. N., MicroRNA biogenesis: coordinated cropping and dicingNat. Rev. Mol. Cell Biol. 6, 376 (2005).

[49] Carrington, J. C. and Ambros, V., Role of microRNAs in plant and animal developmentScience 301 (5631), 336 (2003).

[50] Ambros, V., The functions of animal microRNAsNature 431 (7006), 350 (2004).

[51] Baulcombe, D., RNA silencing in plantsNature 431 (7006), 356 (2004).

[52] Bartel, D. P., MicroRNAs: genomics, biogenesis, mechanism, and functionCell 116 (2), 281 (2004).

[53] He, L. and Hannon, G. J., MicroRNAs: small RNAs with a big role in gene regulationNat. Rev. Genet. 5 (7), 522 (2004).

[54] Meister, G. and Tuschl, T., Mechanisms of gene silencing by double-stranded RNANature 431 (7006), 343 (2004).

[55] Wienholds, E. and Plasterk, R. H., MicroRNA function in animal developmentFEBS Lett. 579 (26), 5911 (2005).

[56] Rodriguez, A., Griffiths-Jones, S., Ashurst, J. L., and Bradley, A., Identification of mammalian microRNA host genes and transcription unitsGenome Res. 14 (10a), 1902 (2004).

[57] Baskerville, S. and Bartel, D. P., Microarray profiling of microRNAs reveals frequent coexpression with neighboring miRNAs and host genesRNA 11 (3), 241 (2005).

[58] Weber, M. J., New human and mouse microRNA genes found by homology searchFEBS J. 272 (1), 59 (2005).

[59] Hutvágner, G. and Zamore, P. D., A microRNA in a multiple-turnover RNAi enzyme complexScience 297, 2056 (2002).

[60] Martinez, J., Patkaniowska, A., Urlaub, H. et al., Single-stranded antisense siRNAs guide target RNA cleavage in RNAiCell 110, 563 (2002).

[61] Schwarz, D. S., Hutvágner, G., Du, T. et al., Asymmetry in the assembly of the RNAi enzyme complexCell 115 (2), 199 (2003).

[62] Liu, J., Carmell, M. A., Rivas, F. V. et al., Argonaute2 is the catalytic engine of mammalian RNAiScience 305 (5689), 1437 (2004).

[63] Meister, G., Landthaler, M., Patkaniowska, A. et al., Human Argonaute2 mediates RNA cleavage targeted by miRNAs and siRNAsMol. Cell 15 (2), 185 (2004).

[64] Mourelatos, Z., Dostie, J., Paushkin, S. et al., miRNPs: a novel class of ribonucleoproteins containing numerous microRNAsGenes & Dev. 16 (6), 720 (2002).

[65] Pillai, R. S., Artus, C. G., and Filipowicz, W., Tethering of human Ago proteins to mRNA mimics the miRNA-mediated repression of protein synthesisRNA 10 (10), 1518 (2004).

[66] Yuan, Y. R., Pei, Y., Ma, J. B. et al., Crystal structure of A. aeolicus Argonaute, a site-specific DNA-guided endoribonuclease, provides insights into RISC-mediated mRNA cleavageMol. Cell 19 (3), 405 (2005).

[67] Landthaler, M., Gaidatzis, D., Rothballer, A. et al., Molecular characterization of human Argonaute-containing ribonucleoprotein complexes and their bound target mRNAsRNA 14 (12), 2580 (2008).

[68] Meister, G., Landthaler, M., Patkaniowska, A. et al., Human Argonaute2 mediates RNA cleavage targeted by miRNAs and siRNAsMolecular cell 15 (2), 185 (2004).

[69] Rivas, F. V., Tolia, N. H., Song, J. J. et al., Purified Argonaute2 and an siRNA form recombinant human RISCNature structural & molecular biology 12 (4), 340 (2005).

[70] Wightman, B., Ha, I., and Ruvkun, G., Posttranscriptional regulation of the heterochronic gene *lin-14* by *lin-4* mediates temporal pattern formation in *C. elegans*Cell 75 (5), 855 (1993).

[71] Moss, E. G., Lee, R. C., and Ambros, V., The cold shock domain protein LIN-28 controls developmental timing in *C. elegans* and is regulated by the lin-4 RNACell 88 (5), 637 (1997).

[72] Olsen, P. H. and Ambros, V., The lin-4 regulatory RNA controls developmental timing in *Caenorhabditis elegans* by blocking LIN-14 protein synthesis after the initiation of translationDev. Biol. 216 (2), 671 (1999).

[73] Seggerson, K., Tang, L., and Moss, E. G., Two genetic circuits repress the *Caenorhabditis elegans* heterochronic gene *lin-28* after translation initiationDev. Biol. 243 (2), 215 (2002).

[74] Doench, J. G., Petersen, C. P., and Sharp, P. A., siRNAs can function as miRNAsGenes & Dev. 17 (4), 438 (2003).

[75] Doench, J. G. and Sharp, P. A., Specificity of microRNA target selection in translational repressionGenes & Dev. 18 (5), 504 (2004).

[76] Bagga, S., Bracht, J., Hunter, S. et al., Regulation by let-7 and lin-4 miRNAs results in target mRNA degradationCell 122 (4), 553 (2005).

[77] Pillai, R. S., Bhattacharyya, S. N., Artus, C. G. et al., Inhibition of translational Initiation by let-7 microRNA in human cellsScience 309, 1573 (2005).

[78] Mello, C. C. and Conte, D., Jr., Revealing the world of RNA interferenceNature 431 (7006), 338 (2004).

[79] Meister, G., Landthaler, M., Dorsett, Y., and Tuschl, T., Sequence-specific inhibition of microRNA- and siRNA-induced RNA silencingRna 10 (3), 544 (2004).

[80] Fire, A., Xu, S., Montgomery, M. K. et al., Potent and specific genetic interference by double-stranded RNA in Caenorhabditis elegansNature 391 (6669), 806 (1998).

[81] Elbashir, S. M., Harborth, J., Weber, K., and Tuschl, T., Analysis of gene function in somatic mammalian cells using small interfering RNAsMethods 26 (2), 199 (2002).

[82] Paddison, P. J., Caudy, A. A., Bernstein, E. et al., Short hairpin RNAs (shRNAs) induce sequence-specific silencing in mammalian cellsGenes Dev 16 (8), 948 (2002).

[83] Hutvagner, G. and Zamore, P. D., A microRNA in a multiple-turnover RNAi enzyme complexScience 297 (5589), 2056 (2002).

[84] Elbashir, S. M., Martinez, J., Patkaniowska, A. et al., Functional anatomy of siRNAs for mediating efficient RNAi in Drosophila melanogaster embryo lysateEmbo J 20 (23), 6877 (2001).

[85] Pasquinelli, A. E., Reinhart, B. J., Slack, F. et al., Conservation of the sequence of *let-7* heterochronic regulatory RNANature 408, 86 (2000).

[86] Lagos-Quintana, M., Rauhut, R., Yalcin, A. et al., Identification of tissue-specific microRNAs from mouseCurr. Biol. 12 (9), 735 (2002).

[87] Bernstein, E., Kim, S. Y., Carmell, M. A. et al., Dicer is essential for mouse developmentNat Genet 35 (3), 215 (2003).

[88] Yi, R., Pasolli, H. A., Landthaler, M. et al., DGCR8-dependent microRNA biogenesis is essential for skin developmentProceedings of the National Academy of Sciences of the United States of America 106 (2), 498 (2009).

[89] Landgraf, P., Rusu, M., Sheridan, R. et al., A mammalian microRNA expression atlas based on small RNA library sequencingCell 129 (7), 1401 (2007).

[90] Aravin, A. and Tuschl, T., Identification and characterization of small RNAs involved in RNA silencingFEBS letters 579, 5830 (2005).

[91] Wienholds, E., Kloosterman, W. P., Miska, E. et al., MicroRNA expression in zebrafish embryonic developmentScience 309, 310 (2005).

[92] Sokol, N. S. and Ambros, V., Mesodermally expressed Drosophila microRNA-1 is regulated by Twist and is required in muscles during larval growthGenes Dev 19 (19), 2343 (2005).

[93] Zhao, Y., Samal, E., and Srivastava, D., Serum response factor regulates a muscle-specific microRNA that targets Hand2 during cardiogenesisNature 436 (7048), 214 (2005).

[94] Lee, R. C. and Ambros, V., An extensive class of small RNAs in Caenorhabditis elegansScience 294 (5543), 862 (2001).

[95] Nelson, P. T., Baldwin, D. A., Kloosterman, W. P. et al., RAKE and LNA-ISH reveal microRNA expression and localization in archival human brainRNA 12 (2), 187 (2006).

[96] Poy, M. N., Eliasson, L., Krutzfeldt, J. et al., A pancreatic islet-specific microRNA regulates insulin secretionNature 432 (7014), 226 (2004).

[97] Lu, J., Getz, G., Miska, E. A. et al., MicroRNA expression profiles classify human cancersNature 435 (7043), 834 (2005).

[98] Farh, K. K., Grimson, A., Jan, C. et al., The Widespread Impact of Mammalian MicroRNAs on mRNA Repression and EvolutionScience (New York, N.Y (2005).

[99] Babar, I. A., Slack, F. J., and Weidhaas, J. B., miRNA modulation of the cellular stress responseFuture oncology (London, England) 4 (2), 289 (2008).

[100] Brennecke, J., Stark, A., and Cohen, S. M., Not miR-ly muscular: microRNAs and muscle developmentGenes & Dev. 19 (19), 2261 (2005).

[101] Kidner, C. A. and Martienssen, R. A., The developmental role of microRNA in plantsCurr. Opin. Plant. Biol. 8 (1), 38 (2005).

[102] Sontheimer, E. J. and Carthew, R. W., Silence from within: endogenous siRNAs and miRNAsCell 122 (1), 9 (2005).

[103] Schaefer, A., O'Carroll, D., Tan, C. L. et al., Cerebellar neurodegeneration in the absence of microRNAsJ Exp Med 204 (7), 1553 (2007).

[104] Bernstein, E., Kim, S. Y., Carmell, M. A. et al., Dicer is essential for mouse developmentNat. Genet. 35 (3), 215 (2003).

[105] Muljo, S. A., Ansel, K. M., Kanellopoulou, C. et al., Aberrant T cell differentiation in the absence of DicerJ. Exp. Med. 202 (2), 261 (2005).

[106] Cobb, B. S., Nesterova, T. B., Thompson, E. et al., T cell lineage choice and differentiation in the absence of the RNase III enzyme DicerJ. Exp. Med. 201 (9), 1367 (2005).

[107] Harfe, B. D., McManus, M. T., Mansfield, J. H. et al., The RNase III enzyme Dicer is required for morphogenesis but not patterning of the vertebrate limbProc. Natl. Acad. Sci. USA 102 (31), 10898 (2005).

[108] Kanellopoulou, C., Muljo, S. A., Kung, A. L. et al., Dicer-deficient mouse embryonic stem cells are defective in differentiation and centromeric silencingGenes Dev 19 (4), 489 (2005).

[109] Tam, O. H., Aravin, A. A., Stein, P. et al., Pseudogene-derived small interfering RNAs regulate gene expression in mouse oocytesNature 453 (7194), 534 (2008).

[110] Landthaler, M., Yalcin, A., and Tuschl, T, The human DiGeorge Syndrome Critical Region Gene 8 and its *D. melanogaster* homolog are required for miRNA biogenesisCurr Biol, in press (2004).

[111] Sohn, S. Y., Bae, W. J., Kim, J. J. et al., Crystal structure of human DGCR8 coreNature structural & molecular biology 14 (9), 847 (2007).

[112] Han, J., Lee, Y., Yeom, K. H. et al., Molecular basis for the recognition of primary microRNAs by the Drosha-DGCR8 complexCell 125 (5), 887 (2006).

[113] Rhoades, M., Reinhart, B., Lim, L. et al., Prediction of plant microRNA targetsCell 110 (4), 513 (2002).

[114] Enright, A. J., John, B., Gaul, U. et al., MicroRNA targets in *Drosophila*Genome Biol. 5:RI, 1 (2003).

[115] Lewis, B. P., Shih, I., Jones-Rhoades, M. W. et al., Prediction of mammalian microRNA targetsCell 115 (7), 787 (2003).

[116] Stark, A., Brennecke, J., Russell, R. B., and Cohen, S. M., Identification of *Drosophila* microRNA targetsPLoS Biol. 1 (3), 397 (2003).

[117] John, B., Enright, A. J., Aravin, A. et al., Human miRNA targetsPLoS Biol. 2 (11), e363 (2004).

[118] Jones-Rhoades, M. W. and Bartel, D. P., Computational identification of plant microRNAs and their targets, including a stress-induced miRNAMol. Cell 14 (6), 787 (2004).

[119] Kiriakidou, M., Nelson, P. T., Kouranov, A. et al., A combined computational-experimental approach predicts human microRNA targetsGenes & Dev. 18, in press (2004).

[120] Rehmsmeier, M., Steffen, P., Hochsmann, M., and Giegerich, R., Fast and effective prediction of microRNA/target duplexesRNA 10 (10), 1507 (2004).

[121] Brennecke, J., Stark, A., Russell, R. B., and Cohen, S. M., Principles of microRNA-target recognitionPLoS Biol. 3 (3), e85 (2005).

[122] Chen, P. Y. , Manninga, H., K., Slanchev et al., The developmental miRNA profiles of zebrafish as determined by small RNA cloningGenes & Dev. 19, 1288 (2005).

[123] Grün, D., Wang, Y. L., Langenberger, D. et al., microRNA target predictions across seven Drosophila species and comparison to mammalian targetsPLoS Comput. Biol. 1 (1), e13 (2005).

[124] Krek, A., Grün, D., Poy, M. N et al., Combinatorial microRNA target predictionNat. Genet. 37, 495 (2005).

[125] Lewis, B. P., Burge, C. B., and Bartel, D. P., Conserved seed pairing, often flanked by adenosines, indicates that thousands of human genes are microRNA targetsCell 120 (1), 15 (2005).

[126] Robins, H., Li, Y., and Padgett, R. W., Incorporating structure to predict microRNA targetsProc. Natl. Acad. Sci. USA (2005).

[127] Xie, X., Lu, J., Kulbokas, E. J. et al., Systematic discovery of regulatory motifs in human promoters and 3' UTRs by comparison of several mammalsNature 434 (7031), 338 (2005).

[128] Rajewsky, N., microRNA target predictions in animalsNat. Genet. 38 Suppl 1 (6s), S8 (2006).

[129] Lim, L. P., Lau, N. C., Garrett-Engele, P. et al., Microarray analysis shows that some microRNAs downregulate large numbers of target mRNAsNature 433 (7027), 769 (2005).

[130] Mencia, A., Modamio-Hoybjor, S., Redshaw, N. et al., Mutations in the seed region of human miR-96 are responsible for nonsyndromic progressive hearing lossNat Genet 41 (5), 609 (2009).

[131] Lewis, M. A., Quint, E., Glazier, A. M. et al., An ENU-induced mutation of miR-96 associated with progressive hearing loss in miceNat Genet 41 (5), 614 (2009).

[132] Aboobaker, A. A., Tomancak, P., Patel, N. et al., Drosophila microRNAs exhibit diverse spatial expression patterns during embryonic developmentProc. Natl. Acad. Sci. USA 102 (50), 18017 (2005).

[133] Lagos-Quintana, M., Rauhut, R., Lendeckel, W., and Tuschl, T., Identification of novel genes coding for small expressed RNAsScience 294 (5543), 853 (2001).

[134] Cheng, L. C., Pastrana, E., Tavazoie, M., and Doetsch, F., miR-124 regulates adult neurogenesis in the subventricular zone stem cell nicheNature neuroscience 12 (4), 399 (2009).

[135] Krichevsky, A. M., King, K. S., Donahue, C. P. et al., A microRNA array reveals extensive regulation of microRNAs during brain developmentRNA 9 (10), 1274 (2003).

[136] Miska, E. A., Alvarez-Saavedra, E., Townsend, M. et al., Microarray analysis of microRNA expression in the developing mammalian brainGenome Biol. 5 (9), R68 (2004).

[137] Sempere, L. F., Freemantle, S., Pitha-Rowe, I. et al., Expression profiling of mammalian microRNAs uncovers a subset of brain-expressed microRNAs with possible roles in murine and human neuronal differentiationGenome Biol. 5 (3), R13 (2004).

[138] Mansfield, J. H., Harfe, B. D., Nissen, R. et al., MicroRNA-responsive 'sensor' transgenes uncover Hox-like and other developmentally regulated patterns of vertebrate microRNA expressionNat Genet 36 (10), 1079 (2004).

[139] Tang, F., Hajkova, P., Barton, S. C. et al., MicroRNA expression profiling of single whole embryonic stem cellsNucleic Acids Res 34 (2), e9 (2006).

[140] Liao, R., Sun, J., Zhang, L. et al., MicroRNAs play a role in the development of human hematopoietic stem cellsJournal of cellular biochemistry 104 (3), 805 (2008).

[141] Kye, M. J., Liu, T., Levy, S. F. et al., Somatodendritic microRNAs identified by laser capture and multiplex RT-PCRRNA 13 (8), 1224 (2007).

[142] Kloosterman, W. P., Wienholds, E., de Bruijn, E. et al., In situ detection of miRNAs in animal embryos using LNA-modified oligonucleotide probesNat Methods 3 (1), 27 (2006).

[143] Obernosterer, G., Martinez, J., and Alenius, M., Locked nucleic acid-based in situ detection of microRNAs in mouse tissue sectionsNat Protoc 2 (6), 1508 (2007).

[144] Silahtaroglu, A. N., Nolting, D., Dyrskjot, L. et al., Detection of microRNAs in frozen tissue sections by fluorescence in situ hybridization using locked nucleic acid probes and tyramide signal amplificationNat Protoc 2 (10), 2520 (2007).

[145] Lein, E. S., Hawrylycz, M. J., Ao, N. et al., Genome-wide atlas of gene expression in the adult mouse brainNature 445 (7124), 168 (2007).

[146] Ryan, D. G., Oliveira-Fernandes, M., and Lavker, R. M., MicroRNAs of the mammalian eye display distinct and overlapping tissue specificityMol Vis 12, 1175 (2006).

[147] Pena, J. T., Sohn-Lee, C., Rouhanifard, S. H. et al., miRNA in situ hybridization in formaldehyde and EDC-fixed tissuesNat Methods 6 (2), 139 (2009).

[148] Smirnova, L., Grafe, A., Seiler, A. et al., Regulation of miRNA expression during neural cell specificationEur. J. Neurosci. 21 (6), 1469 (2005).

[149] Johnston, R. J. and Hobert, O., A microRNA controlling left/right neuronal asymmetry in Caenorhabditis elegansNature 426 (6968), 845 (2003).

[150] Hobert, O., Common logic of transcription factor and microRNA actionTrends Biochem. Sci. 29 (9), 462 (2004).

[151] Chang, S., Johnston, R. J., Jr., Frokjaer-Jensen, C. et al., MicroRNAs act sequentially and asymmetrically to control chemosensory laterality in the nematodeNature 430 (7001), 785 (2004).

[152] Papagiannakopoulos, T. and Kosik, K. S., MicroRNAs: regulators of oncogenesis and stemnessBMC medicine 6, 15 (2008).

[153] Giraldez, A. J., Cinalli, R. M., Glasner, M. E. et al., MicroRNAs regulate brain morphogenesis in zebrafishScience (2005).

[154] Davis, T. H., Cuellar, T. L., Koch, S. M. et al., Conditional loss of Dicer disrupts cellular and tissue morphogenesis in the cortex and hippocampusJ Neurosci 28 (17), 4322 (2008).

[155] Stark, K. L., Xu, B., Bagchi, A. et al., Altered brain microRNA biogenesis contributes to phenotypic deficits in a 22q11-deletion mouse modelNat Genet 40 (6), 751 (2008).

[156] Schaeffer, C., Beaulande, M., Ehresmann, C. et al., The RNA binding protein FMRP: new connections and missing linksBiol Cell 95 (3-4), 221 (2003).

[157] Jin, P., Zarnescu, D. C., Ceman, S. et al., Biochemical and genetic interaction between the fragile X mental retardation protein and the microRNA pathwayNature neuroscience 7 (2), 113 (2004).

[158] Bassell, G. J. and Warren, S. T., Fragile X syndrome: loss of local mRNA regulation alters synaptic development and functionNeuron 60 (2), 201 (2008).

[159] Bolduc, F. V., Bell, K., Cox, H. et al., Excess protein synthesis in Drosophila fragile X mutants impairs long-term memoryNature neuroscience 11 (10), 1143 (2008).

[160] Caudy, A. A., Myers, M., Hannon, G. J., and Hammond, S. M., Fragile X-related protein and VIG associate with the RNA interference machineryGenes Dev 16 (19), 2491 (2002).

[161] Sokol, N. S., Xu, P., Jan, Y. N., and Ambros, V., Drosophila let-7 microRNA is required for remodeling of the neuromusculature during metamorphosisGenes Dev 22 (12), 1591 (2008).

[162] Schratt, G. M., Tuebing, F., Nigh, E. A. et al., A brain-specific microRNA regulates dendritic spine developmentNature 439 (7074), 283 (2006).

[163] Klein, M. E., Lioy, D. T., Ma, L. et al., Homeostatic regulation of MeCP2 expression by a CREB-induced microRNANature neuroscience 10 (12), 1513 (2007).

[164] Blight, A. R., Remyelination, revascularization, and recovery of function in experimental spinal cord injuryAdvances in neurology 59, 91 (1993).

[165] Burns, S. P., Golding, D. G., Rolle, W. A., Jr. et al., Recovery of ambulation in motor-incomplete tetraplegiaArchives of physical medicine and rehabilitation 78 (11), 1169 (1997).

[166] Baker-Herman, T. L., Fuller, D. D., Bavis, R. W. et al., BDNF is necessary and sufficient for spinal respiratory plasticity following intermittent hypoxiaNature neuroscience 7 (1), 48 (2004).

[167] Yuan, B., Latek, R., Hossbach, M. et al., siRNA Selection Server: an automated siRNA oligonucleotide prediction serverNucleic Acids Res 32 (Web Server issue), W130 (2004).

[168] Grimm, D., Streetz, K. L., Jopling, C. L. et al., Fatality in mice due to oversaturation of cellular microRNA/short hairpin RNA pathwaysNature 441 (7092), 537 (2006).

[169] Elbashir, S. M., Lendeckel, W., and Tuschl, T., RNA interference is mediated by 21 and 22 nt RNAsGenes & Dev. 15, 188 (2001).

[170] Hafner, M., Landgraf, P., Ludwig, J. et al., Identification of microRNAs and other small regulatory RNAs using cDNA library sequencingMethods (San Diego, Calif 44 (1), 3 (2008).

[171] Abramoff, M.D., Magelhaes, P.J., Ram, S.J., Image Processing with ImageJBiophotonics International 11 (7), 36 (2004).

[172] Kosik, K. S., The neuronal microRNA systemNat Rev Neurosci 7 (12), 911 (2006).

[173] Thompson, R. C., Deo, M., and Turner, D. L., Analysis of microRNA expression by in situ hybridization with RNA oligonucleotide probesMethods (San Diego, Calif 43 (2), 153 (2007).

[174] Nuovo, G. J., In situ detection of precursor and mature microRNAs in paraffin embedded, formalin fixed tissues and cell preparationsMethods (San Diego, Calif 44 (1), 39 (2008).

[175] Bak, M., Silahtaroglu, A., Moller, M. et al., MicroRNA expression in the adult mouse central nervous systemRNA 14 (3), 432 (2008).

[176] Sempere, L. F., Christensen, M., Silahtaroglu, A. et al., Altered MicroRNA expression confined to specific epithelial cell subpopulations in breast cancerCancer Res 67 (24), 11612 (2007).

[177] Wang, W. X., Rajeev, B. W., Stromberg, A. J. et al., The expression of microRNA miR-107 decreases early in Alzheimer's disease and may accelerate disease progression through regulation of beta-site amyloid precursor protein-cleaving enzyme 1J Neurosci 28 (5), 1213 (2008).

[178] Feldman, M. Y., Reactions of nucleic acids and nucleoproteins with formaldehydeProg Nucleic Acid Res Mol Biol 13, 1 (1973).

[179] Masuda, N., Ohnishi, T., Kawamoto, S. et al., Analysis of chemical modification of RNA from formalin-fixed samples and optimization of molecular biology applications for such samplesNucleic Acids Res 27 (22), 4436 (1999).

[180] Tymianski, M., Bernstein, G. M., Abdel-Hamid, K. M. et al., A novel use for a carbodiimide compound for the fixation of fluorescent and non-fluorescent calcium indicators in situ following physiological experimentsCell calcium 21 (3), 175 (1997).

[181] Pall, G. S., Codony-Servat, C., Byrne, J. et al., Carbodiimide-mediated cross-linking of RNA to nylon membranes improves the detection of siRNA, miRNA and piRNA by northern blotNucleic Acids Res 35 (8), e60 (2007).

[182] Kaur, H., Arora, A., Wengel, J., and Maiti, S., Thermodynamic, counterion and hydration effects for the incorporation of locked nucleic acid (LNA) nucleotides in duplexNucleic Acids Symp Ser (Oxf) (52), 425 (2008).

[183] Zuker, M., Mfold web server for nucleic acid folding and hybridization predictionNucleic Acids Res 31 (13), 3406 (2003).

[184] Devore, Jay L., Probability and statistics for engineering and the sciences, (2004).

[185] Lagos-Quintana, M., Rauhut, R., Meyer, J. et al., New microRNAs from mouse and humanRNA 9 (2), 175 (2003).

[186] Aravin, A. A., Lagos-Quintana, M., Yalcin, A. et al., The small RNA profile during *Drosophila melanogaster* developmentDev. Cell 5 (2), 337 (2003).

[187] Pfeffer, S., Zavolan, M., Grasser, F. A. et al., Identification of virus-encoded microRNAsScience 304 (5671), 734 (2004).

[188] Pfeffer, S., Sewer, A., Lagos-Quintana, M. et al., Identification of microRNAs of the herpesvirus familyNature Meth. 2 (4), 269 (2005).

[189] Pfeffer, S., Lagos-Quintana, M., and Tuschl, T., in Current Protocols in Molecular Biology, edited by F.M. Ausubel, R. Brent, R. E. Kingston et al. (John Wiley and Sons, New York, 2003), pp. 26.4.1.

[190] Grewal, S. I. and Jia, S., Heterochromatin revisitedNature reviews 8 (1), 35 (2007).

[191] Nakayashiki, H., RNA silencing in fungi: mechanisms and applicationsFEBS letters 579 (26), 5950 (2005).

[192] Seto, A. G., Kingston, R. E., and Lau, N. C., The coming of age for Piwi proteinsMolecular cell 26 (5), 603 (2007).

[193] Vaucheret, H., Post-transcriptional small RNA pathways in plants: mechanisms and regulationsGenes Dev 20 (7), 759 (2006).

[194] Zaratiegui, M., Irvine, D. V., and Martienssen, R. A., Noncoding RNAs and gene silencingCell 128 (4), 763 (2007).

[195] Bartel, D. P., MicroRNAs: target recognition and regulatory functionsCell 136 (2), 215 (2009).

[196] Bushati, N. and Cohen, S. M., microRNA functionsAnnual review of cell and developmental biology 23, 175 (2007).

[197] Jones-Rhoades, M. W., Bartel, D. P., and Bartel, B., MicroRNAS and their regulatory roles in plantsAnnual review of plant biology 57, 19 (2006).

[198] Calin, G. A. and Croce, C. M., MicroRNA signatures in human cancersNat Rev Cancer 6 (11), 857 (2006).

[199] Kim, J., Inoue, K., Ishii, J. et al., A MicroRNA feedback circuit in midbrain dopamine neuronsScience (New York, N.Y 317 (5842), 1220 (2007).

[200] Thum, T., Gross, C., Fiedler, J. et al., MicroRNA-21 contributes to myocardial disease by stimulating MAP kinase signalling in fibroblastsNature 456 (7224), 980 (2008).

[201] Kloosterman, W. P., Steiner, F. A., Berezikov, E. et al., Cloning and expression of new microRNAs from zebrafishNucleic Acids Res 34 (9), 2558 (2006).

[202] McGhee, J. D. and von Hippel, P. H., Formaldehyde as a probe of DNA structure. II. Reaction with endocyclic imino groups of DNA basesBiochemistry 14 (6), 1297 (1975).

[203] Rasmussen, S. R., Larsen, M. R., and Rasmussen, S. E., Covalent immobilization of DNA onto polystyrene microwells: the molecules are only bound at the 5' endAnalytical biochemistry 198 (1), 138 (1991).

[204] Fedorova, O.A., Cyanogen bromide induced chemical ligation: Mechanisms and optimization of the reaction conditionsNucleosides & Nucleotides 16 (6), 1137 (1996).